

Antarctica's subglacial sedimentary basins and their influence on ice-sheet change

Alan R.A. Aitken¹, Lu Li¹, Bernd Kulesa², Dustin M Schroeder³, Tom A. Jordan⁴, Joanne M Whittaker⁵, Sridhar Anandakrishnan⁶, Douglas A Wiens⁷, Olaf Eisen⁸, and Martin J. Siegert⁹

¹University of Western Australia

²Swansea University

³Stanford University

⁴British Antarctic Survey

⁵University of Tasmania

⁶Pennsylvania State University

⁷Washington University

⁸Alfred Wegener Institute Helmholtz Center for Polar and Marine Research

⁹Imperial College London

April 3, 2023

1 **Antarctica's sedimentary basins and their influence on ice sheet**

2 **dynamics**

3 A.R.A. Aitken^{1,2}, L. Li¹, B. Kulesa^{3,4}, D. Schroeder^{5,6}, T.A. Jordan⁷, J. Whittaker⁸, S. Anandakrishnan⁹, E.J.
4 Dawson⁵, D. A. Wiens¹⁰, O. Eisen^{11,12}, M.J. Siegert¹³

- 5 1. School of Earth Sciences, The University of Western Australia, Perth, Western Australia, Australia
- 6 2. Australian Centre of Excellence for Antarctic Science, The University of Western Australia, Perth,
7 Western Australia, Australia
- 8 3. School of Biosciences, Geography and Physics, Swansea University, Wales, UK
- 9 4. School of Geography, Planning and Spatial Sciences, The University of Tasmania, Hobart Tasmania,
10 Australia
- 11 5. Department of Geophysics, Stanford University, Stanford, California, USA
- 12 6. Department of Electrical Engineering, Stanford University, Stanford, California, USA
- 13 7. British Antarctic Survey, Cambridgeshire, UK
- 14 8. The Institute of Marine and Antarctic Science, The University of Tasmania, Hobart, Tasmania,
15 Australia
- 16 9. College of Earth and Mineral Sciences, Pennsylvania State University, Pennsylvania, USA
- 17 10. Department of Earth & Planetary Sciences, Washington University, St. Louis, Missouri, USA
- 18 11. Glaciology, Alfred Wegener Institute, Helmholtz Centre for Polar and Marine Research,
19 Bremerhaven, Germany
- 20 12. Department of Geosciences, University of Bremen, Bremen, Germany
- 21 13. Grantham Institute and Department of Earth Science and Engineering, Imperial College London,
22 London, UK

23
24 Corresponding author: Alan Aitken (alan.aitken@uwa.edu.au)

25 **Key Points**

- 27 • Recent advances in detection and characterization of subglacial sedimentary basins are
28 reviewed
- 29 • A new map of Antarctica's sedimentary basins is presented and implications for glacial
30 processes are discussed
- 31 • Some future directions in Antarctic subglacial sedimentary basins research are explored

32

33 **Abstract**

34 Building a knowledge of Antarctica's sedimentary basins develops our understanding of the coupled
35 evolution of tectonics, ice, ocean, and climate. In comparison to non-basin regions, sedimentary basins have
36 distinct subglacial properties that impact ice sheet dynamics and may influence future ice sheet change.
37 Despite this importance, our knowledge of Antarctic sedimentary basins is restricted. Remoteness, the harsh
38 surface environment, the overlying ice sheet, fringing ice shelves and sea ice all make fieldwork challenging.
39 Nonetheless, in the past decade the geophysics community has made great progress in internationally
40 coordinated data collection and compilation. Parallel advances in data processing and analysis also support a
41 new level of insight into Antarctica's subglacial environment. Here, we summarize recent progress in
42 understanding Antarctica's sedimentary basins. We review advances in the technical capability of radar,
43 potential fields, seismic and electromagnetic techniques to detect and characterize basins beneath ice. In
44 addition, we review advances in integrated multi-data interpretation including emerging machine learning
45 approaches. These new capabilities permit a new continent-wide mapping of Antarctica's sedimentary
46 basins and their characteristics, aiding definition of the tectonic development of the continent. Crucially,
47 Antarctica's sedimentary basins interact with the overlying ice sheet through key dynamic feedbacks that
48 have the potential to contribute to rapid ice sheet change. Looking ahead, future research directions include
49 increasing data coverage within logistical constraints, and resolving major knowledge gaps, including
50 insufficient sampling of the ice sheet bed and poor definition of subglacial basin structure and stratigraphy.
51 Translating the knowledge of sedimentary basin processes into ice sheet modelling studies is critical to
52 underpin better capacity to predict future change.

53 **Plain Language Summary**

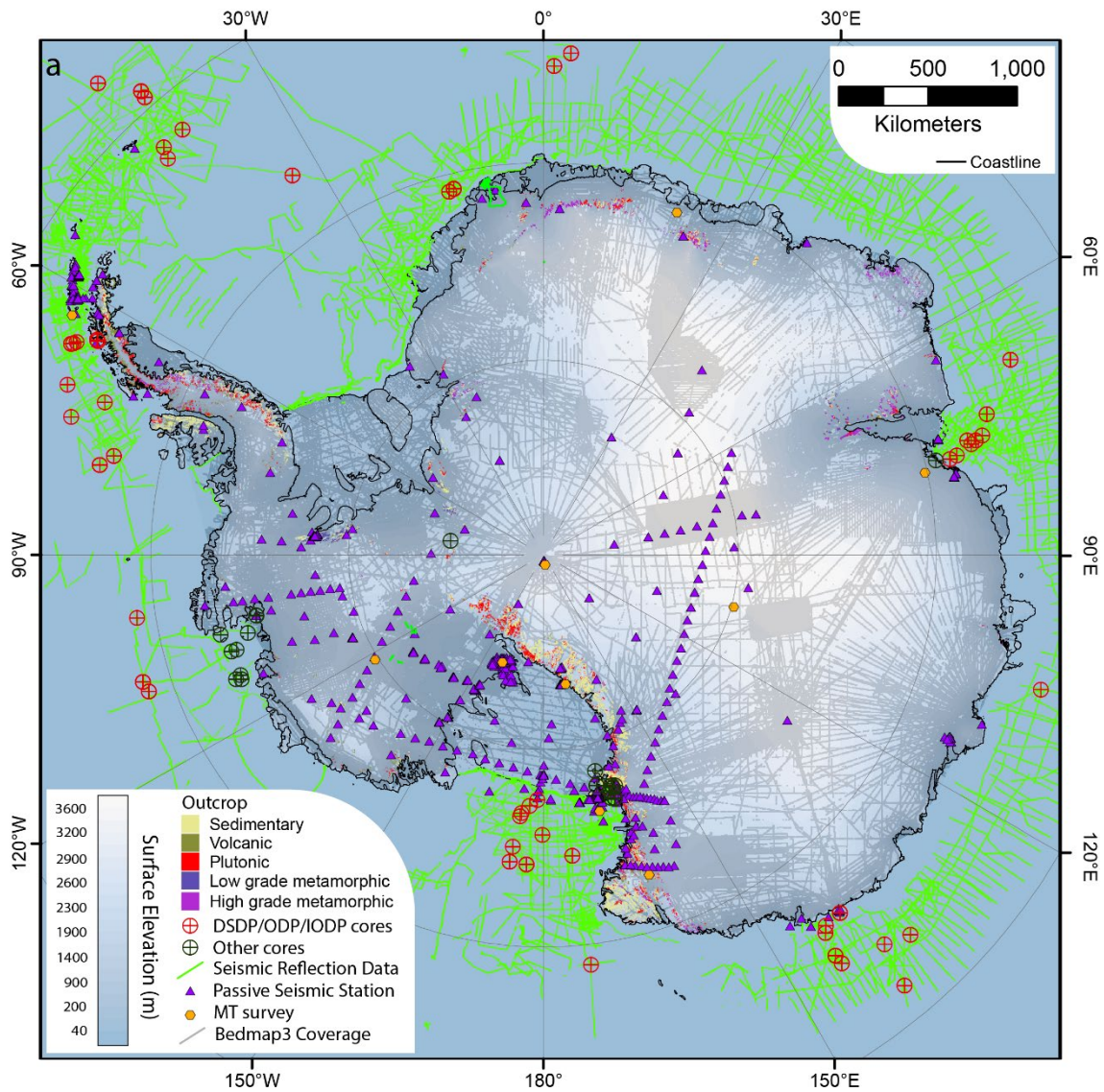
54 Antarctica is the keystone to the former supercontinent Gondwana and, because of its unique isolated
55 location at the South Pole, it has important consequences for understanding changing global climate and
56 ocean change. In several ways, sedimentary basins beneath the ice sheet interact with the ice sheet above
57 and can potentially contribute to rapid ice sheet changes that impact global sea level and climate. These
58 sedimentary basins have not all been systematically mapped due to the challenge of studying them beneath
59 thick ice. In this work we review technical progress towards the understanding of sedimentary basins in the
60 subglacial environment, and we map out the sedimentary basins beneath Antarctica's ice. We explore how
61 improved knowledge of Antarctica's basins helps to (1) understand important tectonic events in the
62 continent, (2) unravel the evolution of the landscape and the ice sheet, and (3) contribute to improved
63 predictions of future ice sheet change. Remaining challenges to further advance Antarctic sedimentary
64 basins research are identified and some future directions for study are discussed.

65 1 Introduction

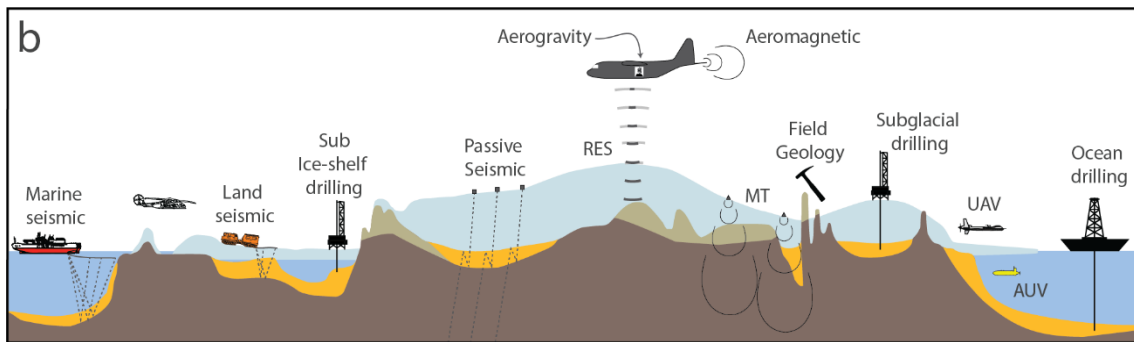
66 Sedimentary basins are widely preserved on all Earth's continents and provide distinct environments for
67 physical, chemical and biological processes [Evenick, 2021]. Antarctica is no exception and possesses several
68 major sedimentary basins and many smaller ones distributed across the continent. Seasonally ice-free
69 marine regions, including the Ross, Weddell, and Amundsen seas, and much of the East Antarctic continental
70 margin are relatively well surveyed (Fig 1). However, the unique challenge of ice-covered inland Antarctica,
71 with very limited and spatially clustered outcrop (Fig 1), a kilometers-thick ice sheet and severe
72 environmental and logistical challenges has meant that the distribution and nature of sedimentary basins is
73 poorly known inland. On the continental shelf, ice shelves and perennial sea-ice limit access to both marine
74 and terrestrial techniques. Sedimentary basins are important not just for the understanding of Antarctic
75 geology, but also because they provide key boundary conditions for glacial processes, with major impacts on
76 the dynamics of the overlying ice sheet [Bell et al., 1998; Gooch et al., 2016; Kulesa et al., 2019; Li et al.,
77 2022; Person et al., 2012; Siegert et al., 2018; Studinger et al., 2001; Tankersley et al., 2022; Zhang et al.,
78 2018].

79 The discovery of sedimentary basins in Antarctica has been a continuing theme since the earliest Antarctic
80 expeditions [Anderson, 1965]. The earliest expeditions captured both the existence of extensive sedimentary
81 rocks in outcrop [Ferrar, 1907; Mawson, 1940] and speculated on the presence of major sedimentary basins
82 in the marine regions, especially the Ross, Weddell and Scotia Seas [Mawson, 1928]. A more comprehensive
83 record emerged in the second half of the 20th Century, in particular the period following the 1957/8
84 International Geophysical Year (IGY) [Naylor et al., 2008], when geophysical mapping of subglacial geology
85 became a consistent feature of Antarctic exploration [Bailey et al., 1964; Bentley et al., 1960; Evans and
86 Robin, 1966]. Key techniques such as radio echo sounding (RES), since the 1960s [Bingham and Siegert,
87 2007a; Schroeder et al., 2020; Turchetti et al., 2008], active and passive seismic, since the 1950s and 1990s
88 respectively [Anandakrishnan et al., 2000; Bentley et al., 1960; Lawrence et al., 2006; Robin, 1958] and
89 airborne magnetic and gravity surveys, since the 1960s and 1990s respectively [Behrendt et al., 1966; Bell et
90 al., 1999b] were developed and adapted to Antarctic requirements. This led to the first continent-scale
91 compilations, including for ice thickness and bed elevation BedMap [Lythe and Vaughan, 2001], for magnetic
92 data ADMAP [Golynsky et al., 2001; Golynsky et al., 2006] and for gravity ADGRAV [Bell et al., 1999a].

93 The 21st Century has seen continued development and refinement of these approaches, and of course the
94 broadening of coverage over the continent, and the last decade has seen the development of much more
95 detailed and comprehensive compilations [Frémand et al., 2022b; Fretwell et al., 2013; Golynsky et al., 2018;
96 Scheinert et al., 2016]. New techniques for compilation have emerged including the integration of satellite
97 gravity and magnetic data [Ebbing et al., 2018; Ebbing et al., 2021; Scheinert et al., 2016], the inclusion of
98 mass-conservation techniques [Morlighem et al., 2020] and geostatistical approaches [Mackie et al., 2021].



99



100

101 *Figure 1: a) Map of data coverage in Antarctica indicating outcropping regions, drill core sites, passive*
 102 *seismic and MT stations, active seismic reflection lines offshore and limited onshore data. Bedmap3 data*
 103 *coverage mostly is derived from airborne RES data [Frémand et al., 2022b], but not all surveys measured*
 104 *gravity or magnetic data. b) Approaches to detection and characterization of sedimentary basins, including*
 105 *direct characterization of rocks, and indirect characterization from geophysical data. MT – magnetotelluric,*

106 *RES – Radio Echo Sounding, UAV - Unmanned Aerial Vehicle, AUV – Autonomous Underwater Vehicle.*
107 *Modified from Kennicutt et al. [2019]*

108 These advances in the coverage and quality of key geophysical datasets, coupled with the development of
109 new data processing and analysis techniques, mean it is now feasible to map with some confidence the
110 sedimentary basins of the Antarctic continent [Li et al., 2022]. In this review, we explore the state of the art
111 with respect to defining the subglacial sedimentary basins of Antarctica, and we summarize the extent and
112 nature of these across the continent. The evolving tectonic setting of basin formation since Pangea is
113 discussed. We explore the interactions of sedimentary basins with glacial processes and consider possible
114 implications for ice sheet dynamics. Finally, we look ahead to the next set of challenges in defining the
115 extent, characteristics and importance of sedimentary basins in Antarctica.

116 2 Defining Subglacial Sedimentary Basins

117 2.1 What is a sedimentary basin?

118 A sedimentary basin is defined by the development of accommodation-space into which sediments have
119 been deposited. This definition needs several concepts to align: First, the development of a topographic
120 depression or shallow-sloped platform is required; second, there must be a source of sediment derived from
121 mechanical erosion, or from chemical or biological processes; third the deposition and accumulation of
122 sediments must occur and fourth, these must be preserved to the present day. The most common situation
123 on continents is that sediments eroded from highlands are deposited and preserved in a topographic
124 depression, forming a sedimentary basin [Allen et al., 2015].

125 Sedimentary and metasedimentary rocks are commonly interpreted to represent their sedimentary basin,
126 potentially defining such properties as extent and thickness of fill and the depositional environment. Later
127 uplift, erosion, deformation, intrusion by magmatic rocks, or other events may make definition of the
128 original depositional basin hard to achieve. Furthermore, in metamorphic rocks, physical properties may
129 become dominated by crystal structures rather than fluid-filled pore networks, and this affects both the
130 geophysical expression [Enkin et al., 2020] and the nature of their interaction with glacial processes
131 [Krabbendam and Glasser, 2011]. For these reasons we exclude from this study exposed metasedimentary
132 rocks of greenschist facies or above. Also, we exclude exposures of recent sediment deposits such as
133 moraines except where these form part of a basin sequence, as the extents of these cannot be reliably
134 defined at a large scale.

135 For this paper we define two major classes of sedimentary basin. We define a type 1 basin to exist where a
136 substantial amount of basin-fill, including sediments and sedimentary rocks, is preserved in the original
137 depositional basin, with no evidence for substantial uplift, major deformation or metamorphism. A certain
138 degree of compaction, diagenesis and deformation are expected in all basins. In contrast, we define type 2

139 basins to exist where exposures or other evidence indicate the presence of sedimentary rocks but not
140 preserved in their original depositional basin.

141 2.2 Recent progress in characterization of subglacial sedimentary basins

142 Globally, the analysis of sedimentary basins is commonly achieved through extensive use of outcrops, where
143 available, supported by drill core and high resolution active seismic reflection studies allowing detailed basin
144 characterization. In Antarctica these key data are available only in selected areas (Fig 1), and in the general
145 case, the major challenge is to define and characterize basins in the subglacial environment, for which
146 specialized techniques are needed.

147 2.2.1 Direct geological characterization

148 Direct access to rocks through outcrop, detrital samples or drill core is fundamental to sedimentary basin
149 analysis, permitting a full assessment of sedimentary characteristics and enabling application of detrital
150 geochronology, thermochronology and other key analysis techniques. In marine and some sub-ice shelf
151 settings of Antarctica (Fig 1), drilling programs with linked seismic surveys have revealed many key features
152 of sedimentary basins on the continental shelf, in particular in the Ross Sea, Prydz Bay and Amundsen Sea
153 [Gohl *et al.*, 2017; Marschalek *et al.*, 2021; McKay *et al.*, 2016; Whitehead *et al.*, 2006]. Ice shelf and sea-ice
154 cover is a major limitation for offshore studies, leading to a substantial data gap on the inner continental
155 shelf. Developing offshore exploration technologies including Autonomous Underwater Vehicles [Batchelor
156 *et al.*, 2020; Davies *et al.*, 2017; Dowdeswell *et al.*, 2008], seafloor drilling [Gohl *et al.*, 2017] and sub-ice shelf
157 drilling [Gong *et al.*, 2019] are enabling these data gaps to be filled.

158 For onshore regions, Antarctica possesses high-quality sedimentary rock outcrops in numerous areas, and
159 these can provide the core-knowledge for basin studies in those regions. The collation of Antarctic geological
160 data has progressed, with continent-scale compilations of key data [Cox *et al.*, 2019; Sanchez *et al.*, 2021].
161 While much knowledge has been gained by these approaches, a severe limitation is the tendency for
162 outcrop to occur only on major highlands, isolated nunataks and coastal islands, leaving unsampled the low-
163 lying regions that contain the bulk of sedimentary rocks. This leads to some undesirable bias towards older
164 and/or uplifted sedimentary rocks and, therefore, the utility of outcrop-based data to infer subglacial
165 geology is limited. Outcrop data is also focused in spaced clusters (Fig 1), often with a high degree of internal
166 complexity, meaning that interpolation between these clusters carries high uncertainty.

167 Detrital samples from much younger sediments can mitigate exposure bias [Maritati *et al.*, 2019; Mulder *et*
168 *al.*, 2019; Thomson *et al.*, 2013], but the lack of a precisely known source location for these samples renders
169 their use to characterize inland basins highly uncertain. Plainly, for a more representative sampling of the
170 Antarctic bedrock, drilling is necessary. As with offshore drilling, onshore sub-ice drilling techniques are
171 developing [Gong *et al.*, 2019; Goodge *et al.*, 2021; Hodgson *et al.*, 2016; Kuhl *et al.*, 2021; Talalay *et al.*,

172 2021] and have seen operation in several locations (Fig 1), with an intent to expand towards more
173 systematic coverage in the future. Notably, the alignment of these records with major ice-coring initiatives
174 has strong potential to inform glacial evolution on multiple timescales.

175 2.2.2 Indirect characterization

176 Despite the benefits of these direct methods, a systematic coverage of Antarctica requires indirect
177 characterization from geophysical data to survey the regions where no direct information exists. The major
178 techniques include ground and/or ship-based techniques including active and passive seismic methods and
179 magnetotellurics, as well as airborne techniques including gravity and magnetic methods and radio-echo
180 sounding (RES).

181 2.2.2.1 Radio-echo sounding

182 RES is an efficient geophysical method to characterize the morphology and nature of the ice sheet bed. In
183 the context of basin studies, RES data can define both the large-scale morphology of topographic
184 depressions, but also the detailed character of the bed, as defined by along-track roughness. While radar
185 data can give a robust characterization of the bed at fine resolutions, hundreds of meters or less, the
186 technique cannot directly indicate a sedimentary origin, nor is it able to define the thickness or properties of
187 the sedimentary cover.

188 RES systems have been used for more than five decades to determine the thickness of ice sheets in an
189 effective way [Schroeder *et al.*, 2020]. Over that period, more than 1.5 million line-kilometers of RES data
190 have been collected with airborne surveys predominating in recent times [Frémand *et al.*, 2022b; Morlighem
191 *et al.*, 2020]. By subtracting the radar-defined ice thickness from surface elevation data, bed topography can
192 be determined. Surface elevation may be obtained from the RES data itself, from other sensors (e.g. LIDAR)
193 on the same platform, or from remote sensing products (e.g. DEMs from satellite studies). The final product
194 is bed elevation profiles of the ice-bed interface that are interpolated to produce gridded bed topography
195 products. Interpolation may be done in numerous ways, including direct spline-based interpolation [Fretwell
196 *et al.*, 2013] or geostatistical interpolation [MacKie *et al.*, 2021]; with the inclusion of ice sheet flow data,
197 mass-conservation approaches may be used also [Morlighem *et al.*, 2020].

198 For the nadir-facing acquisition geometry of RES, specular and quasi-specular returns from the surface and
199 bed are typically the most prominent features in a radar trace [Haynes *et al.*, 2018], which allows for
200 straightforward interpretation of along profile ice thickness and bed topography. Although the earliest
201 systems were incoherent [Schroeder *et al.*, 2019] the development of coherent systems [Gogineni *et al.*,
202 1998] and synthetic aperture radar processing with range migration [Heliere *et al.*, 2007; Peters *et al.*, 2007]
203 improved the azimuth resolution of radargrams and the resulting extracted thickness profiles as well as
204 improving clutter mitigation in regions of high topographic relief and layover. More recently, swath

205 [Holschuh *et al.*, 2020], tomographic [Paden *et al.*, 2010], and array-based [Young *et al.*, 2018] systems as
206 well as the availability of ultra-wideband systems [Arnold *et al.*, 2020; Hale *et al.*, 2016] have further
207 improved the geometric resolution of RES observations, with range resolution in the tens of centimeters and
208 along-track resolution in the tens of meters [Kjær *et al.*, 2018].

209 The roughness of the bed encodes information on the morphologic and geologic character of the subglacial
210 interface [Jordan *et al.*, 2010a; Rippin *et al.*, 2014; Siegert *et al.*, 2005]. This roughness can be estimated
211 directly from thickness profiles [Bingham and Siegert, 2007b] and – with assumptions on the fractal
212 character of the bed – extrapolated to finer scales [Jordan *et al.*, 2017b]. Where perpendicular crossovers
213 are available, the anisotropy of this bed roughness can also be estimated [Cooper *et al.*, 2019; Eisen *et al.*,
214 2020]. In addition to its resolvable along-profile signature, finer-scale (i.e. wavelength-scale) roughness is
215 also encoded in the bed echo character including its abruptness [Jordan *et al.*, 2017b], specularity [Schroeder
216 *et al.*, 2015; Young *et al.*, 2016], and amplitude distribution [Grima *et al.*, 2019]. Notably, these fine-scale
217 relative metrics are insensitive to (even large) absolute errors in ice thickness (e.g. from firn correction or
218 surface registration). Finally, the radiometric signature of bed echoes can also encode information on bed
219 materials [Christianson *et al.*, 2016; Tulaczyk and Foley, 2020] and thermal state [Chu *et al.*, 2018]. These
220 signatures are often difficult to unambiguously interpret at the glacier to ice sheet scale [Matsuoka, 2011],
221 without multi-frequency [Broome and Schroeder, 2022] or multi-static observations [Bienert *et al.*, 2022] or
222 polarimetric [Corr *et al.*, 2007; Dall *et al.*, 2010; Frémand *et al.*, 2022a; Scanlan *et al.*, 2022] observations.
223 These approaches can characterize and constrain the wavelength-scale roughness (tens of centimeters or
224 smaller) and sub-Fresnel-zone geometry [Haynes *et al.*, 2018; Jordan *et al.*, 2017b] (meters to tens of
225 meters) of the bed, orders of magnitude finer-scale constraints than along-profile approaches [Bingham and
226 Siegert, 2009].

227 2.2.2.2 Gravity and magnetic data

228 These passive techniques measure the intensity and in some cases the direction of the Earth’s naturally
229 occurring gravity and magnetic fields. Magnetic and gravity data do not require large power-sources, nor a
230 coupling to the Earth’s surface, and airborne surveys have been widely deployed across Antarctica, most
231 commonly in combination with RES surveys from the same platform (Fig 1).

232 Gravity data are sensitive to the summed effects of mantle and crustal masses, including sedimentary rocks.
233 Due to their porosity, sedimentary rocks typically have lower density than the crystalline basement, causing
234 relative gravity lows over sedimentary basins [Aitken *et al.*, 2016a; Bell *et al.*, 1998; Frederick *et al.*, 2016].
235 Airborne gravity data collections systems include several major types of gravity meter, the conventional
236 stabilized-platform air-sea gravimeter [Bell *et al.*, 1999b] and derivations of this technology [Studiver *et al.*,
237 2008]. More recently, so-called “strapdown” systems have been used, which are based on inertial navigation
238 sensors including triads of high specification accelerometers and gyroscopes rigidly attached to the aircraft

239 [Jordan and Becker, 2018]. In either approach the observed accelerations are dominated by aircraft
240 accelerations, and a well constrained gravity solution is dependent on an accurate recording of the aircraft
241 location and elevation and careful removal from the recorded signal of aircraft accelerations and motion as
242 well as temporal gravity variations such as tides. Accurate navigational systems such as differential GNSS are
243 therefore essential to achieve the best quality data.

244 Older spring-based meters were restricted to straight and level flight, constraining operational logistics, and
245 limiting the ability to collect other data types at the same time. This sensitivity to aircraft dynamics meant
246 accuracies of 3-5 mGal were typical [Jordan et al., 2010b]. In recent times advances in sensor technology and
247 processing methods have allowed collection of gravity data during more dynamic draped flights and an
248 overall improvement in data quality, with accuracies of 1-2 mGal now typical [Jordan and Becker, 2018;
249 Studinger et al., 2008]. Despite these improvements, gravity data processing imposes a low pass filter on the
250 data, typically 70 seconds or more, that leads to spatial resolution in the order of 5-10 km, depending on
251 aircraft velocity. This may be between 60 and 140 m/s for the fixed-wing platforms used in Antarctica. A
252 recent innovation is the adoption of helicopter-borne operations, which promises further improvement in
253 spatial resolution [Jensen and Forsberg, 2018; Wei et al., 2020]. Future application of strapdown gravity on
254 slower-flying Unmanned Aerial Vehicle (UAV) platforms also holds the promise of higher resolution and
255 potentially lower cost gravity surveys. An additional limit on the wavelengths resolved by gravity surveys is
256 the ice sheet thickness, which means observations are often made several kilometers from the bed
257 interface, limiting the minimum resolvable wavelength. These factors limit the capacity for detection of
258 abrupt spatial changes in gravity, such as may be associated with glacial landforms and fault-bounded
259 sedimentary basins. Despite these residual limitations, the improved accuracy of gravity sensor technology
260 allows modern airborne gravity data to be applied with confidence at scales of 5 kilometers and above.

261 The observed gravity field is a summation of several components including topography and crustal thickness,
262 as well as sedimentary mass deficits, therefore, to understand sedimentary basins these other factors must
263 be accounted for. Ice, ocean and bed topography is corrected for using the Bouguer correction or an
264 equivalent, which models and subtracts the effect of known topography and bathymetry, assuming
265 reference densities for rock, ice and water [Hirt et al., 2016; Scheinert et al., 2016]. In Antarctica, the thick
266 ice sheet load in the continental interior also generates a Moho down warp causing distinct negative
267 Bouguer anomalies that do not reflect crustal geology, and it is desirable to correct for this. Because
268 topographic loads may be balanced by the Moho or other masses in the deep crust or uppermost mantle, for
269 the isostatic residual anomaly, the condition is imposed that surface loads are balanced by variable crustal
270 thickness, either locally in the Airy case, or via an elastic or visco-elastic flexure [Paxman et al., 2017]. Airy
271 isostasy models are easy to apply and provide a consistent convention for interpretation, but are prone to
272 overcorrection, whereas carefully applied flexural models may provide superior removal of isostatic effects

273 [Jordan *et al.*, 2013a; Paxman *et al.*, 2017]. Negative isostatic-residual gravity anomalies often indicate
274 sedimentary basins, although low-density basement rocks, such as granitic intrusions, can also give rise to
275 negative anomalies, requiring differentiation with other data [Jordan *et al.*, 2010b].

276 Despite the intricacies of processing and interpretation, sedimentary basin structure can potentially be
277 defined from gravity data for wavelengths >10 km, and for sedimentary rock thicknesses greater than ~500
278 m, although larger and thicker basins are resolved with more confidence. Gravity-derived thicknesses are
279 ambiguous, varying linearly with density contrast, and an inability to separate clearly the basin source from
280 other possible sources is a limiting factor to be overcome during interpretation.

281 For magnetic data, oxidation of magnetite to hematite during weathering means that sedimentary rocks in
282 general have low magnetization relative to crystalline basement [Enkin *et al.*, 2020]. While low-
283 magnetization rocks do not generate a magnetic anomaly, their presence increases the distance between a
284 basement source and the aircraft sensor — this distance also includes the thickness of water and ice and the
285 height of the aircraft above the surface. Increased source-sensor separation causes anomalies to have
286 reduced amplitude and increased wavelength and sedimentary basins are thus characterized by reduced
287 magnetic anomaly gradients [Reid, 1980; Reid *et al.*, 1990]. Analysis of the anomaly gradients using depth to
288 magnetic source estimation techniques is often applied to define sedimentary basin thickness and
289 distribution [Aitken *et al.*, 2014; Ferraccioli *et al.*, 2009a; Tankersley *et al.*, 2022].

290 Airborne magnetic data are collected from magnetometers that, most commonly, are attached to aircraft by
291 a tail-boom, at wingtips, or in some cases towed. Fixed-wing surveys dominate [Aitken *et al.*, 2020; Jordan
292 and Becker, 2018; Tinto *et al.*, 2019] modern data collection but helicopter surveys are also used in specific
293 settings [Damaske *et al.*, 2003; Ferraccioli and Bozzo, 2003; Ferraccioli *et al.*, 2009b; Gohl *et al.*, 2013a;
294 Wilson *et al.*, 2007]. In contrast to gravity surveys, instrument precision is not a major source of error, and
295 improvements in practice have focused on managing the highly unusual magnetic environment of
296 Antarctica, being close to the magnetic pole, and so especially vulnerable to space weather and intense
297 diurnal variations. In addition, the need for longer-range surveys and multi-year campaigns demands
298 additional care in data processing. The most recent approaches consider more fully the complexities of the
299 four-dimensional magnetic field [e.g. Aitken *et al.*, 2020], however the Antarctic geomagnetic environment
300 and logistical constraints remain substantial limitations on dataset accuracy relative to aeromagnetic data on
301 other continents.

302 A limitation of both gravity and magnetic approaches is the inability for airborne surveys to accurately
303 recover field components at wavelengths longer than the scale of the survey [Scheinert *et al.*, 2016]. For this,
304 the expansion of satellite-based gravity, gravity gradiometry and magnetic data, including the GRACE, GOCE
305 and SWARM missions has provided a crucial new understanding of the long-wavelength structure of the

306 continent [Ebbing et al., 2018; Ebbing et al., 2021; Pappa et al., 2019a; Pappa et al., 2019b], these also
307 underpinning more accurate compilations [Ebbing et al., 2021; Golynsky et al., 2018; Hirt et al., 2016]. The
308 GOCE mission in particular has allowed new understandings of crustal structure, including efforts to define
309 sedimentary basins [Capponi et al., 2022; Haeger and Kaban, 2019].

310 Overall, the ability to define sedimentary basins through gravity and magnetic approaches has improved
311 substantially in recent years, with particularly more accurate gravity recovery at shorter wavelengths, and
312 the incorporation of satellite magnetic and gravity data at longer wavelengths. These improvements mean
313 that, where airborne data exist, the identification of subglacial sedimentary basins is possible for basins with
314 thicknesses greater than ~500m and with spatial resolutions of 10 kilometers or possibly less. These data are
315 associated with physical non-uniqueness and, given other unknowns they do not unambiguously define the
316 geometry or physical properties of the basin fill. Unless these are otherwise constrained, these uncertainties
317 limit their use for a quantitative 3D understanding of basin morphology.

318 2.2.2.3 Active and Passive Seismic

319 Seismic techniques record elastic waves in the ground, either from natural or non-specific anthropogenic
320 origins (e.g. earthquakes, ambient noise) or artificial sources of a controlled anthropogenic nature (e.g.
321 explosives, airguns, vibrators). Use of the former (passive seismic) typically involves continuous observations
322 from three-component seismometer arrays, while the latter (active seismic) typically uses shorter-term,
323 triggered observations with (usually single component) geophones, although hybrid approaches are also
324 used. Seismometers or geophones must be deployed in or on the ground for on-ice surveys, or in the water
325 for marine surveys. Of these methods active seismic approaches provide the more comprehensive image of
326 basin architecture.

327 Despite this, the application of active seismic techniques in Antarctica has several drawbacks. Active source
328 marine surveys can cover hundreds of kilometers per day in open water, although around Antarctica, the
329 presence of icebergs may disrupt surveying. By contrast, on-ice surveys that use explosive sources and
330 individual geophones as receivers can cover a few km per day in Antarctic conditions [Anandakrishnan et al.,
331 1998; Johnston et al., 2008; Peters et al., 2006]. The use of the vibroseis method over snow with a towed
332 streamer allows the collection of tens of kilometers per day. By this approach it has become possible to
333 obtain larger-scale surveys with several hundred kilometers per field season [Eisen et al., 2015; Smith et al.,
334 2020]. Nevertheless, on-ice active seismic data are currently limited in spatial extent (Fig 1).

335 Unlike radio waves used in RES, seismic waves can penetrate subglacial environments such as water,
336 sedimentary strata, and the basement beneath, providing crucial information necessary to understand
337 glacial dynamics. In addition, due to the simpler timing requirements (relative to RES) sources and receivers
338 can be separated, allowing for bi-static or multi-static configurations that can exploit angle-dependent

339 information from reflections. Several seismic approaches have been employed to detect and define
340 sedimentary basins in Antarctica. The tomographic approach determines the bulk velocity and thickness of a
341 geologic unit underneath the ice. As the seismic wave speed in sedimentary basins is significantly lower than
342 in crystalline basement, the thickness and properties of such a unit can be estimated, especially with long-
343 baseline (wide-angle) reflection and refracted wave seismic surveys [*Blankenship et al., 1986; Leitchenkov et*
344 *al., 2016; Trey et al., 1999*].

345 Seismic waves will reflect and refract at unit horizons where the acoustic impedance (defined as the product
346 of seismic velocity and density) changes. The seismic wave speed and density of sedimentary basin fill is
347 usually lower than that of crystalline basement, resulting in a generally lower acoustic impedance for
348 sedimentary basins. Furthermore, as the acoustic impedance of ice is well known, the reflection from the
349 subglacial interface can be used to determine the properties of that layer. Acoustic impedance
350 measurements along profiles can be used to discriminate between regions of hard bedrock from sediments
351 or water at the bed. Of particular significance is the ability to discriminate different structures associated
352 with tills and tillites that have a direct link to subglacial processes at the bed [*Anandkrishnan et al., 1998;*
353 *Horgan et al., 2021; Muto et al., 2016; Muto et al., 2019b; Peters et al., 2006; Smith et al., 2013*].

354 Reflection seismic methods can be used to map the stratigraphy of the geological units underlying the ice
355 sheet and ice shelf. The active seismic technique is especially important for resolving sub-ice shelf
356 bathymetry and basins [*Rosier et al., 2018; Smith et al., 2020*], as unlike radio waves the seismic waves can
357 penetrate into strata beneath electrically conductive seawater. These data can be used to constrain gravity-
358 based approaches [*Eisermann et al., 2020; Muto et al., 2016*]. The identification of a geologic stratigraphy
359 indicates that a subglacial unit is of probable sedimentary origin, and the details of its structure can be
360 interpreted to understand the depositional environment, and age relationships with faults and volcanic
361 edifices [e.g. *Horgan et al., 2005; Johnston et al., 2008; Kristoffersen et al., 2014*].

362 As reflection seismic surveys have high spatial resolution, they provide a very good estimate of the ice
363 thickness and thus bed topography. In comparison to RES methods, ice-internal structure is not well
364 resolved, but seismic techniques are better able to characterize subglacial properties. Seismic profiles can be
365 analyzed in the same way as RES profiles for bed roughness, however, as they very often record over a larger
366 offset (source-to-receiver distance) spread than RES methods, they are less prone to the influence of side
367 reflections and smoothing given that adequate processing is applied in the form of migration.

368 Our ability to detect and discriminate sedimentary basins in seismic data is improving. Because seismic data
369 quality increases with the square root of the number of observations, data acquisition speed is key. Over the
370 last decade, progress in borehole drilling techniques (e.g. the rapid air movement drill system [*Gibson et al.,*
371 *2020*]), geophone design and deployment (e.g. Georods [*Voigt et al., 2013*]), and a combination of highly

372 efficient source-receiver systems (e.g. vibroseis-snowstream combination [Eisen et al., 2015]) all contributed
373 to increasing the seismic data coverage and thus our ability to detect sub-ice properties. Nevertheless, as
374 active seismic surveys are logistically still demanding, studies have been either only locally constrained or
375 require considerable resources to cover regional distances.

376 Passive seismic methods for detecting and studying sedimentary basins can estimate the seismic velocity
377 structure of the upper few kilometers of the crust using seismograph arrays deployed for periods of time
378 ranging from months to years. These techniques use naturally occurring seismicity within the ice sheet or
379 from earthquakes around the world, as well as seismic 'noise' from ambient sources such as ocean waves.
380 These surveys are relatively simpler than active source surveys as they don't require the source technology
381 (drills and explosive or a vibroseis truck). Passive seismic techniques can map sedimentary basin thickness on
382 a regional scale with a few seismic stations. Thus, passive techniques offer coverage of remote parts of
383 Antarctica, but at lower resolution than is possible for active seismic methods. One common method to
384 estimate the thickness of sedimentary basins is the so-called receiver function method. The P-wave (or S-
385 wave) from a remote earthquake and converted phases at basin boundaries can be used to estimate basin
386 properties with high sensitivity to acoustic impedance contrasts at structural interfaces located beneath the
387 recording station. Another method is to use the background, so-called ambient noise recorded at two
388 stations to estimate an equivalent to a seismic wave between those two stations. Ambient noise studies can
389 resolve broader lateral changes in seismic velocity structure. Joint application of these methods has become
390 common, providing the ability to resolve sedimentary basins.

391 Receiver function analysis provides images of structural interfaces below a seismic station using processing
392 that enhances seismic waves converted from S to P or P to S at structural interfaces [Ammon, 1991]. The
393 depth to the sediment-bedrock interface and thus the sediment thickness is determined from the time delay
394 of the converted phase, after adjusting for ice thickness [Anandakrishnan and Winberry, 2004; Chaput et al.,
395 2014]. The use of higher frequencies compared to typical receiver function analysis (4 Hz vs < 1 Hz) allows
396 detection of sediment thicknesses of a few hundred meters and also can provide some approximate
397 constraints on the velocity of the sediment layer [Dunham et al., 2020]. While low-velocity relative to
398 igneous or metamorphic basement, consolidated sedimentary rocks may not provide sufficient density and
399 velocity contrast to be discernible in receiver functions.

400 Ambient noise analysis uses short-period seismic surface waves obtained from the ambient noise field
401 derived from non-specific sources, in particular ocean waves. By correlating records from two seismic
402 stations, the shallow structure beneath the ice sheet along the interstation path can be constrained [Pyle et
403 al., 2010; Shen et al., 2018]. The correlation yields the Green's Function for wave propagation between the
404 stations, from which the phase and group velocity and ultimately the shear-wave velocity structure is
405 obtained. If the distribution of seismic stations is dense enough, sediment and sedimentary rock thicknesses

406 can be mapped throughout the region from phase and group velocity tomography maps, so results are not
407 restricted to the locations of seismographs. The use of both Rayleigh and Love waves provides better results,
408 since Love waves have superior resolution at shallow depths [Zhou *et al.*, 2022]. Constraints on shallow
409 structure from ambient noise Rayleigh waves can be improved by also measuring the ratio of horizontal to
410 vertical displacement [Lin *et al.*, 2012; Pourpoint *et al.*, 2019]. Joint inversion of several of these datasets
411 using a Bayesian formalism, including receiver functions, surface wave group and phase velocities, and
412 horizontal to vertical ratios, can improve resolution of sedimentary material beneath the ice sheet [Dunham
413 *et al.*, 2020; Pourpoint *et al.*, 2019].

414 Sedimentary basin thicknesses have been estimated using passive seismic techniques throughout West and
415 Central Antarctica. Pourpoint *et al.* [2019] found thicknesses ranging from 0.1 to 1.5 km beneath seismic
416 stations near the Thwaites Glacier drainage area, with the thickest sediment in the deep topography of the
417 Byrd Basin and Thwaites Glacier bed. Dunham *et al.* [2020] found sediment thicknesses ranging from 0.1 to
418 0.9 km beneath seismographs in the West Antarctic Rift System (WARS) and Ellsworth Mountains region.
419 Zhou *et al.* [2022] mapped sedimentary basin thicknesses throughout West and Central Antarctica with
420 ambient noise surface wave methods. They found 4-5 km thick basins beneath the Ross Ice Shelf but in other
421 regions of the study area maximum thicknesses were at most about 1.5 km, except in small regions where
422 spatial resolution is lacking. They interpreted the lack of thick sedimentary basins, as found for intracratonic
423 basins in other continents, as indicating that basins in this region of Antarctica may have been sediment
424 starved throughout most of their post-Gondwana geological history, although erosion may also have been
425 significant.

426 2.2.2.4 *Electromagnetic and magnetotelluric*

427 Electromagnetic techniques also include active and passive techniques. Due to their limited depth
428 penetration, airborne approaches are not widely applicable to subglacial geology, although can be applied in
429 ice-free regions [Foley *et al.*, 2015]. Ground based electric and electromagnetic techniques saw limited use in
430 the past, however the most broadly applied approach in recent times is passive magnetotellurics [Hill, 2020].
431 The magnetotelluric technique provides the capacity to image deep within the Earth and is generally
432 applicable to detect and to image sedimentary basins through their electrical properties, which are
433 commonly related to water content, salinity and temperature. Assuming that subglacial sediments and
434 sedimentary rocks are water-saturated, the key expected controls on bulk resistivity values are the
435 connected porosity of the pore space and the salinity of the waters within them, defined empirically [see
436 Glover, 2016].

437 Although a relatively old technique, the magnetotelluric method has been increasingly applied due in large
438 part to improved ability to generate robust model solutions with high performance computing and improved
439 sensor technologies. Magnetotelluric applications to crustal and upper mantle imaging in the polar regions

440 are reviewed in Hill [2020]. Building on most recent relevant work [Gustafson et al., 2022; Key and Siegfried,
441 2017; Kulesa et al., 2019; Siegert et al., 2018] we focus here on examining the potential scope and
442 limitations of magnetotelluric imaging of the hydrogeological and thermal properties of subglacial
443 sedimentary basins.

444 The source fields of the magnetotelluric technique are inherently wideband, ranging from $\sim 10^{-5}$ Hz to 10^4 Hz,
445 generated when electrical storms and interactions between the solar wind and the ionosphere produce
446 fluctuations in Earth's magnetic field. These fluctuations then induce correspondingly wideband telluric
447 currents in ice sheets and the underlying crust and mantle. Signal period is a proxy for depth, with longer-
448 period signals representing structure deeper in the Earth. Under favorable circumstances and depending on
449 the bandwidth and collection procedure of the survey, temporally coincident measurements of magnetic
450 and electric potential fields allow the bulk electrical resistivity distributions to be estimated from the near
451 surface at the highest frequencies, to depths of ~ 400 km at the lowest frequencies. Data collection is
452 typically focused in the high frequencies for near-surface studies (AMT 10^0 Hz to 10^4 Hz), across a central
453 broad band (BBMT 10^{-3} Hz to 10^2 Hz) for general crust and mantle studies, and long-period MT (LPMT 10^{-1} Hz
454 to 10^{-4} Hz) for mantle-focused studies. For the investigation of subglacial sedimentary basins beneath the
455 Antarctic Ice Sheet the higher-frequency band of the magnetotelluric spectrum is of most interest. On the
456 one hand this is attractive in that high-quality magnetotelluric data can be acquired with day-long station
457 occupations if wind speeds are low ($\ll 10$ m s^{-1}), as compared with station occupations of a week or more
458 required for upper mantle studies.

459 Many challenges arise in ice sheet settings related to potential violations of fundamental source field
460 assumptions owing to the proximity to the geomagnetic south pole, high contact resistances of electrodes
461 buried in firn, and spin drift of charged snow particles generating strong broadband electrical noise [see Hill,
462 2020]. The last is a particular challenge in the imaging of subglacial sediment basins because the broadband
463 frequencies exploited in doing so are particularly susceptible to noise contamination by drifting snow. A
464 second specific challenge arises when firn is absent and ice is exposed at the surface instead, forming a
465 major barrier to the deployment of electrodes and magnetometers and associated wiring. This could be a
466 problem especially in coastal regions where seasonal melting and refreezing is widespread.

467 Notwithstanding these challenges, a growing number of Antarctic measurement campaigns have
468 demonstrated that high-quality magnetotelluric data can be acquired with careful survey planning and using
469 bespoke electrode pre-amplifiers [Hill, 2020]. Subglacial sediment basins are particularly well suited for
470 magnetotelluric exploration because they are expected to be several orders of magnitude less resistive
471 (order of $10^{-1} - 10^1$ Ω m) than both the underlying crystalline crust (typically $> 10^2$ Ω m) and the overlying ice.
472 Cold Antarctic ice has typical bulk resistivities of $\sim 10^4 - 10^6$ Ω m but these can exceed 10^8 Ω m for temperate
473 clean-ice glaciers [Kulesa, 2007].

474 Magnetotelluric imaging of subglacial sedimentary basins remains poorly documented, however, with only a
475 few studies in Antarctica. Although not yet widely applied, magnetotelluric surveying can reveal high-quality
476 images of subglacial sediment basins and has unique potential for detecting and defining liquid groundwater
477 within them [Gustafson *et al.*, 2022]. The use of seismic data to constrain magnetotelluric inversions has not
478 yet been attempted with cutting edge joint inversion schemes but will very likely result in even higher-
479 quality images in the future [Key and Siegfried, 2017; Kulesa *et al.*, 2019; Siegert *et al.*, 2018].

480 There are two major complications for interpretation, however, in that Archie's law contains a cementation
481 exponent that has never been calibrated for subglacial sediments; even more significantly, Archie's law is not
482 applicable where sediments have noticeable clay mineral contents requiring a significantly adapted
483 formulation [Kulesa *et al.*, 2006]. This is likely a particular problem for coastal subglacial sedimentary basins
484 where contents of marine clays are not normally negligible.

485 Finally, it is expected that a significant geothermal gradient will exist between the base and top of subglacial
486 sedimentary basins, especially where they have a vertical extent of several kilometers and also are buried
487 beneath several kilometers of cold ice. [Kulesa *et al.*, 2019] demonstrated with a conceptual model that
488 such temperature gradients will likely result in a multi-fold increase in bulk resistivity between the base and
489 top of subglacial sediment basins, largely due to a temperature-controlled decrease in ionic mobility in
490 sediment pore waters. This inference suggests that bulk resistivity models can be used to infer temperature
491 changes in subglacial sedimentary basins and implied geothermal heat flux into the ice sheet base, a key
492 unknown in ice sheet modelling, especially in high-heat flux settings.

493 Overall, magnetotelluric measurements are powerful tools to explore subglacial sedimentary basins, the
494 associated groundwater and geothermal heat fluxes, and their interactions with the ice sheet base. In most
495 Antarctic situations, porosity, pore-fluid salinity, clay mineral contents and temperature changes will
496 combine to control bulk resistivity magnitudes, a complication that may be further compounded for coastal
497 sediment basins. These ambiguities require external constraint to develop a quantitative interpretation of
498 sedimentary properties from bulk resistivities.

499 2.2.3 Integrated Studies

500 As we have seen above, each of the listed methods has the capacity to define the existence of sedimentary
501 basins beneath ice, and in many cases also particular characteristics such as thickness, internal geometry,
502 seismic velocity, density, electrical conductivity. These characteristics each may resolve different aspects of
503 the basin, and furthermore, each technique has different uncertainties and so the methods are
504 complementary. In particular, the inherent ambiguities in most data available can lead to major errors when
505 any single technique is used. For example, outcrops may be selected for erosion resistance through
506 landscape forming processes while low-roughness topography may be caused by glacial erosion [Jamieson *et*

507 *al.*, 2014] and low gravity anomalies and/or smooth magnetic gradients may be caused by low-density or
508 non-magnetic basement rocks.

509 Integrated studies that use multiple datasets are necessary to properly resolve these ambiguities [*Grikurov*
510 *et al.*, 2003]. For airborne geophysical surveys, the combination of RES, gravity and magnetic data has
511 proved powerful, and this is especially enhanced where suitable ground observations are also collected.
512 Major recent, ongoing, and upcoming data collection programs have sought to synergize multidisciplinary
513 data collection and modelling [*MacGregor et al.*, 2021; *Scambos et al.*, 2017]. The co-interpretation of
514 multiple complex and sparse geoscience datasets has a high task-complexity, that may lead to difficulty
515 making reliable judgements [*Swink and Speier*, 1999]. As a human-led process which relies on interpreter
516 skill, the background, knowledge and biases of the investigator can have substantial impacts on results
517 [*Wilson et al.*, 2019]. Although clearly not without uncertainty, multi-data analyses provide the potential to
518 manage subjectivity in interpretation and support the ability to make sound judgements [*Aitken et al.*, 2018].

519 A consistent data-based mapping at continental scale is challenged by highly variable data quality, resolution
520 and availability as well as the challenge of combining multiple datasets into a consistent map that accounts
521 for all data. To define basal boundary conditions, we may seek initially to define the presence or absence of
522 sedimentary cover, which is a prerequisite to understanding its thickness, age, and other properties.

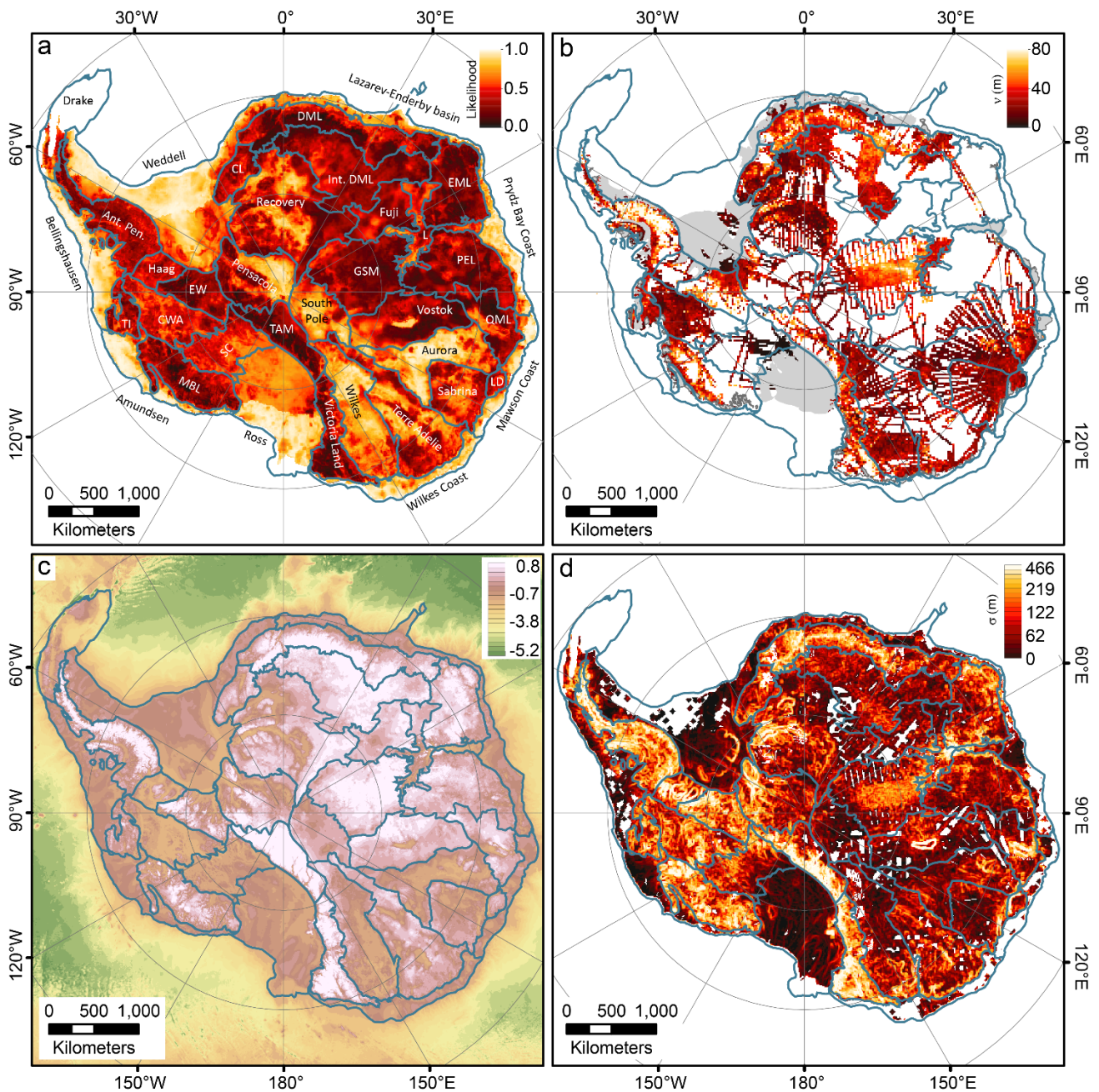
523 Geostatistical and machine learning techniques provide relatively unbiased and data-based approaches to
524 understanding this in a probabilistic sense. *Li et al.* [2022] apply the random forest approach with multiple
525 data types to map for all Antarctica the likelihood of sedimentary basins at the bed. *MacKie et al.* [2021]
526 apply a trained logistic regression model to simulated topographic roughness model to infer geological bed
527 type associated with the presence of sediments. Such techniques are highly valuable with respect to their
528 consistent response to data, provided those data are not too variable in their properties (resolution,
529 accuracy etc), but they are not able always to accommodate irregularly sampled or sparse data, while non-
530 numerical data can also be problematic to include. In this work we use the results of such techniques with a
531 wide range of prior findings and datasets (Fig. 2) to develop a new understanding of sedimentary basins
532 beneath the Antarctic Ice Sheet.

533 3 Antarctica's Sedimentary Basins

534 3.1 Methods & Validation

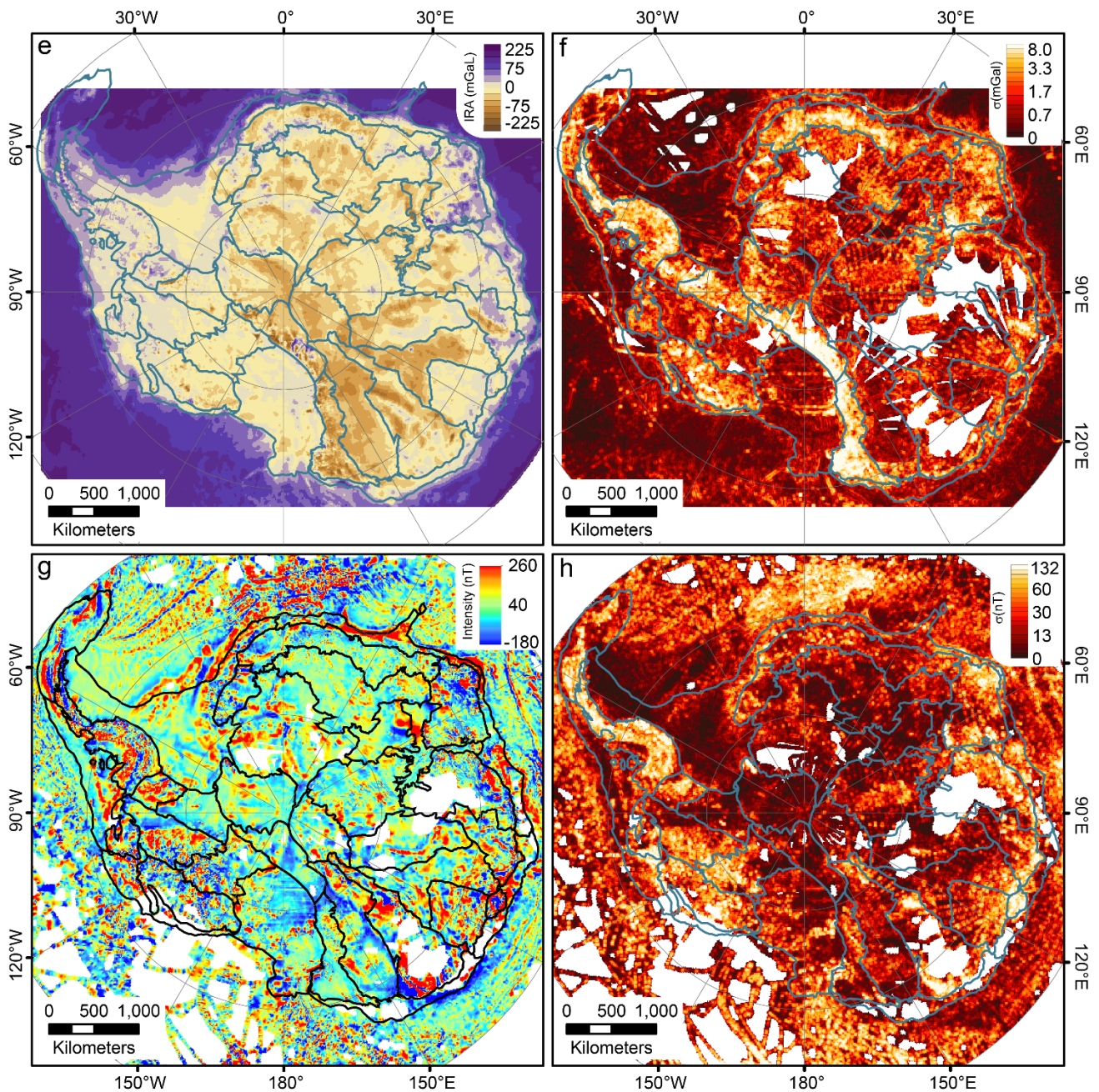
535 The sedimentary basin distribution is mapped continent wide using a flexible basin classification approach
536 applied in a GIS. The map presented here (Figure 3) is manually classified based on a wide range of
537 continent-scale datasets and derivative products. To develop the map, an initial classification into basins and
538 non-basins was automatically derived from the machine learning derived likelihood map of *Li et al.* (2022),
539 using a threshold of 0.5. From this initial point (Fig 2a) the polygons for individual regions were scrutinized

540 and edited considering additional data including outcrop information, along-track roughness (Fig 2b) bed
 541 elevation (Fig 2c) and its spatial variability (Fig 2d), gravity magnitudes (Fig 2e) and their spatial variability
 542 (Fig 2f), aeromagnetic data (Fig 2g) and their spatial variability (Fig 2h) and sedimentary basin thickness
 543 estimates from passive and active seismic datasets. The results and interpretations from many published
 544 studies and maps were also accommodated in the mapping process.



545
 546 *Figure 2: Key models and datasets for defining basin distribution in Antarctica including a) model of*
 547 *sedimentary basin likelihood from machine learning [Li et al., 2022], b) along-track roughness using airborne*
 548 *RES data compiled from Eisen et al. [2020] and other data. Along track roughness v was calculated using a*
 549 *spatial technique as in Eisen et al. [2020], c) a bed elevation model and d) its large-scale spatial variability*

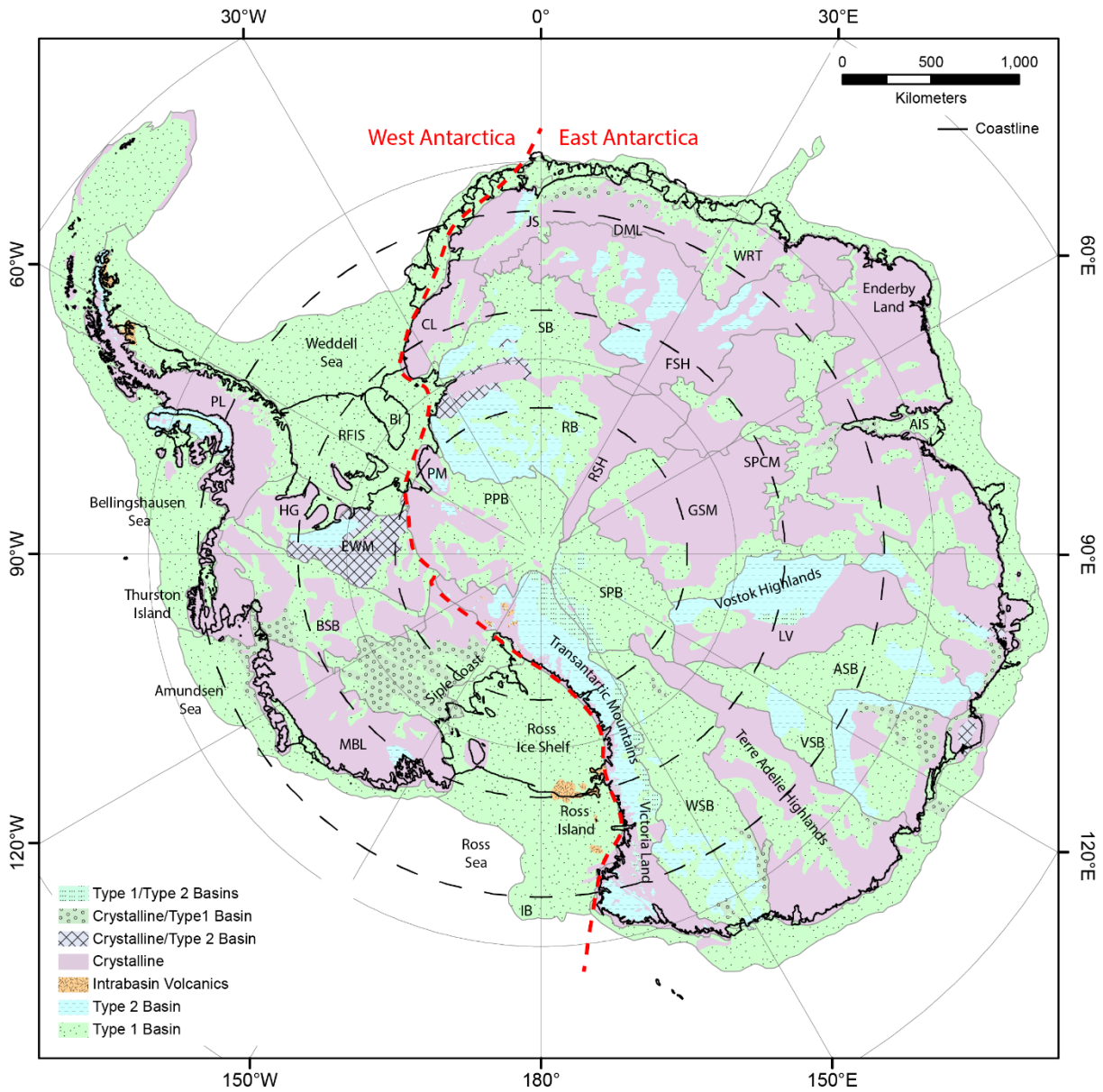
550 defined as standard deviation in a 30 km by 30 km window; both from BedMachine Antarctica [Morlighem,
 551 2020]. Major sedimentary basin regions used for classification are outlined. CWA – Central West Antarctica,
 552 EW – Ellsworth Whitmore, SC – Siple Coast, CL, TAM – Transantarctic Mountains, DML -Dronning Maud Land,
 553 GSM – Gamburtsev Subglacial Mountains, EML- Enderby-Mac Robertson Land, PEL – Princess Elizabeth Land,
 554 QML – Queen Mary Land, LD – Law Dome



555
 556 *Figure 2 (continued): e) Airy isostatic residual gravity anomaly and f) spatial variability (standard deviation,*
 557 *30 km window) of Bouguer gravity anomaly. Gravity data after AntGG [Scheinert et al., 2016] and additional*
 558 *data [Forsberg et al., 2018; Kvas et al., 2021; Olesen et al., 2020; Paxman et al., 2019a; Sandwell et al., 2014;*
 559 *Tinto et al., 2019; Young et al., 2017a] g) magnetic field intensity anomaly and h) its spatial variability.*

560 Magnetic data after ADMAP-2 [after Golynsky et al., 2018] and additional data [Ferraccioli et al., 2020;
 561 Forsberg et al., 2018; Paxman et al., 2019a; Tinto et al., 2019; Young et al., 2017b].

562 3.1.1 Geology classification



563
 564 Figure 3: Classification of geological bed type in Antarctica showing the main classes of type 1 and type 2
 565 basins, intra-basin volcanics, and crystalline basement, as well as regions of mixed type classification. Major
 566 sedimentary basin regions are outlined in grey. The coastline shows both the ice sheet grounding line and the
 567 ice shelf edge. Dashed lines indicate locations of annular profiles (Fig. 6). PL – Palmer Land, RFIS – Ronne-
 568 Filchner Ice Shelf, BI – Berkner Island, HG – Haag Block, EWM – Ellsworth Whitmore Mountains, PM –
 569 Pensacola Mountains, BSB – Byrd Subglacial Basin, MBL – Marie Byrd Land IB – Iselin Bank, CL – Coats Land,
 570 PPB – Pensacola-Pole Basin, RB – Recovery Basin, RSH – Recovery Subglacial Highlands, JS – Jutulstraumen,
 571 DML -Dronning Maud Land, WRT -West Ragnhild Trough, FSH – Fuji Subglacial Highlands, AIS – Amery Ice

572 *Shelf, SPCM – Southern Prince Charles Mountains, GSM – Gamburtsev Subglacial Mountains, SPB – South*
573 *Pole Basin, LV – Lake Vostok, ASB – Aurora Subglacial Basin, VSB – Vincennes Subglacial Basin, WSB – Wilkes*
574 *Subglacial Basin*

575 As discussed above, the principal distinction we wish to make here is between crystalline basement
576 dominated regions, and sedimentary basins. However, a binary classification is inadequate to cover the
577 range of circumstances that the geology presents. Retaining simplicity, we classify the bed type into four
578 main classes: crystalline basement, intra-basin volcanic, and type 1 and type 2 basins (Fig 3). Often, the data
579 contain characteristics of more than one of these types, due either to variable bed types present in small
580 areas, or due to transitional conditions from one type to another and so we also have three mixed-type
581 classes, although their distribution is relatively restricted compared to the major types (Fig 3).

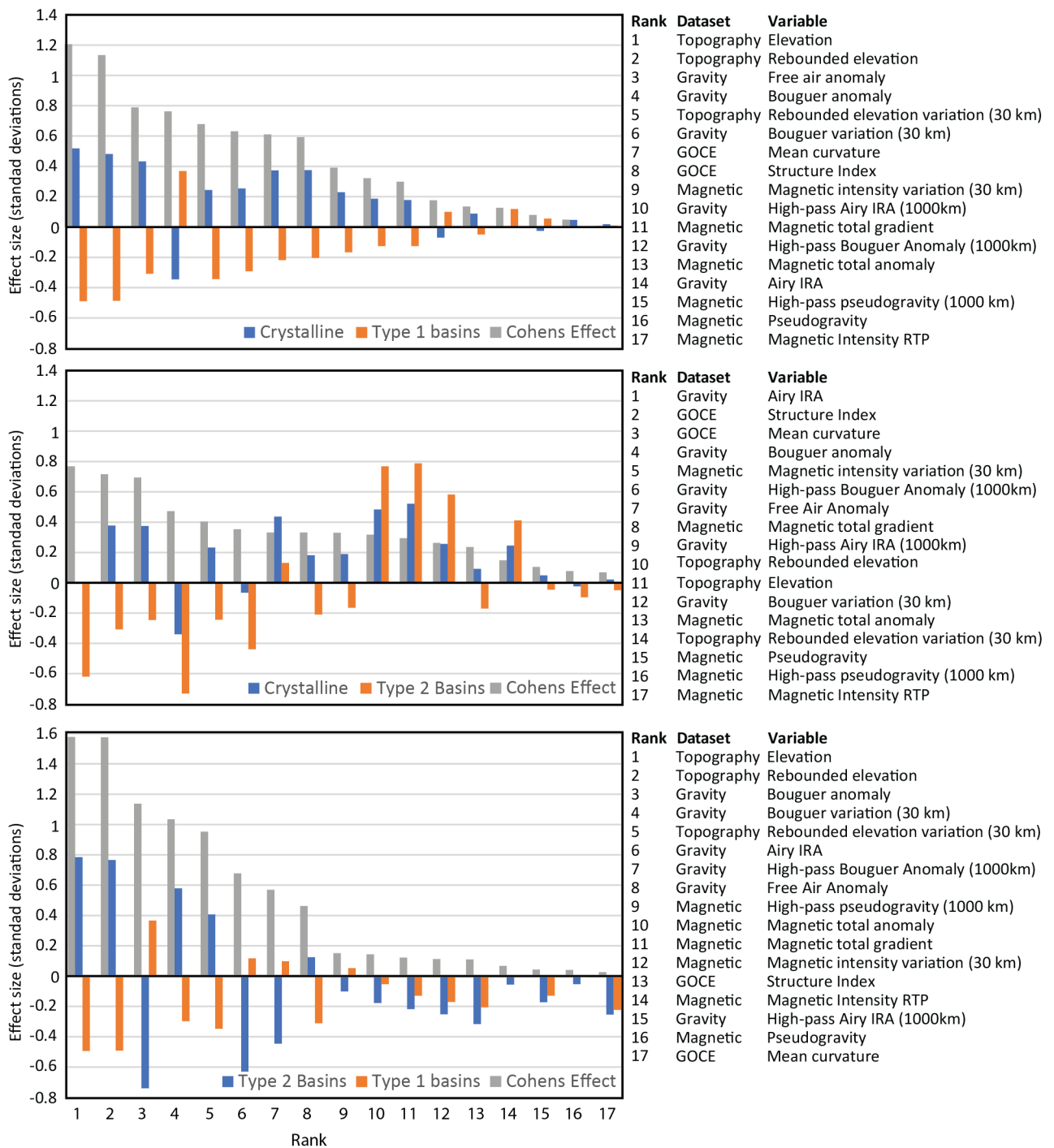
582 The crystalline basement class indicates where the bed is interpreted to consist of igneous or metamorphic
583 rocks (including high-grade metasedimentary rocks), with either no sedimentary cover, or a thin veneer that
584 is below the detection thresholds of the datasets used. Typically, these regions possess the characteristics of
585 high elevation and high gravity with high variability in topography, gravity, and magnetic data. Along track
586 roughness tends to be high for this class. Type cases for this class include regions in the Transantarctic
587 Mountains, Dronning Maud Land, Marie Byrd Land and the Gamburtsev Subglacial Mountains.

588 The type 1 basin class represents regions where sedimentary basins are preserved in relatively unmodified
589 basins, with typical characteristics of low elevation and low gravity, and low variability in gravity and
590 magnetic data. Along-track roughness tends to be low. Commonly, basins of this type have sufficient
591 thickness for this to be modeled in gravity and aeromagnetic data and detected in seismic data (Fig 6). Type
592 cases for this class include the Ross and Weddell embayments, and the Wilkes, Aurora and Pensacola-Pole
593 Subglacial Basins.

594 The intra-basin volcanics class includes areas where volcanic rocks are interpreted to be emplaced within a
595 type 1 basin sequence, that is they are younger than the base of the basin and may interfinger with or
596 overlie sedimentary rocks. Typically, this class relies on outcrop data and aeromagnetic data to define the
597 extents of volcanic complexes where they are dominant. It is noted that basins may contain volcanic rocks
598 without them being evident in geophysical data and the extent of volcanic rocks is likely underestimated.
599 The type case for this class is the McMurdo Volcanic Complex in the Ross Sea.

600 Finally, we define the type 2 basin class where sedimentary rocks are known or inferred but the original
601 depositional basin is not preserved. These rocks tend to predate the formation of the present landscape, are
602 often uplifted to high elevations, may be intruded by younger igneous rocks, may be heavily eroded and
603 overall have geophysical characteristics more similar to crystalline basement than type 1 basins. The type
604 case for this class is the Beacon Supergroup, with its characteristic high elevation exposures through the

605 TAM and mesa-like topography as a consequence of widespread Jurassic dolerite intrusions. Type 1 basins
 606 are prominent in the TAM and in the Ellsworth Whitmore mountains, with subglacial examples inferred in
 607 Dronning Maud Land, and subglacial highlands in Vostok and Aurora regions (Fig 3).



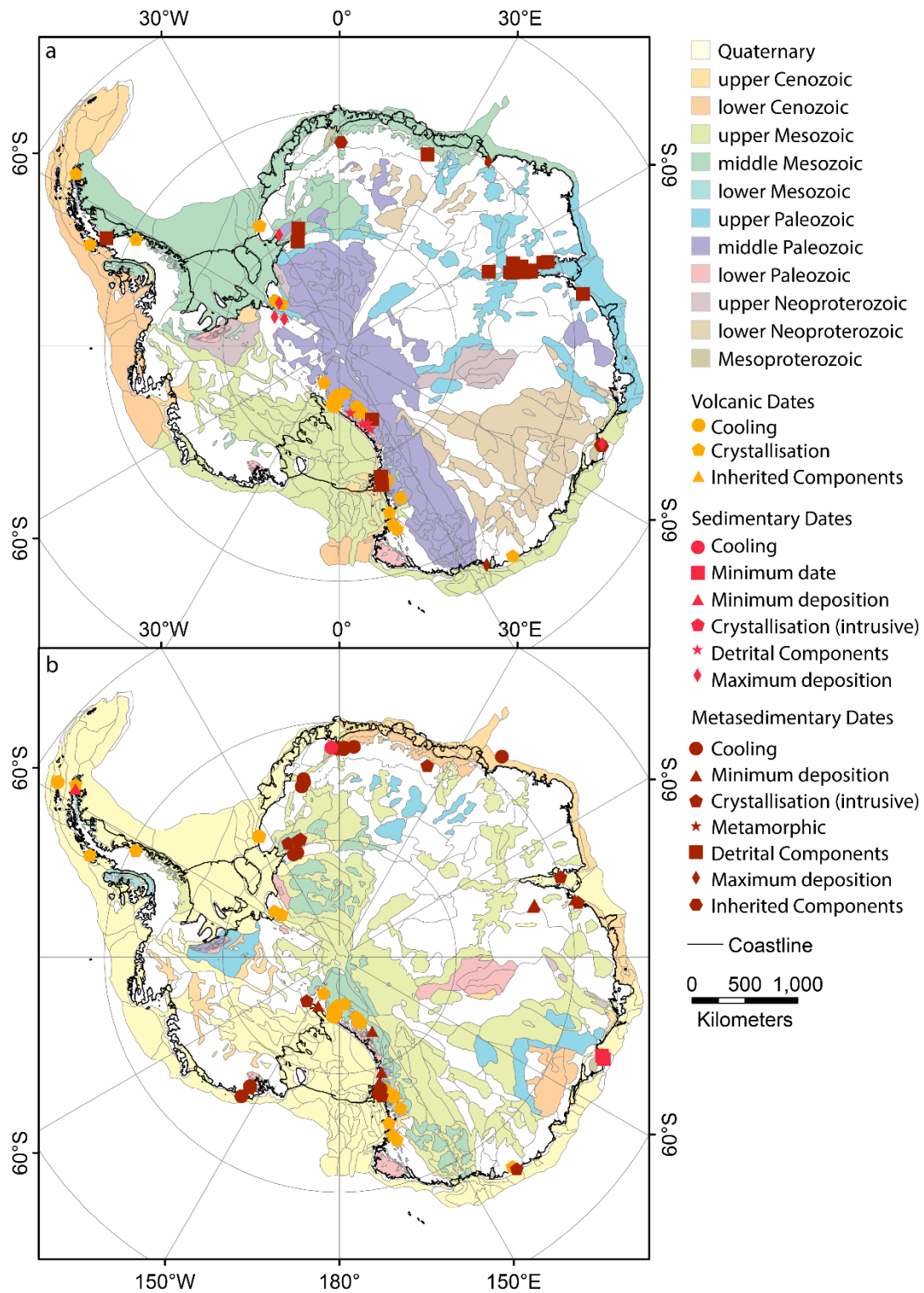
608
 609 *Figure 4: Relative effect sizes for selected datasets for a) crystalline basement vs type 1 basins, b) crystalline*
 610 *basement vs type 2 basins, c) type 1 basins vs type 2 basins. For each, datasets are ordered by Cohen's effect*
 611 *size indicating the ability of the dataset to discriminate those classes. The listing on the right highlights the*
 612 *datasets in rank order. Effect sizes above 0.8 may be considered a large effect, and below 0.5 a small effect.*

613 3.1.1.1 Class Validation

614 For validation, we may review this geological bed type classification against the major numerical datasets
615 available to the interpretation. Summary statistics for each input dataset were calculated for each class using
616 a Zonal Statistics GIS tool. These statistics allow to define the distinctiveness of the class-level populations, in
617 terms of differences of means, factoring in standard deviation, and so illuminate the data that most strongly
618 differentiate between classes (Fig 4). In figure 4 we show, with orange and blue lines the extent to which the
619 zonal mean for the class differs from the mean for the entire region. Where these differ substantially,
620 especially in sign, that dataset can discriminate the two selected classes. Furthermore, we may directly
621 compare the population-level distinctiveness between classes, for which we derive Cohen's effect size (Fig
622 4). Values above 0.8 may be considered a large effect, indicating a strong discriminator while values below
623 0.5 may be considered a small effect, indicating a weak discriminator.

624 The primary classification we seek is the distinction between type 1 basins and crystalline basement. For
625 these two classes, large effect sizes are seen for topography elevation datasets, while medium effect sizes
626 are seen for free air and Bouguer gravity, topography and gravity variation and satellite gravity-gradient
627 components (Fig 4a). In contrast, the distinction between crystalline basement and type 2 basins is weaker,
628 with medium effect sizes seen for Airy IRA and satellite gravity-gradient components (Fig 4b). The
629 distinction between type 1 and type 2 basins is strong, with large effect sizes for subglacial topography
630 elevation datasets, Bouguer gravity datasets and variability measures for these, and medium effect sizes for
631 Airy IRA and high pass filtered Bouguer gravity (Fig 4c). Finally, the in-basin volcanics class is sharply defined
632 relative to all other classes, these being most clearly differentiated with large or medium effect sizes for
633 magnetic data products as well as for variability in topography and gravity data.

634 The relationships highlighted above support the following as key criteria in classifying subglacial geology
635 class: type 1 basins are defined most by their low topography at large scales, accompanied by relatively high
636 Bouguer gravity, perhaps counter to expectations (note the opposite sign to topography in Fig 4a, 4c). With
637 respect to their classification from type 1 basins, type 2 basins show similar characteristics to the crystalline
638 basement class, but with a stronger effect from gravity data, reflecting characteristic gravity lows. Type 2
639 basins can be separated from crystalline bed by their low response in Bouguer and Airy IRA gravity
640 anomalies and satellite gravity gradiometry components. The magnetic dataset does not discriminate
641 strongly between these three classes but is strongly linked to the in-basin volcanics class, which is also
642 identified by high spatial variability in all datasets.



643

644 *Figure 5: Interpreted ages for a) base of the basin sequence and b) top of the basin sequence. Locations of*
 645 *selected age information for volcanic, sedimentary, and metasedimentary rocks are derived from PetroChron*
 646 *Antarctica [Sanchez et al., 2021], and broadly indicate where basin ages are better constrained.*

647

648 3.1.2 Age Classification

649 In addition to geological class we seek to define the age of the basins, which besides its importance for
650 tectonic understanding, may correspond to very different conditions for the ice sheet for basins of different
651 age. The interpreted age distribution indicates the evolving tectonic conditions of Antarctica and its
652 landscape, although due to the general paucity of robust age-dating outside of outcropping regions, and also
653 the very limited capacity for stratigraphic correlation beneath the ice, these interpretations are on
654 necessarily broad timescales.

655 For each basin, we define an interpreted age for the base and the top of the basin sequence (Fig. 5). The
656 base of basin age (Fig. 5a) represents a maximum bound on basin age, either from a known maximum age
657 (e.g. from maximum deposition), or from the interpreted age of the underlying crust. The top of basin age
658 (Fig. 5b) represents a minimum bound on basin age, either from a known minimum age (e.g. cooling age),
659 from a capping or intruding unit or from geomorphological criteria including interpreted regions of glacial
660 erosion and deposition.

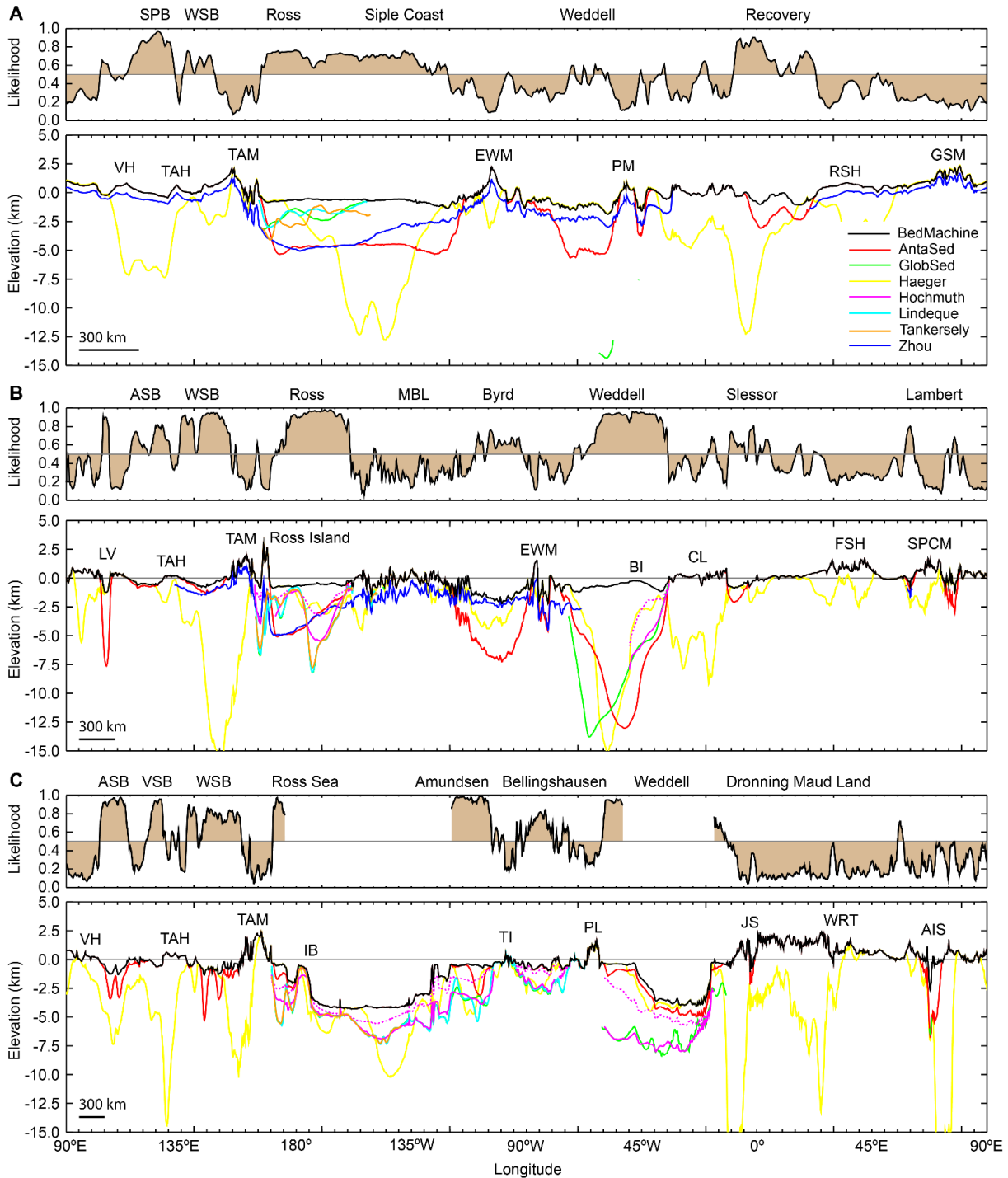
661 3.1.3 Basin Thickness

662 Except for RES data, the data types in the preceding section can all be used to generate models of the
663 thickness of sedimentary cover. It is possible to interpolate sedimentary thickness between existing data
664 points, giving an estimate of the thickness of sedimentary cover across the continent [*Baranov et al.*, 2021].
665 However, the fundamental differences between basin-sensing techniques, their differing resolution and
666 accuracy, and specific features of individual surveys and models leads to major uncertainty in defining basin
667 thickness.

668 Figure 6 shows several sedimentary basin thickness models, including models derived from gravity [*Haeger*
669 *and Kaban*, 2019], interpolation of seismic data [*Baranov et al.*, 2021], passive seismic models [*Zhou et al.*,
670 2022], seismic reflection data and magnetic depth to basement [*Tankersley et al.*, 2022] and marine seismic
671 reflection data [*Hochmuth et al.*, 2020; *Lindeque et al.*, 2016b; *Straume et al.*, 2019]. While there is some
672 commonality between these models, there are also many differences and only the seismic reflection models
673 show strong consistency with each other.

674 Three major factors contribute to this discrepancy. First, the resolution of techniques differs and so distinctly
675 separate features in one technique are likely to be merged in another. Consequently, thickness models will
676 differ greatly in the presence of complexity (e.g. Ross Island in Fig. 6b). Second, the physical properties
677 detected with each technique differ and furthermore, not all techniques have agreed criteria for the
678 definition of the basin-basement interface. Finally, the different techniques have different capacity to image
679 deep basin fill, and to accurately define the base of basins is often challenging, for example depth to
680 magnetic basement commonly defines sills within the basin sequence, and there is often no solution

681 possible for the basement beneath. Ultimately, while a general agreement can be reached on the extent of
 682 sedimentary basins, their thicknesses remain poorly constrained in Antarctica, except where seismic
 683 reflection data have been collected.



684
 685 *Figure 6: Annular profiles at latitudes of a) 82.5°S b) 77.5°S and c) 72.5°S (see figure 3 for locations). For*
 686 *each, the upper panel shows the basin likelihood model of [Li et al., 2022] and the lower panel bed*
 687 *topography [Morlighem, 2020] and base-basin elevation for several basin thickness model [Baranov et al.,*
 688 *2021; Haeger and Kaban, 2019; Hochmuth et al., 2020; Lindeque et al., 2016b; Straume et al., 2019;*

689 Tankersley et al., 2022; Zhou et al., 2022]. SPB – South Pole Basin, WSB – Wilkes Subglacial Basin, VH -
690 Vostok Highlands, TAH – Terre Adelie Highlands TAM – Transantarctic Mountains, EWM – Ellsworth
691 Whitmore Mountains, PM – Pensacola Mountains, RSH – Recovery Subglacial Highlands, GSM – Gamburtsev
692 Subglacial Mountains, ASB – Aurora Subglacial Basin, MBL – Marie Byrd Land, LV – Lake Vostok, BI- Berkner
693 Island, CL – Coats Land, FSH – Fuji Subglacial Highland, SPCM – Southern Prince Charles Mountains, VSB –
694 Vincennes Subglacial Basin, IB – Iselin Bank, TI – Thurston Island, PL – Palmer Land, JS – Jutulstraumen, WRT -
695 West Ragnhild Trough, AIS – Amery Ice Shelf.

696 3.2 West Antarctic Basins

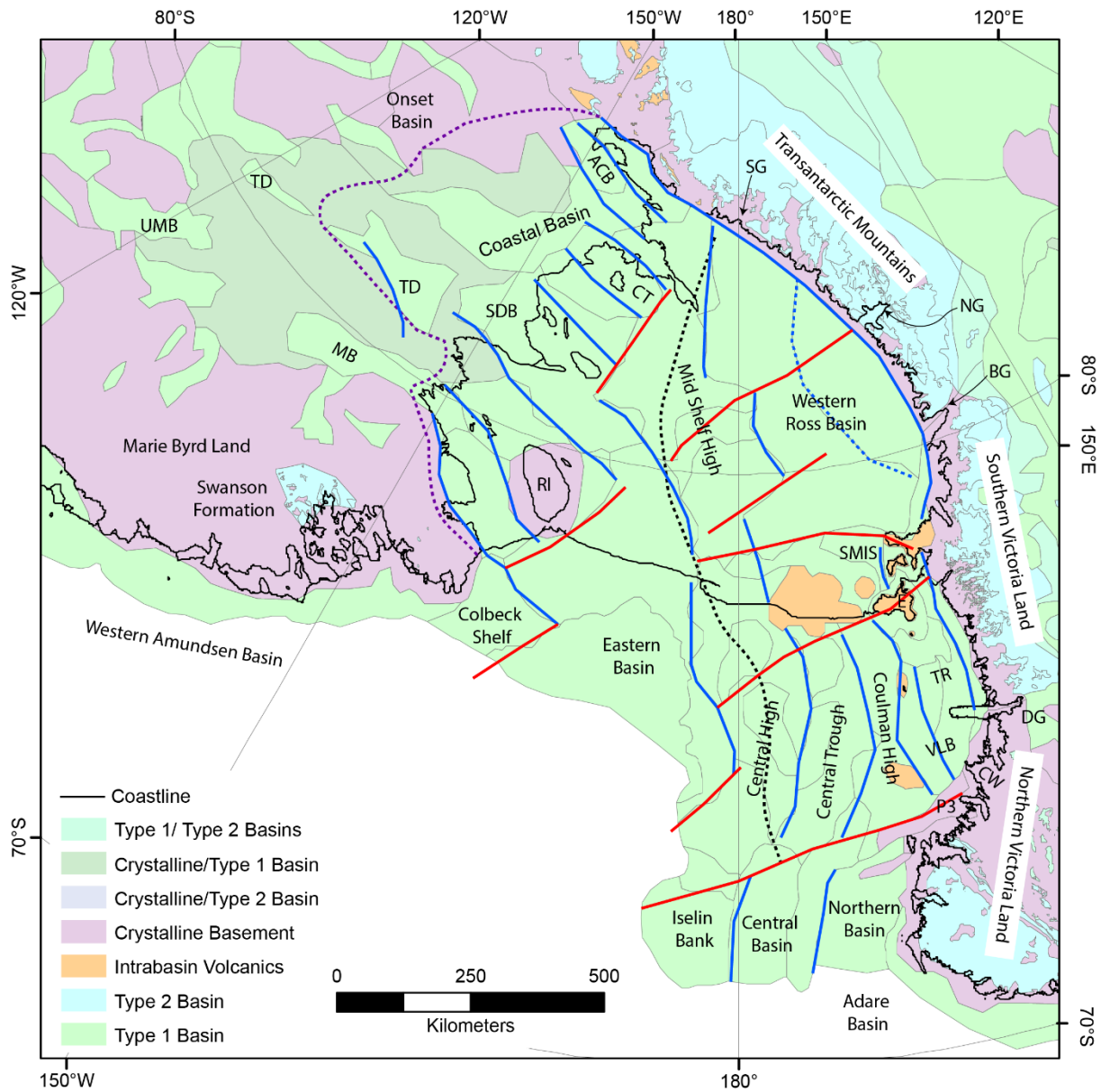
697 West Antarctica, in a geomorphological division, includes the continental regions on the Pacific-facing side of
698 the chain of mountains extending from Northern Victoria Land through the Transantarctic and Pensacola
699 Mountains to Coats Land (Fig 3). This region possesses several major basin-dominated regions, in particular
700 the Ross, Amundsen and Weddell regions, and is characterized by the low-elevation topography associated
701 with these. West Antarctica's crust has a varied history but the majority has formed since the Cambrian as a
702 result of accretionary tectonics at Gondwana's paleo-Pacific margin [Jordan et al., 2020]. It is noted that the
703 inferred boundary between the Paleozoic crust and the Proterozoic crust of East Antarctica, is not co-located
704 with the geomorphological boundary. Rather it traverses centrally through the Ross Embayment [Tinto et al.,
705 2019], and also has been affected by later translation of the Haag and Ellsworth-Whitmore and Marie-Byrd
706 Land blocks [Jordan et al., 2020]. This basement hosts a series of basins of diverse origin extending from the
707 Cambrian to the Quaternary

708 3.2.1 The Ross Embayment and Siple Coast

709 This sector of West Antarctica is bounded by the Transantarctic Mountains to the west and the West
710 Antarctic Ice Sheet (WAIS) divide to the south with the basement-dominated Marie Byrd land to the east. In
711 Marie Byrd land, small type 1 basins are interpreted in glacial troughs (Fig. 7) but the major known basin
712 (type 2) is defined by the variably metamorphosed <520 Ma to >440 Ma Swanson Formation, dominated by
713 turbidites and flysch. These rocks represent a middle-Cambrian to Ordovician basin, with sediments derived
714 from the Ross Orogen and a variety of Proterozoic sources [Yakymchuk et al., 2015]. These sediments were
715 deposited along the Gondwana margin, initially on the continental slope and rise in the Cambrian – lower
716 Ordovician but possibly later in a fore-arc/accretionary prism setting as a convergent margin setting
717 developed [Jordan et al., 2020].

718 The Ross Sea is of the most well studied regions in Antarctica and the existence of major sedimentary basins
719 is well established, with their stratigraphy revealed in multi-channel seismic data as well as numerous drill
720 cores (Fig 1). These studies define a thick sequence of late Cretaceous to Quaternary sedimentary rocks

721 separated into several packages by regional unconformities [Davey and Brancolini, 1995; Lindeque et al.,
 722 2016a; Pérez et al., 2021].



723
 724 *Figure 7: Sedimentary basins of the Ross Sea and Siple Coast regions, showing basin regions and*
 725 *reinterpreted basin structures, rift parallel (blue) and transverse (red). Basin faults are reinterpreted from*
 726 *prior studies [Davey et al., 2021; Lindeque et al., 2016b; Pérez et al., 2021; Sauli et al., 2021; Studinger et al.,*
 727 *2001; Tankersley et al., 2022; Wilson et al., 2012; Wilson, 1999]. Also shown are the interpreted East*
 728 *Antarctica-West Antarctica basement boundary (black) [Tinto et al., 2019], and the seismically defined*
 729 *extents of thick basin cover [Zhou et al., 2022] (purple). UMB – Upstream MacAyeal Basin, MB - MacAyeal*
 730 *Basin, TD - Trunk D Basin, ACB – Amundsen Coast Basin, CT - Crary Trough, SDB - Siple Dome Basin, TR –*
 731 *Terror Rift, VLB – Victoria Land Basin, P3 – Polar 3 Anomaly, RI – Roosevelt Island, SG – Shackleton Glacier,*

732 SMIS – Southern McMurdo Ice Shelf, NG – Nimrod Glacier, BG – Byrd Glacier, CW – Cape Washington, DG –
733 David Glacier, E - Erebus

734 The Ross Sea basin has four major depocenters, the Victoria Land Basin, the Central Trough, the Eastern
735 Basin and the Northern Basin [Davey and Brancolini, 1995] separated by basement highs with much less fill,
736 the Coulman High and Central High; only Roosevelt Island appears sediment free [Wilson and Luyendyk,
737 2006]. These basins initiated with rifting in the late Cretaceous, but with relatively little basin-fill deposited.
738 The first major sequence (RSS-1) is discontinuous and is observed in isolated grabens in the eastern to
739 central Ross Sea, and may represent this rifting event, with thermal subsidence perhaps extending into the
740 early Cenozoic [Luyendyk et al., 2001]. A later phase of Eocene to Oligocene rifting is interpreted in the
741 Victoria Land Basin [Fielding et al., 2008]. A basin-wide unconformity (RSU-6) indicates a period of erosion in
742 the Oligocene, occurring not later than 26 Ma in the Eastern Basin [Kulhanek et al., 2019], potentially
743 associated with sea-level fall associated with large-scale glaciation in Antarctica. Correlation of RSU-6 into
744 the Victoria Land Basin has been problematic [cf. Davey et al., 2000; Fielding et al., 2008], but may align with
745 a mid-Oligocene unconformity that marks the end of the early rift stage of Fielding et al. [2008]. Subsequent
746 to this, basin deposition was episodic, but with relatively little extension, the glacial evolution of the
747 continent being the major driver of basin evolution in most of the Ross Sea [Anderson et al., 2019; De Santis
748 et al., 1999; Kim et al., 2018; Lindeque et al., 2016a; Marschalek et al., 2021; Pérez et al., 2021]

749 Upper Oligocene to Lower Miocene strata (RSS-2) are preserved in the major basins of the Ross Sea, but are
750 thin to absent on the basement highs [Pérez et al., 2021]. These sediments are interpreted to be deposited
751 in a glacio-marine setting associated with a fluctuating ice sheet margin including glaciation of local
752 bathymetric highs [De Santis et al., 1999]. Early to middle Miocene (18-15 Ma) sedimentary deposition (RSS-
753 3 & RSS-4) is interpreted in detail in Pérez et al. [2021]. In contrast to the thick and structurally segmented
754 packages of the lower sequence, this package overall is laterally continuous across the southern Ross Sea,
755 but with complex internal structure that is representative of changeable ice sheet dynamics, as documented
756 in several drill core records [Levy et al., 2016; Marschalek et al., 2021; McKay et al., 2016]. A major mid-
757 Miocene erosional event (RSU-4), indicating the advance of a major ice sheet over the Ross Sea is
758 interpreted associated with the Mid-Miocene Climate Transition [Bart, 2003; Pérez et al., 2021]. The post
759 mid-Miocene sedimentary basin record is similarly characterized by numerous and repeated ice sheet
760 advance and retreat cycles [Anderson et al., 2019; Bart et al., 2000; Halberstadt et al., 2018; McKay et al.,
761 2012a; McKay et al., 2012b; Naish et al., 2009]. Consequently, sediment thicknesses are relatively low,
762 except in deeper water in the northeast where substantial progradation of the shelf edge is seen [Hochmuth
763 and Gohl, 2019; Pérez et al., 2021], and in the west where the Terror Rift has substantially deepened the
764 bathymetry [Sauli et al., 2021; Wenman et al., 2020].

765 The Terror Rift has generated the ~ 4 km thick rhombic Discovery Graben, extending from Cape Washington
766 to, at least, Ross Island [Sauli et al., 2021], with a seismically defined extension into the southern McMurdo
767 Ice Shelf [Johnston et al., 2008], and possibly further south [Tankersley et al., 2022]. Stratigraphic
768 considerations suggest that after Eocene- Oligocene rifting, a period of thermal subsidence persisted until
769 renewed extension from ~13 Ma drove the renewed tectonic development of accommodation space in the
770 Discovery Graben [Fielding et al., 2008], however a more continuous evolution may be considered [Granot
771 and Dymant, 2018; Sauli et al., 2021]. Within the western Ross Sea, the McMurdo Volcanic Complex
772 represents widespread and prominent volcanism, and some of these volcanoes are associated with flexural
773 basin development [e.g. Horgan et al., 2005; Wenman et al., 2020] generating repositories of Neogene
774 sedimentation and glacial development [McKay et al., 2012a; McKay et al., 2012b; McKay et al., 2016; Naish
775 et al., 2009].

776 The northwestern Ross Sea has a distinct Cenozoic evolution. The Northern Basin is directly associated with
777 the adjacent Adare Basin, which formed during seafloor spreading from 43 to 26 Ma, while the oceanic crust
778 beneath the Central Basin, north of the Central Trough, may have formed from 61 to 53 Ma [Cande and
779 Stock, 2004]. The Northern Basin is offset from the Victoria Land Basin by the Polar 3 magnetic anomaly,
780 inferred to represent an intrusion emplaced into a transcurrent fault zone. With the implication that this
781 fault zone extends further offshore to the Iselin Bank, Davey et al. [2021] present a three-stage
782 reconstruction of the northern Ross Sea involving: 10 to 26 Ma – Terror Rift opening and minor extension of
783 WARS [Granot and Dymant, 2018], 26 to 43 Ma – Opening of the Adare Basin and Northern Basin; 53 to 61
784 Ma – Opening of the Central Basin and northern Central Trough, accommodated by Polar-3 transfer and its
785 extension to the Iselin Rift [Davey et al., 2021].

786 The extension of the basin forming events known from the southern Ross Sea beneath the Ross Ice Shelf is
787 highly likely, although the structure of these basins has not been fully demonstrated, due to the lack of
788 extensive seismic data and ambiguous gravity signals [Karner et al., 2005]. Recent geophysical data have
789 begun to reveal the structure of this basin: Airborne geophysical surveying across the Ross Ice Shelf has
790 allowed the identification of several depocenters from depth to magnetic basement calibrated against the
791 southern Ross Sea [Tankersley et al., 2022]. These show continuation of the Ross Sea systems into Eastern
792 and Western depocenters separated by a mid-shelf high connecting with the Central High. The Eastern
793 depocenter narrows inland to a distinct trough beneath Siple Dome. A smaller depocenter is located to the
794 east of Roosevelt Island. The western depocenter beneath the Ross Ice Shelf is broad with a weakly defined
795 ridge separating two sub-basins. In addition, recent passive seismic models map sedimentary thickness in
796 the region using ambient noise tomography, also revealing thick sedimentary basins beneath the Ross Ice
797 shelf and southern Ross Sea [Zhou et al., 2022]. The structure of these is different to the magnetic studies,
798 likely reflecting the different spatial sensitivities of these techniques. Similarly, the mapping of Li et al. [2022]

799 indicates a high likelihood of major basins beneath the Ross Ice Shelf (Fig 2a). Despite these first
800 considerations being addressed, the absence of seismically constrained basin geometry and stratigraphy
801 limits the understanding of Cenozoic deposition and erosion patterns beneath the Ross Ice Shelf.

802 A further extension of the WARS into the Siple Coast region suggests a likely continuation of the basin-
803 forming processes; however, the Siple Coast has distinctly different characteristics to the Ross Embayment.
804 Although sedimentary cover is widely recognized in many geophysical surveys, sedimentary deposits are
805 apparently thinner (in general < 1 km) and not ubiquitous. Ambient noise tomography resolves a broad basin
806 region extending ~400 km inland from the coast [Zhou *et al.*, 2022]. Aeromagnetic data at the coast suggest
807 several ~75 km wide depocenters beneath Siple Dome aligned with the previously identified Trunk D Basin
808 [Bell *et al.*, 1998], the Crary Trough, and on the Amundsen Coast, respectively north and south of the Crary
809 Ice Rise [Tankersley *et al.*, 2022]. The southernmost of these has recently been defined using magnetotelluric
810 and passive seismic data [Gustafson *et al.*, 2022]. In the mapping of Li *et al.* [2022] the Siple Coast region
811 returns sedimentary bed likelihoods dominantly between 0.25 and 0.75 indicating the relatively ambiguous
812 nature of this region at large scales, however high likelihood basin regions are identified for the MacAyeal
813 Ice Stream, for the Siple Dome/Trunk D Basin, the Crary Trough and the Amundsen Coast. Inland, beyond the
814 limit of the broad basin-dominated region [Zhou *et al.*, 2022] a basement-dominated pattern is seen
815 however, four smaller basins are identified associated with the uppermost MacAyeal Ice Stream, Trunk D
816 [Peters *et al.*, 2006], the Onset Basin linking to the Crary Trough [Bell *et al.*, 1998; Peters *et al.*, 2006] and a
817 southern basin linking to the Amundsen Coast [Studinger *et al.*, 2001]. The rest of the region is here
818 classified as mixed type 1 basin/crystalline basement. The exact configuration of sedimentary cover is not
819 well resolved, but nonetheless there is likely to be sufficient sedimentary cover for basin-influenced
820 processes to occur widely.

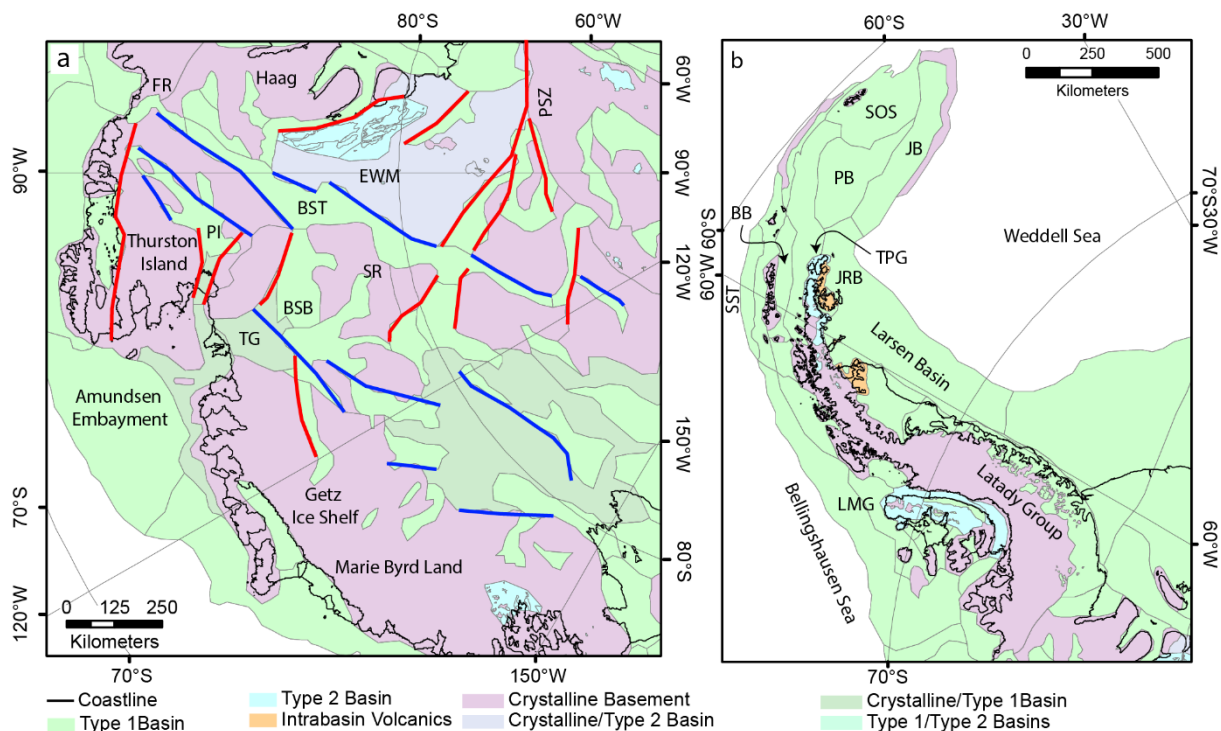
821 The transition from the Ross Sea to the Siple Coast involves, in the west, several transitions in basin
822 architecture (Fig 7) – one located from the Polar-3 anomaly to Iselin Bank, which separates the Northern
823 Basin from the Victoria Land Basin and the Central Basin from the Central Trough [Davey *et al.*, 2021];
824 another located at the Discovery Accommodation Zone, separating the Victoria Land Basin and Central
825 Trough from the Western Ross Basin [Wilson, 1999], and a third located outboard of Shackleton Glacier
826 separating this broad basin from the narrower basins of the Amundsen Coast and Crary Trough [Tankersley
827 *et al.*, 2022]. The situation in the east is simpler, with the Eastern Basin separating at Roosevelt Island into
828 two narrower depocenters – one extending to Siple Dome, the other to MacAyeal Ice Stream [Tankersley *et al.*,
829 *et al.*, 2022; Zhou *et al.*, 2022]. In general, the tendency is for narrower and more defined depocenters
830 developing inland, indicating a probable combination of deeper exposure level inland due to repeated
831 glaciation events with reduced Cenozoic subsidence and sediment loading [Paxman *et al.*, 2019b; Wilson *et al.*,
832 *et al.*, 2012], and potentially stronger lithosphere under WAIS divide.

833 3.2.2 Interior West Antarctica

834 Interior West Antarctica includes a prominent low-lying region east of the WAIS divide including the Byrd
835 Subglacial Basin and the Bentley Subglacial Trough (each extending > 2 km below sea level), the central West
836 Antarctica region is bounded to three sides by high-standing regions, the Ellsworth Whitmore and Haag
837 regions to the west, the Thurston Island region to the north and Marie-Byrd Land to the northeast. To the
838 southwest, an indistinct transition leads to the Siple Coast.

839 The Ellsworth Whitmore Mountains preserve the oldest known sedimentary rocks in West Antarctica, with a
840 ~ 13 km thick sequence of Cambrian to Permian sedimentary rocks [Castillo *et al.*, 2017; Craddock *et al.*,
841 2017]. The lowermost unit, the Heritage Group, comprises lower- to middle-Cambrian sedimentary rocks
842 including a lower sequence of terrestrial volcanoclastic, shallow marine clastic sediments and limestones, an
843 overlying sequence of transitional terrestrial to marine sedimentary rocks and overlying these Late-Middle to
844 Late Cambrian carbonate-dominated rocks [Curtis and Lomas, 1999]. Thin transitional beds divide the
845 Heritage Group from the Upper Cambrian to Devonian Crashsite Group, deposited in a fluvial to shallow-
846 marine environment [Curtis and Lomas, 1999]. The glacial-derived Whiteout Conglomerate is interpreted to
847 represent the early Permian Gondwanide glaciation at ca. 300 Ma [Isbell *et al.*, 2008] and is overlain by the
848 Polarstar Formation including argillite, sandstone and coal measures, interpreted to represent post-glacial
849 deposition in the Gondwana Basin [Elliot *et al.*, 2017]. Overall, this basin has been interpreted to represent a
850 transition from a rift setting in the early Cambrian to a passive margin setting extending into the Permian
851 [Castillo *et al.*, 2017; Craddock *et al.*, 2017]. Isolated exposures elsewhere in the Ellsworth-Whitmore Block
852 [Cox *et al.*, 2019] also possess sedimentary rocks and we infer the unexposed region to be of mixed type
853 class, preserving the Paleozoic basin intruded by younger granite suites.

854 Seismic observations suggest that the central West Antarctica region is not occupied by a major broad
855 sedimentary basin [Zhou *et al.*, 2022], but sedimentary rocks likely exist in association with low lying regions
856 [Li *et al.*, 2022]. The low-elevation areas possess markedly smooth beds, and in many cases low isostatic
857 residual gravity anomalies indicating relatively young sedimentary rocks are present [Jordan *et al.*, 2010b].
858 Three basins are interpreted in this region, each with different glacial catchments: The Pine Island Rift Basin
859 underlies the upper Pine Island Glacier catchment [Jordan *et al.*, 2010b]; The Byrd Subglacial basin underlies
860 the upper portion of the Thwaites Glacier catchment [Studinger *et al.*, 2001]; and the Bentley Subglacial
861 Trough flanks the Ellsworth Whitmore block, connecting to the Ferrigno Rift Basin [Bingham *et al.*, 2012].
862 The thickness of sedimentary rocks in these is variable but locally may be up to 2 km thick. The geometry of
863 these basins indicates several phases of extension, with ~E-W oriented basins overprinted by later extension
864 generating ~NE-SW aligned basins (Fig 8). The former set may relate to structures in the southern Weddell
865 Sea while the latter are aligned with WARS rift axis and the Siple Coast basins.



866

867 *Figure 8: Sedimentary basins of the a) Central West Antarctica and b) Antarctic Peninsula Drake and eastern*
 868 *Weddell Sea regions. Structures in a) are reinterpreted from prior studies [Bell et al., 1998; Bingham et al.,*
 869 *2012; Haeger and Kaban, 2019; Jordan et al., 2010b; Jordan et al., 2013b; Jordan et al., 2020; Studinger et*
 870 *al., 2001] as associated with the WARS (blue) and WSRS (red). PI – Pine Island Rift Basin, FR – Ferrigno Rift,*
 871 *BSB – Byrd Subglacial Basin, BST – Bentley Subglacial Trough, EWM - Ellsworth Whitmore Mountains, SR –*
 872 *Sinuuous Ridge, PSZ – Pagano Shear Zone, SST – South Shetland Trench, BB – Bransfield Basin, PB – Powell*
 873 *Basin, JB – Jane Basin, SOS – South Orkney Shelf, TPG – Trinity Peninsula Group, LMG – LeMay Group, JRB –*
 874 *James Ross Basin.*

875 The nature of the bed in the glacial troughs connecting these inland basins to the coast is not clearly defined.
 876 Evidence from seismic and RES data suggests in each case a complex bed evolving with, in places thick and
 877 partially lithified sedimentary deposits, and in other places basement rocks or volcanoes [Alley et al., 2021;
 878 Bingham et al., 2012; Brisbane et al., 2017; Muto et al., 2016; Muto et al., 2019a; Muto et al., 2019b; Smith
 879 et al., 2013]. These are classed as mixed-crust, similar to the Siple Coast region, implying a bed condition
 880 that is not well resolved within the trough, and also is potentially quite time-variable but likely contains
 881 enough sedimentary material to support enhanced till production and hydrogeology [Alley et al., 2021].

882 3.2.3 Pacific Margin

883 The Pacific margin of West Antarctica includes the basin regions of the Amundsen and Bellingshausen Seas,
 884 and the extension of this margin along the western Antarctic Peninsula (Fig 8). Each of these is characterized
 885 by a thick sequence of sedimentary rocks on the continental shelf, with up to 7 km in the Amundsen Sea and
 886 5 km in the Bellingshausen Sea [Hochmuth et al., 2020; Lindeque et al., 2016b]. Based on a partial continuity

887 of Cenozoic seismic stratigraphy extending from the eastern Ross Sea, the Pacific margin preserves, from
888 west to east, a progressively younger base-of-basin, from 80-67 Ma in the Ross Sea to 36 Ma on the
889 Antarctic Peninsula margin, and correspondingly a younger onset of transitional glacial conditions, from 34-
890 30 Ma in the Ross Sea to 21 Ma in the eastern Amundsen Sea, and 25 Ma on the Antarctic Peninsula margin
891 [*Lindeque et al.*, 2016b]. In the transition to glacial Antarctica, and in subsequent glacial conditions these
892 basins record selective deposition focused especially in the Amundsen Sea Embayment and the eastern
893 Bellingshausen Sea [*Hochmuth et al.*, 2020; *Lindeque et al.*, 2016b]. This margin has substantial shelf-edge
894 progradation, since the middle to late Miocene in the Amundsen Sea and since the late Miocene/early
895 Pliocene for the Bellingshausen Sea, and the early Pliocene for the Antarctic Peninsula margin [*Hochmuth et*
896 *al.*, 2020].

897 The Amundsen Sea Embayment receives sediments from the Pine Island and Thwaites Glaciers and
898 possesses the thickest accumulation of sedimentary rocks on the Pacific margin. The inner shelf however is
899 dominated by exposed basement, extending 200 to 250 km from the coast [*Gohl et al.*, 2013a]. Within this
900 region some minor basin regions are interpreted where both the bed and the magnetic data are relatively
901 smooth. The middle and outer shelf are thickly sedimented, comprising basal strata from early Cretaceous
902 rifting, a thick passive-margin sequence of Late Cretaceous to Oligocene sediments, and Early/Middle
903 Miocene to Pleistocene characterized by episodic glacial advances and progradation of the shelf edge,
904 especially during the Pliocene [*Gohl et al.*, 2013a; *Gohl et al.*, 2013b; *Gohl et al.*, 2021].

905 3.2.4 South Shetland and South Orkney Shelf

906 At the northern Antarctic Peninsula, the Pacific margin of Antarctica changes from a passive margin to a
907 convergent margin with the former Phoenix Plate (Antarctic Plate) descending under the South Shetland
908 Islands. The main features of this margin are the South Shetland trench and the active spreading centre in
909 Bransfield Strait behind, both associated with ongoing basin forming processes. At the South Shetland
910 Trench, the margin preserves a thick accretionary complex and fore-arc system imposed on the older
911 continental shelf [*Maldonado et al.*, 1994]. These sediments were predominantly accumulated during
912 subduction of the former Phoenix Plate, which ceased between 3.6-2.6 Ma, but also preserve evidence of
913 younger deformation suggesting ongoing thrust faulting [*Maldonado et al.*, 1994]. Since ~ 4 Ma, the
914 Bransfield Basin is actively subsiding through rifting with segmented depocenters up to 2 km thick, and with
915 active volcanism and seismicity [*Almendros et al.*, 2020].

916 On the opposite side of the Antarctic Peninsula shelf, the Powell Basin records rifting of the South Orkney
917 microcontinent from the Antarctic Peninsula, with rifting commencing in the late Eocene or early Oligocene,
918 progressing to seafloor spreading from ~30 to ~20 Ma [*Eagles and Livermore*, 2002]. The adjacent Jane Basin
919 opened in a back-arc setting from ~18 to ~14 Ma [*Bohoyo et al.*, 2002]. Across these basins, sediments are
920 deposited in several sequences including syn-to post rift packages initially in individual depocenters,

921 transitioning to a broader shared sequence since the mid-Miocene [*Lindeque et al.*, 2013; *Maldonado et al.*,
922 2006].

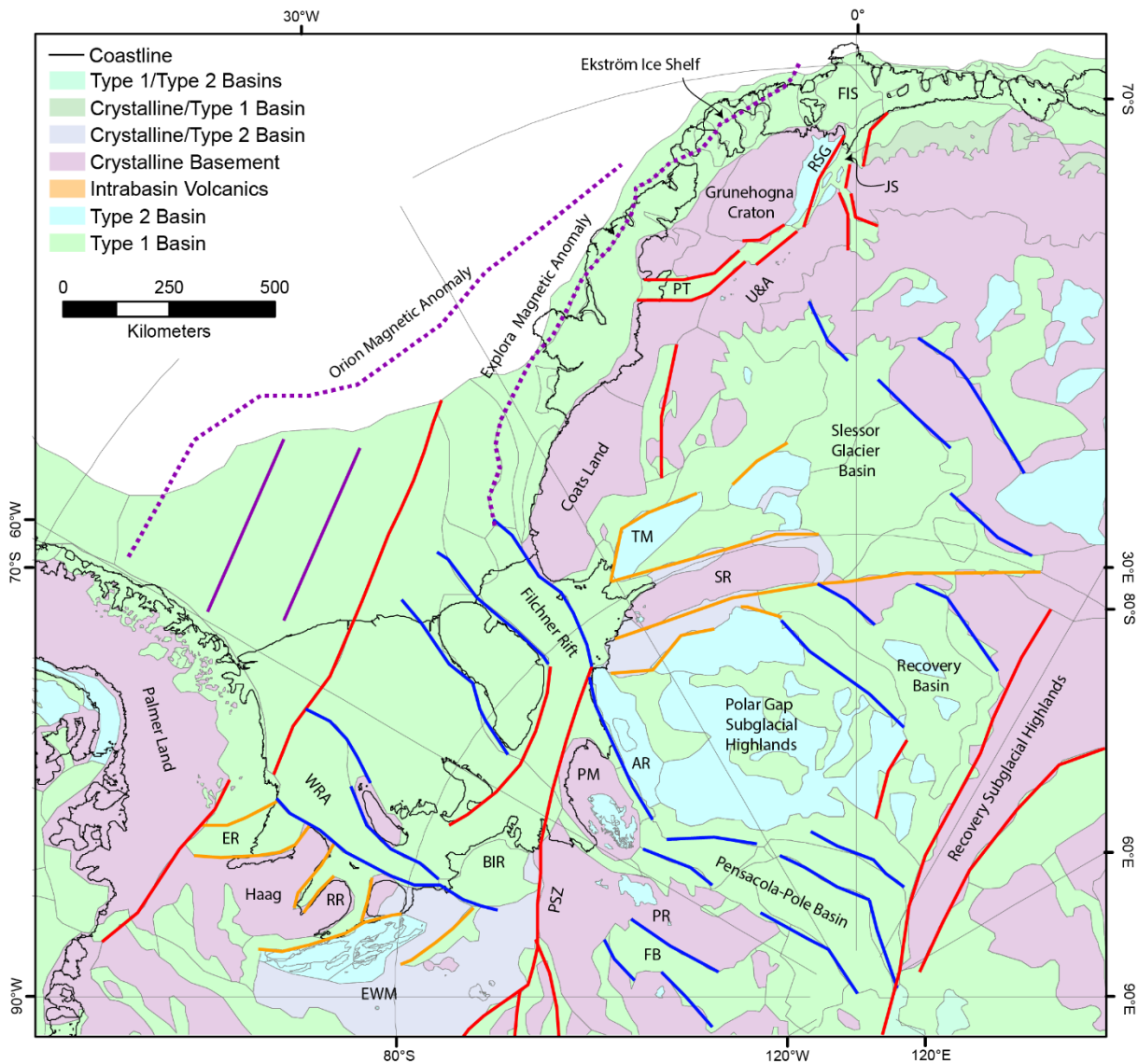
923 3.2.5 Antarctic Peninsula and Weddell Sea

924 The Antarctic Peninsula and the Weddell Sea record the evolution of the Weddell Sea Rift with a partly
925 shared basin evolution in the Mesozoic to Cenozoic. The oldest sedimentary rocks on the Antarctic Peninsula
926 are preserved in the Trinity Peninsula Group, outcropping on the northern Antarctic Peninsula. These rocks
927 comprise an upper Carboniferous to Triassic sequence that formed on the margin of Gondwana in
928 association with erosion of continental magmatic arc material [*Castillo et al.*, 2015]. The Triassic LeMay
929 Group outcropping on Alexander Island was deposited in a fore-arc accretionary complex coincident with
930 ongoing Triassic arc magmatism in southern Antarctic Peninsula [*Willan*, 2003]. The Late Jurassic to Early
931 Cretaceous Fossil Bluff Group represents a thick sequence of fore-arc deposits derived from adjacent
932 magmatic arc [*Riley et al.*, 2012]. Considering their current setting, all these basins are considered as type 2
933 basins in our classification.

934 The Jurassic-Cretaceous Latady Group outcrops on the south-eastern Antarctic Peninsula, representing the
935 formation of a progressively deepening basin from 185 to 140 Ma, with several kilometers of sediment
936 deposited [*Hunter and Cantrill*, 2006]. Early Jurassic to early-Middle Jurassic terrestrial to shallow marine
937 formations occupy smaller depocenters in grabens or half-grabens, with a transition to a deep marine
938 environment from the late-Middle Jurassic onwards associated with Weddell Sea rifting [*Hunter and Cantrill*,
939 2006]. More sparse outcrops of similarly aged rocks are found to the north in the Larsen basin. Although a
940 distinct depocenter, the Larsen Basin preserves a similar evolution from a terrestrial to shallow marine syn-
941 rift setting in the Early to Middle Jurassic, transitioning to a deep marine setting from the Late Jurassic
942 [*Hathway*, 2000]. The northern Antarctic Peninsula preserves key upper Mesozoic to lower Cenozoic
943 sequences exposed in the James Ross Basin. These sequences preserve a critical record of the high latitude
944 paleoenvironment at the Cretaceous-Tertiary boundary and also support a better knowledge of
945 paleogeography of Antarctica [*Bowman et al.*, 2016; *Francis et al.*, 2006].

946 The formation of the Weddell Sea Rift System is interpreted to commence in line with the above transition
947 from a magmatic-arc setting to back-arc extension at 180-177 Ma [*Riley et al.*, 2020] with the onset of
948 seafloor spreading by 147 Ma [*König and Jokat*, 2006]. The Weddell Sea contains the thickest known
949 sedimentary basin in Antarctica (Fig 6), with up to 15 km of sedimentary rocks [*Leitchenkov and Kudryavtzev*,
950 1997; *Straume et al.*, 2019]. *Jordan et al.* [2017a] define distinct northern and southern provinces from
951 magnetic fabrics, indicating two distinct phases of rifting: In the south, east-west extension is interpreted
952 due to the motion, and possibly rotation, of the Ellsworth-Whitmore and Haag blocks from a position
953 adjacent to the East Antarctic margin, north of the Pensacola Mountains. Movement of the Haag Ellsworth–
954 Whitmore microcontinent likely ceased by ~175 Ma, based on the ages of granites emplaced along the

955 marginal Pagano Shear Zone [Jordan et al., 2013b]. Modelling of Bouguer gravity anomalies suggest highly
 956 thinned continental crust with a bowl-shaped basin geometry beneath the Ronne-Filchner Ice Shelf [Jordan
 957 et al., 2017a; Leitchenkov and Kudryavtzev, 1997]. Distinct positive Bouguer gravity anomalies around the
 958 margins of the Ronne-Filchner ice shelf (Fig 2e), including the Weddell Rift Anomaly, Filchner Rift and Evans-
 959 Rutherford Rift Basin represent areas with thinned crust and low topography, but less thick sedimentary fill than
 960 seen in the central basin.



961
 962 *Figure 9: Sedimentary basins of the Weddell and Weddell Coast regions. Structures are reinterpreted from*
 963 *prior studies including [Bamber et al., 2006; Ferraccioli et al., 2005b; Jones et al., 2002; Jordan et al., 2013b;*
 964 *Jordan et al., 2017a; Paxman et al., 2017; Paxman et al., 2019a; Riedel et al., 2012]. Blue lines indicate*
 965 *structures parallel with the SWRS, Red lines structures aligned transverse to the SWRS, parallel to the Pagano*
 966 *Shear Zone. Orange lines indicate structures of other orientations. Purple lines indicate magnetic trends of*
 967 *the NWRS including the Orion and Explora Anomalies. ER - Evans Rift, RR - Rutherford Rift, EWM – Ellsworth*

968 *Whitmore Mountains, WRA – Weddell Rift Anomaly, BIR – Bungenstock Ice Rise, FB – Foundation Basin, PR*
969 *Patuxent Range, PM – Pensacola Mountains, AR – Argentina Range, SR -Shackleton Range, TM – Theron*
970 *Mountains, U&A – Urfjell and Amelang Groups, PT - Pencksokket Trough, RSG – Ritscherflya Supergroup, JS –*
971 *Jutulstraumen, FIS – Fimbul Ice Shelf*

972 After development of the Southern Weddell Sea Rift System, continental rifting between Southern Africa
973 and Antarctica became the dominant tectonic process [König and Jokat, 2006] forming the Northern
974 Weddell Sea Rift System. The northern province possesses a NE-SW magnetic fabric, and potentially oceanic
975 to transitional crust [Jordan et al., 2020]. This phase of extension appears to crosscut the older back-arc
976 system [Jordan et al., 2017a] and is associated with magmatism giving rise to the Orion and Explora magnetic
977 anomalies (Fig. 9). These magnetic anomalies approximately coincide with the continent-ocean transition,
978 and they may reflect seaward dipping reflector sequences [Kristoffersen et al., 2014], potentially emplaced
979 ca 150-138 Ma [König and Jokat, 2006]. The onset-age of northern Weddell Sea rifting is not uniquely
980 defined: In one model, onset of extension is suggested by 167 Ma with ocean-crust forming by 147 Ma
981 [König and Jokat, 2006], however an alternative model suggests the Northern Weddell Sea Rift reflects
982 separation of a single Skytrain plate from Southern Africa and the Falkland Plateau between 180 and 156
983 Ma, followed by 90 degree rotation of the entire Skytrain plate into its current position by ~126 Ma [Eagles
984 and Eisermann, 2020].

985 Regardless of the tectonic model, interpreted sedimentary rock thicknesses and gravity anomalies are
986 continuous throughout the central part of the Weddell Embayment. This suggests that most of the
987 sedimentary fill has been deposited after tectonic motions ceased due to thermal subsidence associated
988 with ongoing slow spreading at the margin. The oldest sedimentary horizons were deposited over the
989 seaward dipping reflectors and the oceanic crust from ~160 to 145 Ma, with ongoing deposition continuing
990 until at least ~114 Ma in the southeastern Weddell Sea [Rogenhagen et al., 2004], and progressively younger
991 toward the northwest, in line with the generation of oceanic crust and its subsidence [Lindeque et al., 2013].
992 The youngest sediments of the pre-glacial regime may be as young as mid-Miocene, with deposition
993 controlled by the proto-Weddell gyre [Lindeque et al., 2013].

994 Glacial influences on the northern Weddell Sea are substantial, with major sedimentary packages deposited
995 associated with the transition to glacial conditions, in the Oligocene (in the southeast) to early Miocene (in
996 the northwest), and to full glacial conditions in the mid-Miocene [Lindeque et al., 2013], with substantial
997 shelf progradation since the late Miocene [Hochmuth and Gohl, 2019]. The youngest cover relates to
998 Quaternary sediments recovered in marine sediment cores which preserve normally consolidated, over-
999 compacted sediments and glacial till [Hillenbrand et al., 2014] as well as glacio-marine landforms in seabed
1000 topography [Arndt et al., 2017]. The distribution of these young units is not comprehensively mapped, and
1001 their thickness and age are likely to be highly variable. Nevertheless, we infer that the Weddell Sea has

1002 received sediment continuously since the Early Jurassic. To the south of the Weddell Ice Shelf, accumulations
1003 of water-saturated sediments are identified beneath the Bungenstock Ice Rise and extending into the
1004 Institute Ice Stream [Siegert *et al.*, 2016]. These sedimentary deposits overly a relatively shallow basement
1005 but are associated with elevated ice velocity suggesting control on ice sheet dynamics [Siegert *et al.*, 2016].

1006 3.3 East Antarctic Basins

1007 3.3.1 Weddell Coast

1008 The continental shelf in the eastern Weddell Sea preserves a sedimentary basin extending along the shelf
1009 from the Filchner Rift to the Fimbul Ice Shelf. The basin is associated with a volcanic rifted margin that
1010 initiated in the Jurassic [Jokat and Herter, 2016; Kristoffersen *et al.*, 2014], but also has upper Cenozoic to
1011 Quaternary sediment deposition [Hillenbrand *et al.*, 2014; Huang and Jokat, 2016; Kristoffersen *et al.*, 2014]
1012 recording repeated glacial advances. Magnetic data indicate the geology of the underlying basement with
1013 high frequency content indicating relatively thin basin cover throughout this basin. Magnetic data also image
1014 the Explora anomaly (Fig 9), associated with Jurassic magmatism [Hunter *et al.*, 1996] and a seaward-dipping
1015 reflector (SDR) sequence, the Explora Wedge [Kristoffersen *et al.*, 2014]. Seismic exploration on the Ekström
1016 Ice Shelf has demonstrated the Explora Wedge to extend beneath the ice shelf, with overlying sedimentary
1017 rocks of up to 1 km thickness [Kristoffersen *et al.*, 2014]. The boundary is marked by a prominent magnetic
1018 gradient that extends along the entire basin, which we infer to delineate the extent of the SDR sequence.
1019 Landward from this magnetic boundary, the basin is characterized by smooth topography with several ice
1020 rises interpreted as representing grounded ice on remnants of shelf sediments while adjacent troughs were
1021 eroded [Kristoffersen *et al.*, 2014].

1022 Inland, as well as extensive crystalline bed, several phases of basin formation are recorded. The oldest phase
1023 is preserved in outcrops on the Pensacola Mountains. The early Cambrian Hannah Ridge Formation was
1024 deposited after 563 Ma and prior to granite intrusion dated at 505 Ma [Curtis *et al.*, 2004]. The Hannah
1025 Ridge Formation is overlain by the Nelson Limestone and the Gambacorta Formation volcanics, dated at 501
1026 Ma. Overlying, the Late Cambrian Wiens Formation and Late Cambrian to Ordovician Neptune Group, were
1027 deposited during and after the Ross Orogeny [Curtis *et al.*, 2004]. Similar rocks may also be preserved in the
1028 Argentina and Shackleton Ranges [Evans *et al.*, 2018]. The second major phase comprises the Devonian to
1029 Permian Beacon Supergroup, including the Upper Devonian Dover Sandstone, the Carboniferous-Permian
1030 Gale Mudstone and the Permian Pecora Formation [Curtis, 2002]. As elsewhere, the Beacon Supergroup is
1031 preserved with characteristic mesa-like landforms in the Polar Gap Subglacial Highlands between Support
1032 Force and Recovery glaciers (Fig 9). Outliers of the Beacon Supergroup also occur on the Theron Mountains
1033 north of Slessor Glacier [Cox *et al.*, 2019]. There is no evidence for Beacon Supergroup to the north of the
1034 Theron Mountains, although the Paleozoic rocks of the Urfjell Group and Amelang Formation outcrop in
1035 western Dronning Maud Land [Cox *et al.*, 2019]

1036 Several type 1 basins are inferred, with a dominant westerly trend, and characterized by low topography,
1037 negative isostatic residual gravity and smooth beds. Major basins exist to the north and east and to the
1038 south of the Polar Gap Subglacial Highlands and are bounded to the east by the Recovery Subglacial
1039 Highlands (Fig 9). The southern basin, the Pensacola-Pole Basin, occupies an elongate trough 150-200 km
1040 wide. Sedimentary rocks in this basin thicken inland reaching a thickness of 3.6 ± 1.1 km [Paxman *et al.*,
1041 2019a]. The basin fill is interpreted to be dominated by the Beacon Supergroup, indicated by the presence of
1042 magnetic features interpreted to represent Jurassic dolerites, but also there is interpreted younger cover of
1043 up to 1 km thickness [Paxman *et al.*, 2019a]. We define the Foundation Basin as a smaller aligned
1044 depocenter with similar characteristics. The northern Recovery Basin occurs inland from the Recovery
1045 Glacier. No thickness for this basin is defined, however, its geophysical character is similar to the Pensacola-
1046 Pole basin. We suggest that the Foundation, Pensacola-Pole and Recovery subglacial sedimentary basins
1047 formed during Jurassic-Cretaceous rifting. This event generated the distinctive topography that was later
1048 incised by glaciers, removing several kilometers of sediments from glacier troughs [Paxman *et al.*, 2017].
1049 These troughs today do not host major basin fill. another major basin is interpreted associated with the
1050 northern Slessor Glacier (Fig 9). This basin has a particularly smooth bed throughout [Bamber *et al.*, 2006;
1051 Eisen *et al.*, 2020] and models of magnetic data suggest 3 km of post-Jurassic fill [Bamber *et al.*, 2006].

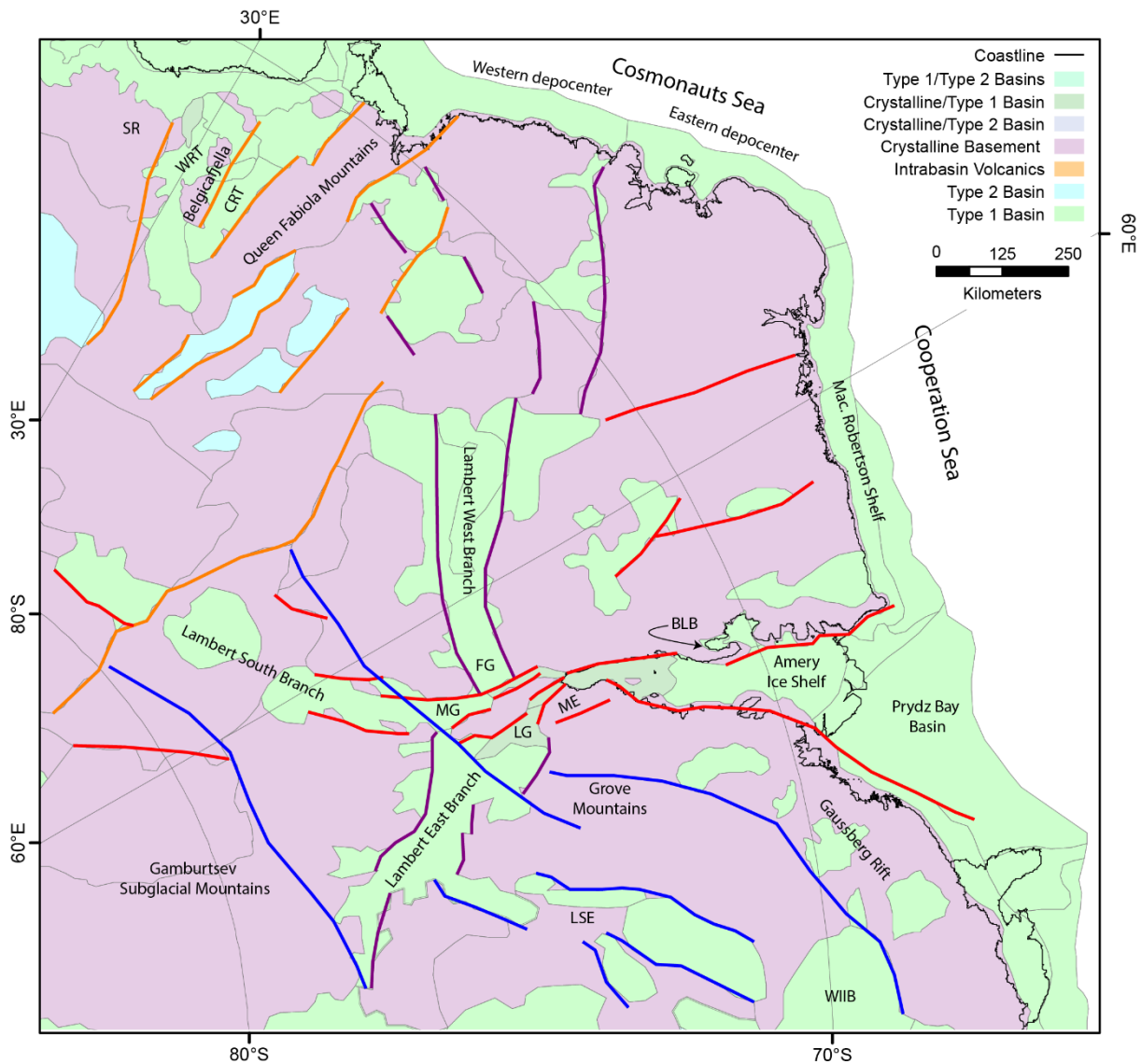
1052 3.3.2 Dronning Maud Land and Enderby Land

1053 Dronning Maud Land preserves evidence for a series of basin forming events. The most prominent is the
1054 Jurassic rifting associated with the Jutul-Penck Graben system, associated with localized crustal thinning
1055 associated with the Jutulstraumen and Pencksokket troughs, with high isostatic residual gravity, and smooth
1056 magnetic field patterns [Ferraccioli *et al.*, 2005a; Ferraccioli *et al.*, 2005b; Riedel *et al.*, 2013]. Interpreted
1057 type 1 basins in interior Dronning Maud Land region are parallel and may also represent this event.

1058 Sedimentary rocks of the ca. 1.1 Ga Ritscherflya Supergroup are exposed adjacent to the Jutulstraumen,
1059 representing a ~2 km thick basin forming on the eastern edge of the Grunehogna Craton, in an interpreted
1060 arc-proximal setting [Marschall *et al.*, 2013]. A series of north-south oriented ancient basins is interpreted in
1061 Interior Dronning Maud Land based on negative isostatic residual gravity and reduced subglacial roughness
1062 relative to their surroundings (Fig 3). One of these was modelled in the work of Eagles *et al.* [2018] who
1063 identified a sedimentary bed incised by a preserved fluvial landscape. The age of these basins is highly
1064 uncertain, however they overlie magnetic trends of the Tonian Ocean Arc Super Terrane [Ruppel *et al.*,
1065 2018], and are aligned with interpreted late Pan-African structures in the Sør Rondane region [Mieth and
1066 Jokat, 2014].

1067 The Dronning Maud Land escarpment separates the type 2 basins of the interior from interpreted type 1
1068 basins along the front of the escarpment, on the coastal plain and continental shelf. These basins are
1069 characterized by low, flat and smooth bed topography, sloping gently southward overall [Eisen *et al.*, 2020]

1070 and, onshore, negative isostatic residual gravity. Numerous ice-rises are present associated with
 1071 sedimentary banks, interpreted as remnant shelf sediments following erosion of adjacent troughs. These
 1072 basins are interpreted to reflect depocenters formed initially during the late Jurassic to Cretaceous
 1073 denudation of the Great Escarpment, and received sediment as part of the sedimentary pathway to the
 1074 major depocenters of the Riiser-Larsen Sea [Eagles *et al.*, 2018]. Further regions along the front of the
 1075 escarpment, and in localized topographic lows, also have relatively high basin likelihood [Li *et al.*, 2022], and
 1076 may represent piedmont deposits.



1077
 1078 *Figure 10: Sedimentary basins of the Enderby-Mac. Robertson and Lambert regions. Red structures indicate*
 1079 *structures aligned with the main north-south Lambert Rift trend while purple structures are aligned with the*
 1080 *east-west trend. Blue structures are aligned with Precambrian structures including the Gamburtsev Suture*
 1081 *[Ferraccioli *et al.*, 2011], the Ruker anomaly and Proterozoic basins in the southern Prince Charles Mountains*
 1082 *[McLean *et al.*, 2008]. Orange lines indicate structures associated with the Fuji Subglacial Highlands block. SR*
 1083 *– Sør Rondane, WRT – West Ragnhild Trough, CRT – Central Ragnhild Trough BLB – Beaver Lake Basin, FG –*

1084 *Fisher Glacier, MG – Mellor Glacier, LG – Lambert Glacier, ME – Mawson Escarpment, LSE – Lake Snow Eagle,*
1085 *WIIB – Wilhelm II Basin.*

1086 The Ragnhild Trough (Fig 10) is a major topographic feature cutting through the escarpment and in its
1087 coastal portion is interpreted to possess a fill of low-density sedimentary material [Eagles *et al.*, 2018], which
1088 is also topographically smooth [Eisen *et al.*, 2020], included here in the escarpment basin. The trough forms
1089 two ~100 km wide sub-troughs either side of Belgica Highlands (Belgicafjella), called West and Central
1090 Ragnhild Troughs, with low gravity, low to moderate topographic roughness and low magnetic roughness. To
1091 the east is the crystalline bed of the Queen Fabiola Mountains block. These linear troughs are interpreted as
1092 rifts forming during Paleozoic to Mesozoic rifting. Similar troughs are interpreted in Enderby Land,
1093 connecting to the west branch of the Lambert Rift System (Fig 10).

1094 The continental shelf fringing the Cosmonauts Sea is narrow, at ca 70 km width [Davis *et al.*, 2018]. Two
1095 separate depocenters are defined with the western depocenter having less rugged topography and lesser
1096 offshore sediment volume relative to the eastern depocenter [Davis *et al.*, 2018]. Seismic data over the shelf
1097 edge image a relatively thin package (0.5 to 2 km) of pre-to syn-rift sediments, with a more voluminous post-
1098 rift sequence [Stagg *et al.*, 2004]. While sedimentation on the shelf may be relatively limited, a substantial
1099 sediment volume was transported to the continental rise since the late Miocene [Hochmuth *et al.*, 2020].

1100 3.3.3 Lambert Graben and Prydz Bay

1101 Mac. Robertson Land is dominated by crystalline basement, with basins associated with the Lambert Rift
1102 System. The Lambert Rift System has a cruciform geometry, with the north-south aligned main branch
1103 extending inland for over 1500 km, complemented by eastern and western branches (Fig 10). Subsidence is
1104 greatest in the northern portion of the main branch, with more limited subsidence to the south, suggesting
1105 that the East and West branches may have accommodated differential strain. Smaller aligned basins are
1106 found on Mac. Robertson land, including the exposed Beaver Lake Basin. The Beaver Lake Basin preserves
1107 the mid-Permian to upper-Triassic Amery Group, comprising clastic sedimentary rocks, with coals in the
1108 lower sequence [McLoughlin and Drinnan, 1997]. These rocks represent a terrestrial depositional setting
1109 with overall north-directed sediment transport. Seismic studies on the Amery Ice Shelf resolve multiple
1110 layers of sedimentary rocks, with a thin layer of young sediments overlying an older package of interpreted
1111 glaciomarine origin [McMahon and Lackie, 2006]. In turn this overlies a > 5 km thick sequence of rift-related
1112 sedimentary rocks [Mishra *et al.*, 1999]. Cenozoic glaciomarine fjordal sedimentary rocks are mapped from
1113 within the Lambert Graben, indicating a series of glacial retreat events since the Oligocene or younger, and
1114 also significant Cenozoic uplift, with exposures preserved at up to 1500 m elevation [Hambrey and McKelvey,
1115 2000].

1116 Inland, the southern branch of the Lambert Rift System occupies the trough to the Mellor Glacier, while the
1117 eastern branch occupies the trough to the Lambert Glacier, and the western branch occupies the catchment
1118 of the Fisher Glacier [Ferraccioli et al., 2011]. Each has characteristics of low isostatic residual gravity
1119 anomalies and smooth topography. The southern branch has several further depocenters indicated
1120 upstream (Fig 10).

1121 Offshore, the Prydz Bay Basin is well-surveyed with relatively dense seismic coverage and multiple drill cores
1122 (Fig 1). The inner shelf is dominated by thick accumulations of Permian to Early Cretaceous sediments, with a
1123 thin veneer of Cenozoic cover [Stagg et al., 2004]. On the outer shelf a sequence is recorded prograding
1124 toward the northeast through the Cenozoic, marked by a number of erosion surfaces and marine deposition
1125 events [Whitehead et al., 2006]. Quaternary deposition is inferred to be present throughout the region
1126 [Whitehead et al., 2006]. The Mac. Robertson Shelf preserves a relatively thin cover of syn- to post-rift
1127 sedimentary rocks [Stagg et al., 2004], with a comparable Cenozoic sequence to the Prydz Bay Basin
1128 [Whitehead et al., 2006].

1129 3.3.4 Princess Elizabeth Land and Queen Mary Land

1130 The Princess Elizabeth Land shelf preserves a thin cover of upper Paleozoic to Cenozoic sedimentary rocks
1131 [Davis et al., 2018], with interpreted Precambrian basement at Drygalski Island, and, at Gaussberg, a volcano
1132 dated at 56 ± 5 ka [Smellie and Collerson, 2021]. Inland, the Princess Elizabeth Land region is dominated by
1133 crystalline basement, however, several regions are identified with subdued magnetic responses and
1134 relatively smooth topography that may represent remnant sedimentary basins. These are arrayed along the
1135 tectonic structure of the Gaussberg Rift, which may share an evolution with the Lambert Rift system
1136 [Golynsky and Golynsky, 2007]. A large basin (the Wilhelm II Basin) is identified with similar characteristics to
1137 the better-known Knox Basin further east (Fig 11). The interior of Princess Elizabeth Land until recently had
1138 one of the largest data gaps in Antarctica [Cui et al., 2020]. Early work identified a significant lake (Lake Snow
1139 Eagle) and associated canyon system [Jamieson et al., 2016] likely aligned with tectonic structures (Fig 10).
1140 More recent subglacial topography [Cui et al., 2020] identified a topographic depression that is aligned en-
1141 echelon with the Wilhelm II Basin and Lake Snow Eagle (Fig 10). We infer a sedimentary basin in this
1142 depression although other geophysical results are not yet available for corroboration.

1143 Queen Mary Land has the well-resolved and substantial Knox Rift system including several sedimentary
1144 depocenters aligned perpendicular to the coast [Maritati et al., 2016]. The basin system may extend over
1145 1000 km inland (Fig 11). This basin possesses up to 3 km of sedimentary rock fill that is interpreted to date
1146 primarily to the Permian-Triassic [Maritati et al., 2016; Maritati et al., 2020]. The region also preserves the
1147 Neoproterozoic to Ediacaran Sandow Group, exposed at the fringes of the Knox Basin [Mikhalsky et al.,
1148 2020]. The coastal region is dominated by Precambrian crystalline basement, including beneath the
1149 Shackleton Ice Shelf, with moderate to thin sedimentary cover interpreted for the Bruce Rise and the Knox

1150 Coast shelf. The Knox coastal plain preserves a low-relief surface [Eisen *et al.*, 2020] potentially indicative of
1151 a thin and relatively young sedimentary cover.

1152 3.3.5 Vostok and Gamburtsev Highlands

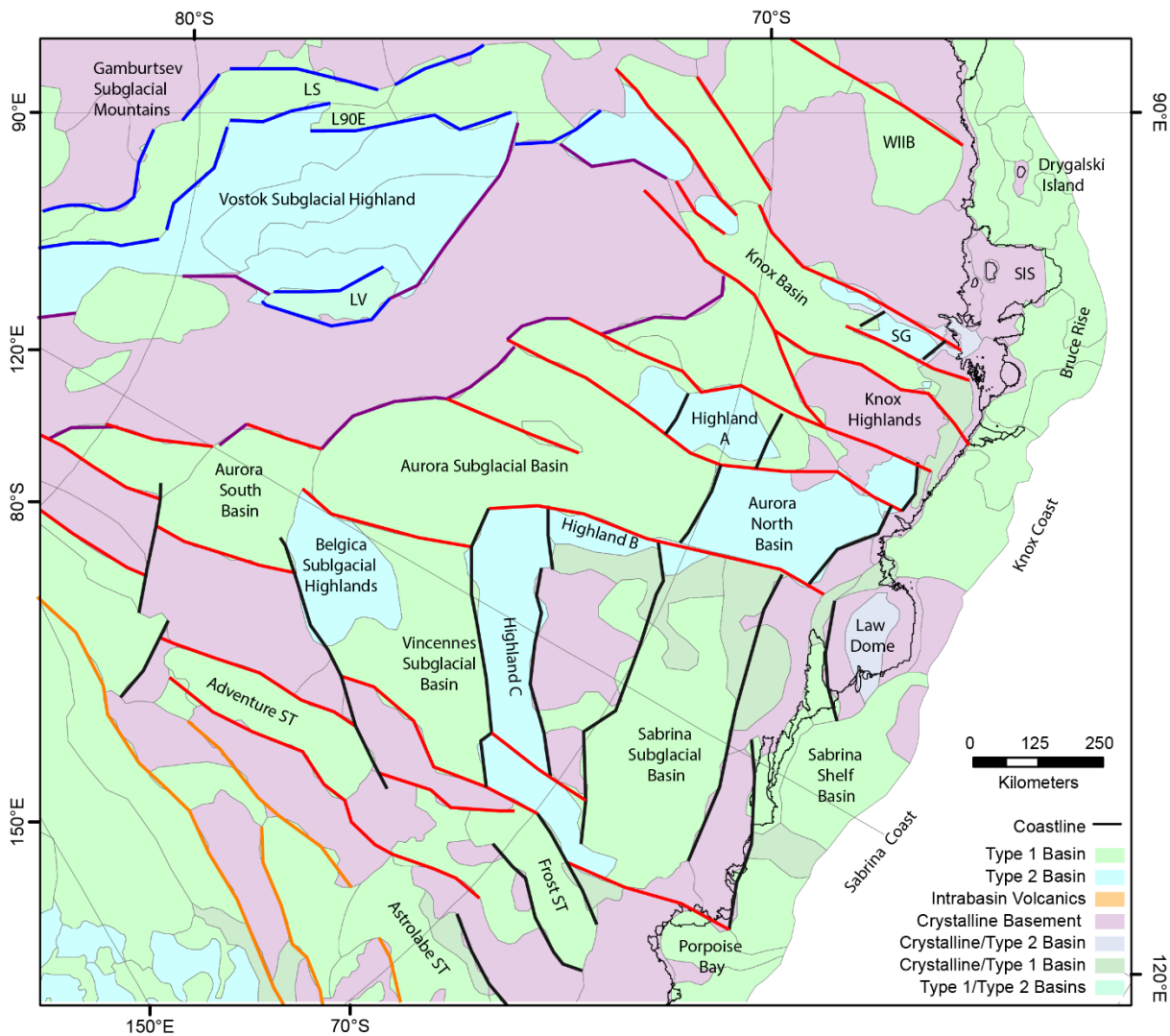
1153 The East Antarctic interior is defined by the subglacial highlands of the Vostok and Gamburtsev regions (Fig
1154 11). Subglacial Lake Vostok has been investigated with seismic techniques that return equivocal results
1155 [Siegert *et al.*, 2011]. Receiver function studies record a low-velocity zone beneath the lake bed, interpreted
1156 to represent a 4-5 km thickness of sedimentary rocks above a crystalline bed [Isanina *et al.*, 2009]. However,
1157 later seismic refraction experiments suggest instead that the lake bed is characterized by a relatively thin
1158 cover of sediments over an acoustically fast basement, likely to be crystalline basement [Leitchenkov *et al.*,
1159 2016]. The same study resolved a lower velocity bedrock for the highlands to the west of Lake Vostok. The
1160 western shore of Lake Vostok, and the lake itself possesses areas with predicted moderate to high
1161 sedimentary basin likelihood [Li *et al.*, 2022], indicated by low isostatic residual gravity anomalies and
1162 smooth magnetic field anomalies [Studinger *et al.*, 2003]. These characteristics notably do not extend to the
1163 eastern shore. While a thick type 1 sedimentary basin in Lake Vostok may not be supported, a type 2 basin is
1164 interpreted extending along the Vostok Subglacial Highland to the west of and beneath Lake Vostok (Fig 11).
1165 This may represent a flexural basin formed in response to collisional processes in the Neoproterozoic
1166 [Studinger *et al.*, 2003].

1167 The Vostok Highlands are separated from the Gamburtsev Subglacial Mountains by a prominent a low-lying
1168 region with relatively smooth bed, also including Lake Sovetskaya and Lake 90°E (Fig 11), forming the eastern
1169 branch of the EARS [Ferraccioli *et al.*, 2011]. This region is interpreted as a type 1 sedimentary basin
1170 although it is not associated with a gravity low, suggesting sedimentary fill is limited in thickness. The main
1171 range of the Gamburtsev Subglacial Mountains (GSM) is dominated by high elevation topography, high
1172 along-track roughness, and high spatial variability in elevation and magnetic data (Fig 2), all indicative of
1173 crystalline basement. To the west, a broad area with low and smooth topography, and low gravity separates
1174 the GSM from the Recovery Subglacial Highlands, suggesting a basin with substantial sedimentary fill,
1175 forming the western branch of the EARS [Ferraccioli *et al.*, 2011]. The southern flank of the GSM is also
1176 marked by a substantial gravity low, and relatively low roughness, indicating a possible sedimentary basin
1177 (Fig 3). The origin of this basin is not known, but it is aligned parallel to the South Pole Basin, and it may be
1178 an uplifted remnant that basin or part of an older basin system [cf McLean *et al.*, 2008].

1179 3.3.6 Wilkes Land and Terre Adelie

1180 Wilkes Land preserves an extensive sedimentary basin system including several major depocenters including
1181 the Aurora, Vincennes and Sabrina basins [Aitken *et al.*, 2014]. These basins are characterized by thick
1182 accumulations of sedimentary rocks, with as much as 10 km of fill possible in the Aurora Basin, but more

1183 typically ~5 km in Aurora, ~4 km in Vincennes and ~2 km in Sabrina Basin [Aitken et al., 2014; Aitken et al.,
 1184 2016b]. The Aurora and Vincennes basins are characterized most fundamentally by low gravity, a very
 1185 smooth surface, and subdued magnetic signals - this same characteristic defining southward extension of the
 1186 Aurora basin (Fig 11). The Sabrina basin has less smooth topography and magnetic data, nevertheless,
 1187 geophysical models suggest a preserved sedimentary basin of up to 3 km thickness that has been variably
 1188 eroded by ice sheet activity, exposing basement in places [Aitken et al., 2016b]. These inland basins are
 1189 separated from the Sabrina Coast by a basement ridge, likely also a feature of glacial erosion.



1190
 1191 *Figure 11: Sedimentary basins of the Vostok, Queen Mary Land, Aurora, and Terre Adelie regions. Purple lines*
 1192 *indicate older structures associated with collisional events [Studinger et al., 2003] while the blue lines*
 1193 *indicate interpreted EARS structures [Ferraccioli et al., 2011]. Black and Red structures indicate Paleozoic-*
 1194 *Mesozoic structures linked to the Knox, Aurora, Vincennes and Sabrina subglacial basins. Orange structures*
 1195 *indicate structures associated with the Wilkes Subglacial Basin, with slightly different trend. Structures*
 1196 *reinterpreted from prior studies [Aitken et al., 2014; Aitken et al., 2016a; Cianfarra and Salvini, 2016; Maggi*

1197 *et al., 2016; Maritati et al., 2016; Tabacco et al., 2006*]. LS – Lake Sovetskaya, L90E – Lake 90°E, LV – Lake
1198 Vostok, WIIB – Wilhelm II Basin, SIS – Shackleton Ice Shelf, SG – Sandow Group.

1199 Tonian to Ediacaran sedimentary rocks have been found in glacial erratics, indicating an early basin forming
1200 phase with potential links to the Centralian Superbasin of Australia [*Maritati et al., 2019*]. The region
1201 preserves several subglacial highlands that are interpreted in gravity models to be sedimentary in nature,
1202 including Highlands A, B and C, the region north of the Aurora Basin, and the Belgica Subglacial Highlands
1203 [*Aitken et al., 2016b*]. Thermochronology suggests that the highlands were uplifted and peneplained in the
1204 Permian-Triassic [*Maritati et al., 2020*], with the main phase of rifting at this time. Although the region was
1205 potentially reactivated during Jurassic-Cretaceous rifting events, to date, no evidence of this exists locally.

1206 Offshore sedimentary sequences along the Australian-Antarctic margin define four major sequences
1207 separated by unconformities of age 95-80 Ma, 65-58 Ma, 50-45 Ma and 34 Ma [*Sauermilch et al., 2019*]. The
1208 first sequence represents the rift-derived basin; the sequence is characterized by deltaic sediment
1209 deposition derived from continental river systems, while the third may derive from clockwise-circulating
1210 bottom currents developing in the Paleocene – Eocene with a decrease in sediment input [*Sauermilch et al.,*
1211 *2019*]. The Sabrina Shelf sedimentary basin may have begun forming at this time, with a distinctive
1212 terrestrial palynoflora interpreted to date to the latest Paleocene to earliest Eocene [*Smith et al., 2019a*].
1213 The Sabrina Shelf is covered by post-Cretaceous sedimentary cover with variable thickness up to 1.3 km
1214 seismically imaged [*Gulick et al., 2017; Montelli et al., 2019*]. Paleocene to late-Miocene strata record a
1215 history of Cenozoic ice sheet evolution including the identification of marine-terminating glaciers in the early
1216 to middle Eocene, a series of retreat and advance events in the Oligocene and Miocene, and an expanded
1217 EAIS since the late Miocene [*Gulick et al., 2017*]. The fourth offshore sequence represents the glacial
1218 development of the margin with in particular the deposition of a high-volume of sediments since the
1219 Oligocene, including apparently variable supply from glacial outlets through time [*Hochmuth et al., 2020;*
1220 *Hochmuth et al., 2022*].

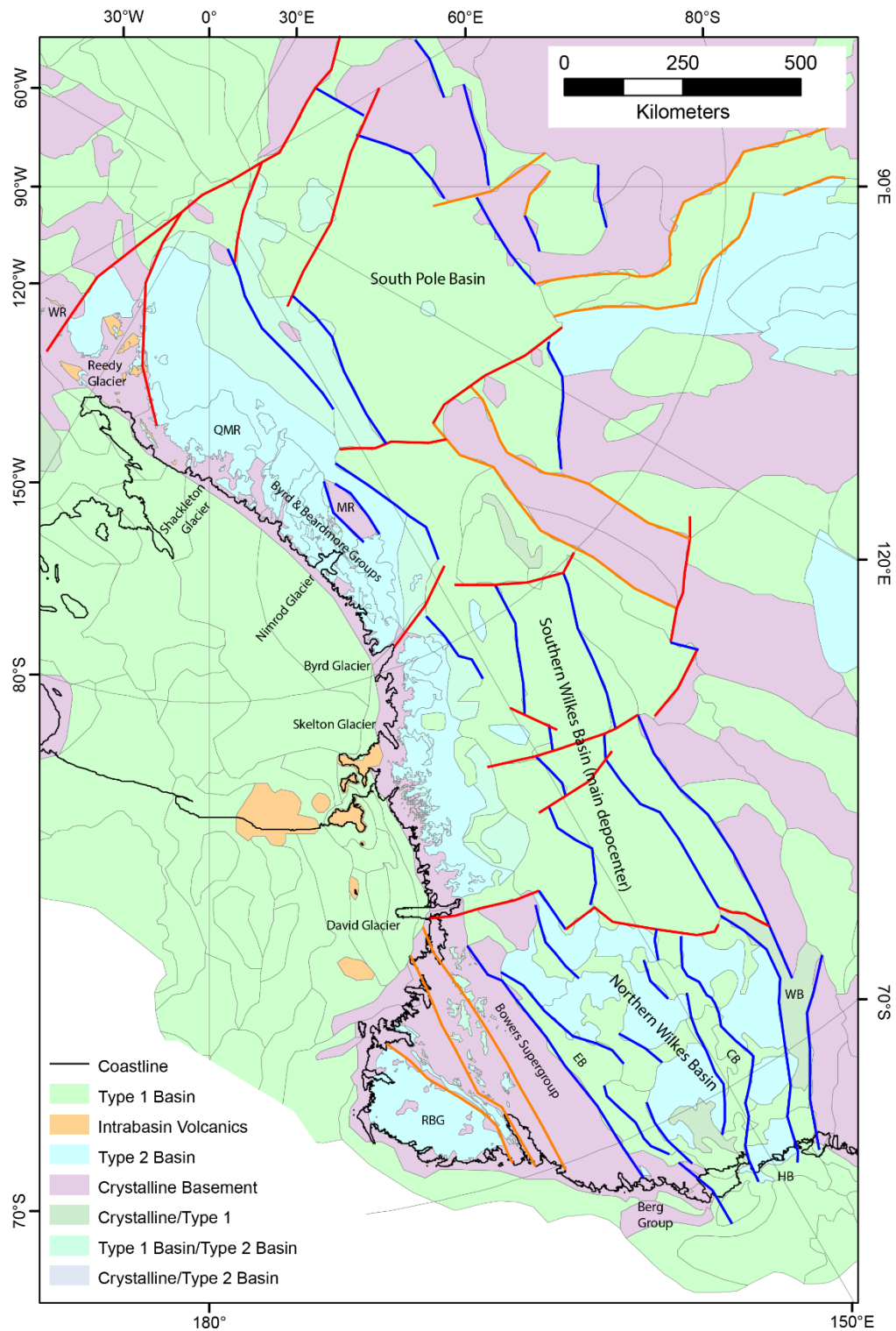
1221 The Terre Adelie Craton provides the eastern boundary to this basin region, with a basement-dominated
1222 ridge extending 1800 km inland from Porpoise Bay. Several smaller basins are identified within this ridge
1223 including the Frost Subglacial Basin, and the Astrolabe and Adventure Subglacial troughs. Smooth beds [*Eisen*
1224 *et al., 2020*] and low gravity suggest these depressions host sedimentary basins, although their age is not
1225 known [*Aitken et al., 2014; Frederick et al., 2016*]. Offshore Terre Adelie, seismic data record the transition
1226 from a deformed Cretaceous rift on the innermost shelf, through a Paleocene to Eocene transpressional
1227 phase, younging to Plio-Pleistocene strata at the shelf edge [*De Santis et al., 2003*], representing
1228 progradation of the shelf through since the Eocene [*Hochmuth and Gohl, 2019*]. Maximum observed
1229 sedimentary thickness is 1.6 km [*De Santis et al., 2003*]. The Mertz and Adelie banks are prominent

1230 bathymetric features representing remnant shelf-sediments, with adjacent basins incised by past glacial
1231 action [Beaman *et al.*, 2011].

1232 3.3.7 Wilkes Subglacial Basin, South Pole Basin and Transantarctic Mountains

1233 The Beacon Supergroup are prominent along the Transantarctic Mountains (TAM) extending from northern
1234 Victoria Land, where outcrop is relatively sparse, to prominent and near continuous exposures extending
1235 from David Glacier to the Ohio Range [Elliot *et al.*, 2017]. The Beacon Supergroup comprises the basal Taylor
1236 Group and the overlying Victoria Group. The Taylor Group consists of Devonian clastic sedimentary rocks,
1237 predominated by shallow marine sediments grading to fluvial sediments [Bradshaw, 2013]. The
1238 unconformably overlying Victoria Group and regional equivalents consists of Permian-Triassic siliciclastic and
1239 volcanoclastic rocks also including glacial deposits and coal beds [Elliot *et al.*, 2017]. Ongoing sedimentation
1240 into the Jurassic is identified from younger rocks exposed along the Transantarctic Mountains including the
1241 Jurassic Section Peak Formation of northern Victoria land, the Mawson Formation of southern Victoria Land
1242 and the Hanson Formation in the central TAM [Elliot *et al.*, 2017]. The sequence is overlain and intruded by
1243 mafic magmatic rocks of the Ferrar Group, often forming the caps to mesa-like exposures. In the context of
1244 their exposed extent the Beacon Supergroup are classed as type 2 basins.

1245 Likely Beacon Supergroup correlatives are exposed at Horn Bluff, on the Wilkes Land coast and also,
1246 magnetic features consistent with Ferrar Group dolerite intrusions are found throughout the northern
1247 Wilkes Subglacial Basin [Ferraccioli *et al.*, 2009a]. From these observations we may infer the Beacon
1248 Supergroup as the dominant sedimentary fill in the Wilkes Subglacial Basin. The Wilkes Subglacial Basin
1249 extends for 1600 km along the edge of the Terre Adelie Craton. The basin may be divided into a southern
1250 sub basin, which consists of a single broad depocenter, with a substantial thickness of sedimentary rocks (~ 5
1251 km) extending to 81°S, in line with the Byrd Glacier [Frederick *et al.*, 2016]. Thinner cover extends
1252 southwards to roughly 84°S, in line with the southern end of the Miller Range. The northern sub-basin
1253 consists of three smaller depocenters and more variable sedimentary cover [Frederick *et al.*, 2016]. Magnetic
1254 analysis suggests possible rifting post-dating the intrusion of the Ferrar Group, and interpreted to be
1255 Cretaceous in age, possibly with Cenozoic reactivation [Ferraccioli *et al.*, 2009a; Jordan *et al.*, 2013a]. The
1256 discontinuity between these basin regimes (Fig 12) connects to the David Glacier and is aligned with several
1257 right-lateral transcurrent faults in northern Victoria Land [Ferraccioli *et al.*, 2009a], that also influenced the
1258 Cenozoic evolution of the Ross Sea [Salvini *et al.*, 1997]. The Wilkes Subglacial Basin is continuous with a
1259 further subglacial sedimentary basin located near the South Pole [Wannamaker *et al.*, 2004]. The furthest
1260 extent of the South Pole Basin is aligned with a structural lineament extending from the South Pole through
1261 the TAM near the Reedy Glacier (Fig 12).



1262

1263 *Figure 12: The Transantarctic Mountains and the Wilkes and South Pole subglacial sedimentary basins. Blue*
 1264 *lines indicate major rift structures of the Wilkes and South Pole subglacial basins and red lines major cross-*
 1265 *basin discontinuities. Orange lines indicate structures from other events. Structures reinterpreted from*
 1266 *[Ferraccioli and Bozzo, 2003; Ferraccioli et al., 2009a; Frederick et al., 2016; Jordan et al., 2013a; Wilson,*
 1267 *1999]. WR – Wisconsin Range, QMR – Queen Maud Range, MR – Miller Range*

1268 Several Neoproterozoic to early Paleozoic sedimentary packages occur along the TAM. Ediacaran
1269 sedimentary rocks are preserved including the Berg Group (northern Victoria Land) and the Beardmore
1270 Group (central and southern TAM), with also metasedimentary units including the Rennick Schist and
1271 Priestley Formation (northern Victoria Land) and Skelton Group (southern Victoria Land) [Goodge, 2020].
1272 Detrital zircon populations indicate these units were deposited after ca 1000 Ma, while Ross Orogeny
1273 metamorphism and granite intrusions provide a lower bound of 600 – 550 Ma; volcanic horizons in the
1274 Skelton Glacier area and Beardmore Group return compatible ages of 670-650 Ma [Goodge, 2020]. The TAM
1275 also preserves extensive lower Paleozoic successions. These include in northern Victoria Land the Bowers
1276 Supergroup, comprising the Sledgers, Mariners and Leap Year Groups, exposed in the Bowers Terrane and
1277 the Robertson Bay Group exposed in the Robertson Bay Terrane. The Bowers Supergroup was deposited in a
1278 marine to terrestrial setting in the Cambrian, deposition beginning prior to 520 Ma and ceasing after 480 Ma
1279 [Goodge, 2020]. The Robertson Bay Group was deposited in a deep marine setting in the early Ordovician,
1280 after 490-465 Ma. The TAM between David Glacier and Byrd Glacier does not preserve a comparable lower
1281 Paleozoic sequence but south of Byrd Glacier the Cambrian-Ordovician Byrd Group is interpreted to extend
1282 to the Shackleton Glacier [Goodge, 2020]. The Byrd Group contains a lower sequence of carbonate rocks
1283 (Shackleton Limestone, 525-515 Ma) transitioning upwards to carbonate-clastics (Holyoake Formation) and
1284 then siliciclastic sedimentary rocks (Starshot Formation and Douglas Conglomerate, 515 – 480 Ma). These
1285 are interpreted to represent the transition from a pre-Ross Orogeny carbonate platform to syn-orogenic
1286 molasse deposit [Goodge, 2020]. The southern TAM, extending from the Queen Maud Range to the
1287 Wisconsin Range preserves the lower Paleozoic siliciclastic LaGorce Formation and Duncan Formation. These
1288 formations contain detrital zircons dated at ~ 560-550 Ma suggesting they were deposited in the early
1289 Cambrian and are intruded by hypabyssal volcanic rocks of the Liv Group dated at 526 Ma. The Liv Group
1290 preserves an early Cambrian lower sequence of silicic volcanics and a middle to late Cambrian upper
1291 sequence of bimodal volcanics.

1292 4 Tectonic architecture, basin formation and the paleolandscape of 1293 Antarctica

1294 Antarctica's sedimentary basins have developed in several key phases in accordance with the evolving plate-
1295 tectonic system. Early phases associated with Pre-Ediacaran tectonic events are well defined at regional
1296 scale, however, their plate tectonic setting remains in many cases cryptic with respect to the global plate
1297 system. The type 1 basins recognized in this study have predominantly developed since the Ediacaran and
1298 we focus on these.

1299 4.1 Tectonic structure of Antarctica's lithosphere

1300 The development of sedimentary basins occurs in parallel with the development of the crust and the
1301 lithospheric mantle beneath. The structure of the crust and mantle have been investigated in a number of
1302 recent studies that reveal key features of relevance to understanding the basin distribution [*An et al.*, 2015;
1303 *Pappa et al.*, 2019a; *Shen et al.*, 2017; *Shen et al.*, 2018] [*Chaput et al.*, 2014; *Hazzard et al.*, 2022; *Lloyd et*
1304 *al.*, 2015; *Lloyd et al.*, 2020]. Most critical to basin forming is the development of accommodation space due
1305 to tectonic subsidence. Most commonly, the thinning of the lithosphere under extension is the main driver
1306 of subsidence.

1307 Antarctica's crustal thickness (Fig 13a) reflects to a large degree the history of extension events that have
1308 occurred since Pangea times, and thinner crust is highly correlated with the presence of major basins,
1309 whereas basement dominated regions tend to have substantially thicker crust. This is most notable in the
1310 Ross and Weddell regions where very thin crust ($h < 15$ km) is linked to the major basin systems in these
1311 regions. This relationship is not universal, and the southern Wilkes Basin and the Aurora Basin are underlain
1312 by thicker crust ($h > 30$ km), suggesting that basin subsidence here was not driven by crustal thinning. Type 2
1313 basins including those in the Vostok Highlands, TAM and Dronning Maud Land regions often overlie thick
1314 crust.

1315 In addition to crustal thickness lithospheric thinning may lead to the upwelling of asthenospheric mantle.
1316 Initially surface uplift is typical due to mantle heating, and then a prolonged post-rift thermal subsidence
1317 phase as the mantle cools over hundreds of millions of years. Lithospheric thickness (Fig 13b) is closely
1318 associated with the thermal state of the mantle, and areas of thin lithosphere are associated with recent to
1319 ongoing tectonic events. Thin lithosphere in West Antarctica is associated with the WARS, and recent higher-
1320 resolution models [*Hazzard et al.*, 2022] suggest it may be less than 30 km thick in regions with recent
1321 volcanism including the Terror Rift, Marie Byrd Land, the Siple Coast and the Antarctic Peninsula. Thicker
1322 lithosphere is found through the Eastern Basin of the Ross Sea, central West Antarctica and Ellsworth-
1323 Whitmore and Haag regions. The Jurassic Weddell Sea Rift System has a lithosphere thickness of ~ 100 km.

1324 In central East Antarctica the thickest lithosphere exceeding 200 km thickness, is centered on the Recovery
1325 Subglacial Highlands, the Gamburtsev Mountains and the Vostok Highlands. The effect of the EARS on the
1326 lithosphere is not clearly delineated, although narrow rifts of ca 100 km width may be below the resolution
1327 of the seismic models for East Antarctica. The major basins of East Antarctica are not all clearly associated
1328 with thinned lithosphere and notably Aurora, Vincennes, South Pole and Southern Wilkes basins all overly
1329 lithosphere exceeding 150 km thickness. The lack of a basin-aligned thermal anomalies suggests that these
1330 basins are probably associated with rifting occurring prior to the Jurassic. The Pensacola-Pole, Recovery and
1331 Sabrina basins rest on more moderate lithosphere thickness, potentially representing partial reactivation,

1332 although other influences on the lithosphere thickness are complicating factors. The Lambert, Slessor Glacier
 1333 and northern Wilkes basins are associated with thinner lithosphere, supporting a more recent (post-Triassic)
 1334 rifting and thermal reactivation in those basins. Thinned lithosphere is observed around the East Antarctic
 1335 margin including lithospheric embayments beneath northern Victoria Land, the southern TAM, Dronning
 1336 Maud Land, Enderby Land, the Sabrina Coast and Terre Adelie.

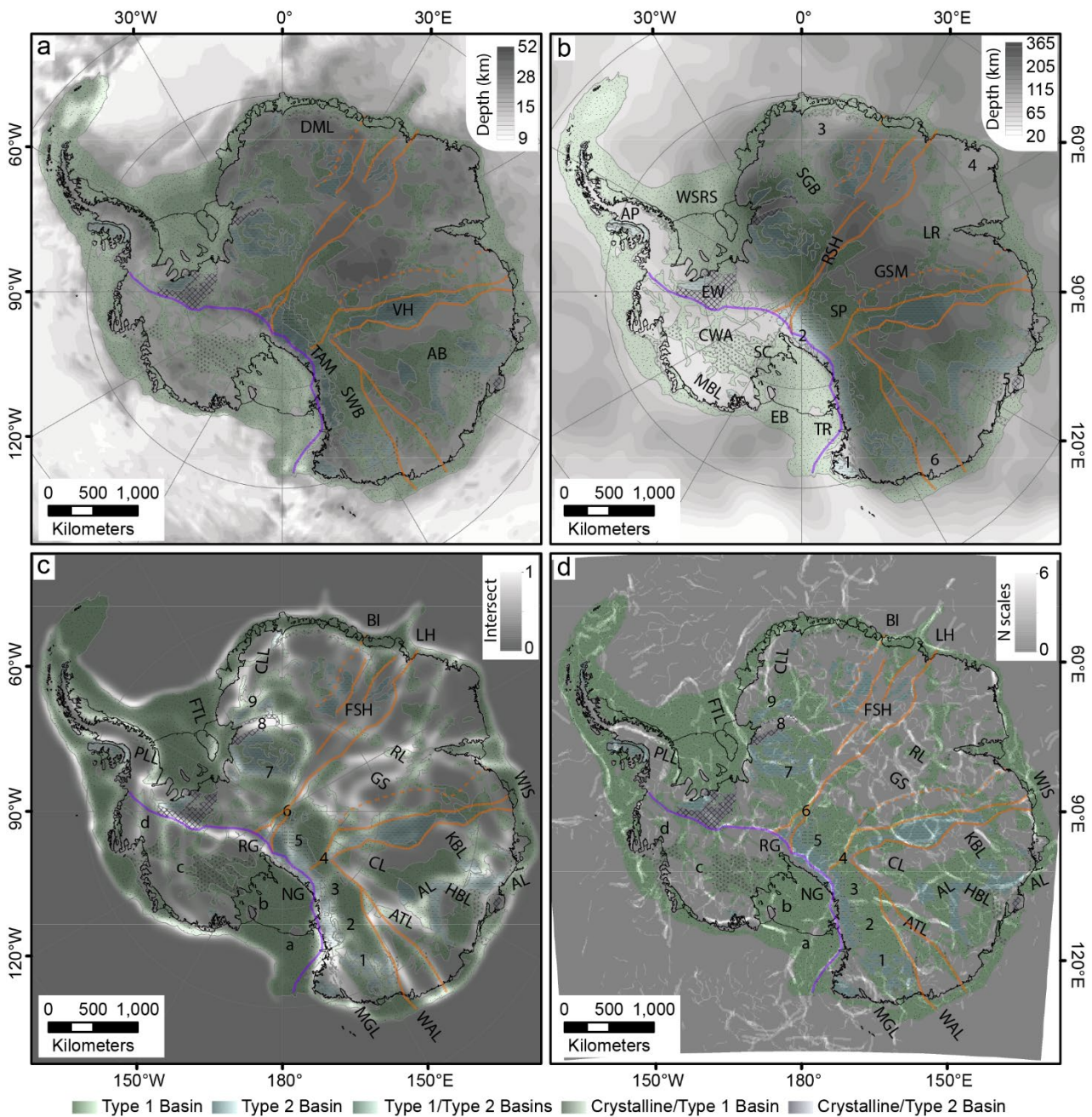


Figure 13: Structure of the Antarctic lithosphere showing basins over a) Moho depth [Pappa et al., 2019a], b) lithosphere-asthenosphere boundary depth [Hazzard et al., 2022], 1 to 6 indicate lithospheric embayments around the East Antarctic margin c) multidata lineament analysis [Stål et al., 2019] and d) multiscale gravity edge analysis. Labelling: a to d cross-rift structures in the WARS, 1 to 9 cross-basin structures in the Beacon Basin, PLL – Palmer Land Lineament, FTL – Filchner Trough Lineament, CLL – Coats Land Lineament, RL – Ruker Lineament, GS – Gamburtsev Suture, KBL Knox Basin Lineament, AL -Aurora lineament, HBL – Highland

1344 *B Lineament, CL – Concordia lineament, ATL -Adventure Trough Lineament, WAL – Wilkes-Adelie Lineament,*
1345 *MGL – Matusevich Glacier Lineament. All images show the WARS bounding TAM front in purple and the East*
1346 *Antarctic lineament sets in orange. WSRS – Weddell Sea Rift System, NG – Nimrod Glacier, RG – Reedy*
1347 *Glacier, GR – Gunnerus Ridge, FSH – Fuji Subglacial Highlands, WIS – West Ice Shelf, DML – Dronning Maud*
1348 *Land, VH – Vostok Highland, AB – Aurora Subglacial Basin, SWB – Southern Wilkes Basin, TAM –*
1349 *Transantarctic Mountains, AP -Antarctic Peninsula, CWA – Central West Antarctica, MBL – Marie Byrd Land,*
1350 *SC – Siple Coast, EB - Eastern Basin, TR – Terror Rift, SP – South Pole Basin, RSH – Recovery Subglacial*
1351 *Highlands, SGB – Slessor Glacier Basin, LR – Lambert Rift, GSM - Gamburtsev Subglacial Mountains.*

1352 In rifting, crust and lithospheric scale structures control the locus of deformation, and strongly influence the
1353 shape and internal structure of basins. Integrated lithospheric scale structures were investigated by [Stål et
1354 al., 2019], who analyzed bed topography, gravity, and seismic tomography models to delineate indicate the
1355 major boundaries of the lithosphere (Fig 13c). We apply a multiscale gravity edge detection approach to the
1356 Bouguer anomaly (Fig 13d). Phase-congruent multiscale edges [Kovesi, 1999] were delineated for 6 scales
1357 with upward continued datasets at 20, 30, 40, 50, 60 and 80 km height; for each of these three sub-scales
1358 were analyzed for phase congruency using windows of 3, 6 and 12 times the height. Ultimately, the analysis
1359 resolves phase-congruent structures between 60 km and 960 km width. Overall, the gravity analysis provides
1360 finer-scaled structures than the integrated lithospheric analysis.

1361 Both analyses indicate major basin-bounding structures of the lithosphere including the WARS-bounding
1362 structures of the TAM front and Bentley Subglacial Trough but also several more subtle basin-aligned
1363 features including in the Ross Sea, and along the Siple Coast, the Pine Island Rift and the Byrd Subglacial
1364 Basin (Fig 10c). The boundaries of the Weddell Sea Rift system are clearly defined including the boundary
1365 with Palmer Land (the Palmer Land Lineament) and the Filchner Trough (the Filchner Trough Lineament),
1366 with again several smaller structures associated with the internal structure of the basin. The gravity analysis
1367 defines additional lineaments associated with the Orion and Explora magnetic anomalies (Fig 13d)

1368 In East Antarctica, key basin-bounding features defined include both the eastern and western edges of the
1369 northern Wilkes Subglacial Basin, with the western boundary (the Wilkes Adelie Lineament) extending inland
1370 for at least 1200 km, while the eastern boundary (the Matusevich Glacier Lineament) is truncated against
1371 the TAM front near David Glacier. Numerous cross-basin structures are seen including the division of
1372 northern and southern WSB, near David Glacier, the boundary with the South Pole Basin near Nimrod
1373 Glacier, and the truncation of the South Pole Basin near Reedy Glacier (Fig 13). Beyond, the Polar Gap
1374 Subglacial Highland is bounded by lineaments associated with Support Force and Recovery Glaciers, and the
1375 final boundary of the Beacon Supergroup basin is seen aligned with Bailey Glacier. Beyond Bailey Glacier the
1376 north-south oriented Coats Land lineament relates to basement structures, likely of Precambrian age, with a
1377 minor basin formed to its west.

1378 The Adventure Subglacial Trench is bounded to the west by a prominent north-south oriented lineament
1379 (the Adventure Trough Lineament) while a parallel structure to the west bounds the Belgica Subglacial
1380 Highlands from the Aurora Subglacial Basin (the Concordia Lineament). The southern boundary of the ASB
1381 possesses a substantial gravity boundary, linked to topographic boundary and truncation of magnetic trends
1382 [Aitken *et al.*, 2014], however it is not associated with a lineament in either analysis. This indicates a diffuse
1383 gradient that is not phase-congruent and may indicate a shallow-dipping structure. The northern edge of the
1384 ASB is associated with a lineament (the Aurora Lineament) trending northwest-southeast towards the Knox
1385 Coast. The northwest-southeast lineament is disrupted by the north-south trending Highland B lineament
1386 and a similar structure to the west defines the eastern boundary of the Knox Subglacial Basin (the Knox Basin
1387 Lineament). Lambert also has a complex structure including the analysis of [Stål *et al.*, 2019] the main north-
1388 south graben, although this is less obvious in the gravity analysis and in both east-west to northwest-
1389 southeast boundaries aligned with basins. In the gravity data analysis, additional northeast-southwest
1390 lineaments are identified aligned with the magnetic Ruker magnetic anomaly (the Ruker Lineament) and the
1391 Gamburtsev suture representing structures in the Precambrian basement [Ferraccioli *et al.*, 2011; McLean *et*
1392 *al.*, 2009].

1393 At the largest scale, we can see in these analyses and models the division of East Antarctica into several
1394 major domains by prominent sets of lineaments along structural culminations. The first lineament set is
1395 observed extending along the Terre Adelie Highlands, bounding the Wilkes Subglacial Basin from the Aurora
1396 region. This trend reflects fundamental boundaries in the geometry of the Mawson continent and its
1397 Neoproterozoic margin [Aitken *et al.*, 2016a; Studinger *et al.*, 2004].

1398 The second set extends from near Nimrod Glacier, along the Vostok Subglacial highlands, where they bound
1399 the Vostok Highlands Basin and lake Vostok Basin, and reaching the coast near the West Ice Shelf. A
1400 potential sub-set to the west extends along a similar trend transecting the Gamburtsev Subglacial
1401 Mountains, Princess Elizabeth Land and emerging into Prydz Bay. In part this trend may represents the EARS
1402 [Ferraccioli *et al.*, 2011], which dominates the domain to the west but likely also is aligned with a more
1403 fundamental lithospheric boundary associated with Neoproterozoic collision [Mulder *et al.*, 2019; Studinger
1404 *et al.*, 2003].

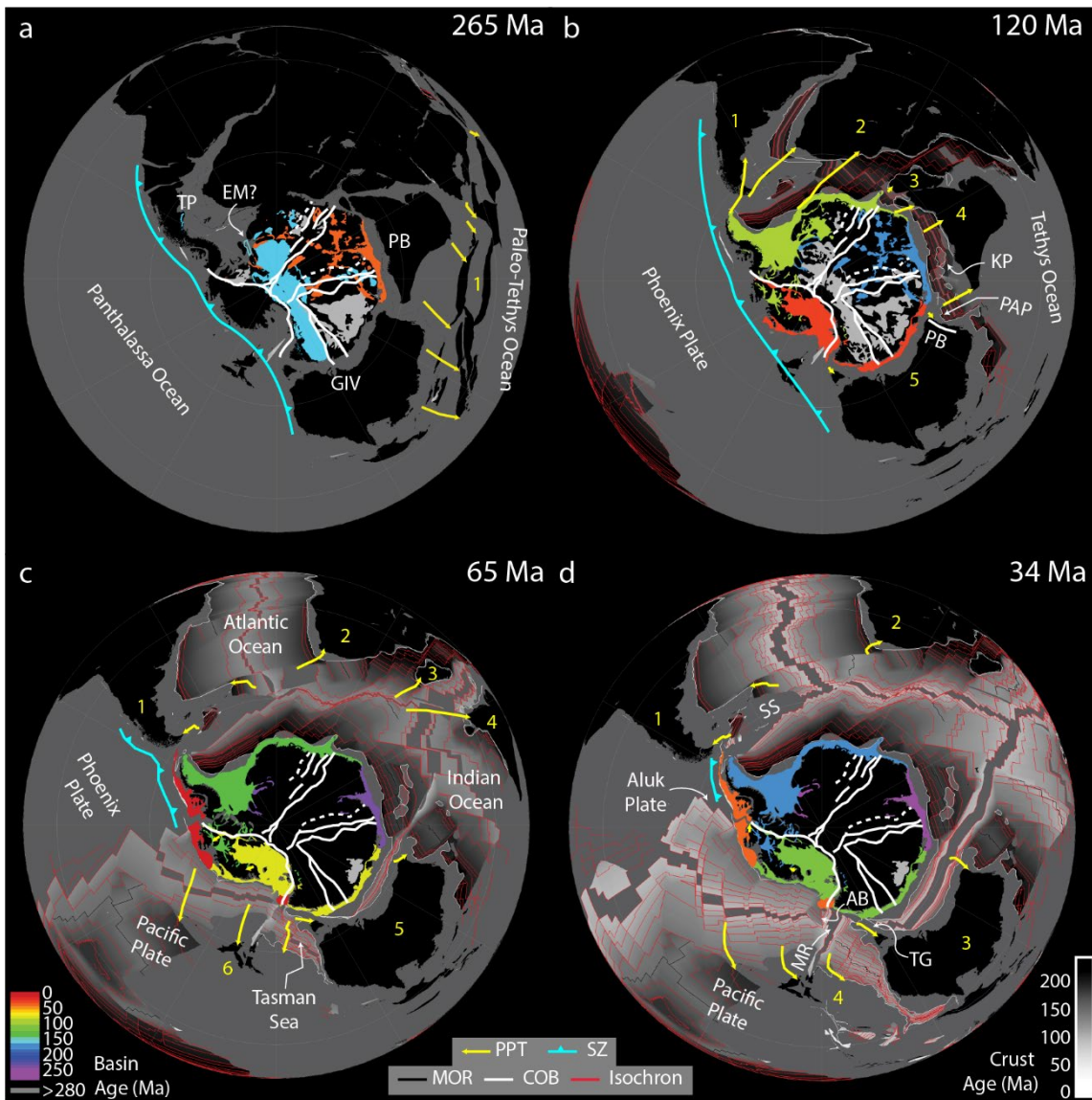
1405 A third set of lineaments extends from Reedy Glacier, through South Pole, extending along the Recovery
1406 Subglacial Highland, and then either side of the Fuji Subglacial Highlands, with branches emerging into
1407 Lutzow-Holm bay, the West Ragnhild Trough and possibly also Borchgrevinkisen. In its southern portion, this
1408 structure separates the South Pole Basin from the Pensacola Pole Basin and is linked to the formation of the
1409 Pensacola Embayment, interpreted in the late Neoproterozoic [Jordan *et al.*, 2022]. To the north, the Fuji
1410 Subglacial Highlands culmination separates the basin-dominated regions to the west (Recovery, Slessor and
1411 Interior DML), and east (Lambert).

1412 These lineament sets represent fundamental structures of the Antarctic lithosphere dating to at least the
1413 Neoproterozoic, but their impact on later tectonics and basins is profound. In a Gondwana reconstruction,
1414 the Fuji Subglacial Highlands lineament trend is aligned with the eventual Africa-Madagascar-Sri Lanka triple
1415 junction, the Vostok Highlands lineament trend is aligned with the Kerguelen Plateau, and the Terre Adelie
1416 Highlands trend is linked to the George V fracture zone of Australian-Antarctic basin (Fig 14). The four
1417 domains of East Antarctica have clearly different basin systems with distinct geometries and structural
1418 trends, with broadly the Pensacola-Recovery-Slessor rift system [Paxman *et al.*, 2017; Paxman *et al.*, 2019a],
1419 the EARS [Ferraccioli *et al.*, 2011], the Aurora-Vincennes-Sabrina system [Aitken *et al.*, 2014], and the Wilkes
1420 Subglacial Basin system [Ferraccioli *et al.*, 2009a; Jordan *et al.*, 2013a; Jordan *et al.*, 2022].

1421 4.2 Phase 1 - Ediacaran to Carboniferous

1422 During the Ediacaran to early Cambrian, a continuous East Antarctica was formed as part of Gondwana,
1423 assembled through the East-African (~650 to ~550 Ma) and Kuunga (~550 to ~490 Ma) orogens. The exact
1424 locations of the associated lithospheric boundaries beneath the ice sheet are not known well, however, it is
1425 likely that type 2 basins in the continental interior potentially formed during these events, including in
1426 Dronning Maud Land, the Vostok Highlands, the Aurora/Sabrina region and the Knox region. In the same
1427 timeframe, the edge of East Antarctica was evolving as a passive margin [Jordan *et al.*, 2022] with associated
1428 basin forming events [Goodge, 2020]. Ediacaran subduction was initiated along the paleo-Pacific margin of
1429 Gondwana. The onset of the Ross Orogeny, marked by metamorphism from 615 Ma and magmatism from
1430 590- 565 Ma [Goodge, 2020] and associated deformation events, saw a change in the locus and nature of
1431 basin formation towards the edge of the craton, with the orogeny ending ~470 Ma when the margin
1432 retreated [Goodge, 2020].

1433 Cambrian to Ordovician sedimentary basins deposited along this margin are interpreted to have formed in
1434 association with arc-related magmatism of the Ross Orogeny, continuing into the post-tectonic phase. Basins
1435 typically include an Early to Middle Cambrian sequence of pre- to syn-orogenic units (e.g. Bowers
1436 Supergroup, Byrd Group, Hannah Ridge Formation, Heritage Group) and a Late Cambrian to Ordovician syn-
1437 to post-orogenic sequence (e.g. the Robertson Bay Group, the Swanson Formation, Neptune Group,
1438 Crashsite Group). Both the Ellsworth-Whitmore and western Marie Byrd blocks were probably adjacent to
1439 East Antarctica at this time [Jordan *et al.*, 2020]. Global tectonic reconstructions of this time period lack
1440 detail relative to those from the Devonian onwards and for regional tectonic reconstructions of this time
1441 period the reader is referred to several regional syntheses [Boger, 2011; Goodge, 2020]. Cambro-Ordovician
1442 basement exhumation occurred inland from the central TAM region as recorded in low temperature
1443 thermochronology [Fitzgerald and Goodge, 2022].



1444

1445 *Figure 14: Tectonic reconstruction snapshots a) 265 Ma, b) 120 Ma, c) 65 Ma and d) 34 Ma showing the*
 1446 *context of basin formation since Pangea [Müller et al., 2019; Young et al., 2019]. East Antarctica is held fixed*
 1447 *in this reconstruction which also does not include rift block motions not involving ocean spreading. Basins are*
 1448 *shown from their base-of-basin age to their top-of-basin age, with basin age indicating the time elapsed*
 1449 *since the former. Each image also shows the major lithospheric boundaries (see Fig 13). Past plate*
 1450 *trajectories (PPTs) are shown for departing plates for the following time periods a) 280 to 265 Ma 1 -*
 1451 *Cimmeria, b) 180 to 120 Ma 1 – South America, 2 – Africa, 3 – Madagascar, 4 -Greater India, 5 - Australia c)*
 1452 *90 to 65 Ma 1 – South America, 2 – Africa, 3 – Madagascar, 4 -Greater India, 5 – Australia, 6 – Zealandia, and*
 1453 *d) 64 to 34 Ma, 1 – South America, 2 – Africa, 3 –Indo-Australia 4 – Zealandia/Pacific. TP – Trinity Peninsula,*
 1454 *EM – Ellsworth Mountains (inferred location) PrB – Prydz Bay, GIV George IV land, KP – Kerguelen Plateau*
 1455 *PAP - Perth Abyssal Plain. PeB – Perth Basin, DP – Drake Passage, SS – Scotia Sea, AB – Adare Basin TG –*
 1456 *Tasman Gateway.*

1457 The Devonian is marked by the deposition of the lower Beacon Supergroup in an interpreted continental
1458 retro-arc setting within Gondwana [Bradshaw, 2013]. This basin is exposed as type 2 in the mountains from
1459 Northern Victoria Land to the Theron Mountains and is also preserved as type 1 in the hinterland. The
1460 distinction of type 1 and type 2 in this case is primarily a consequence of later uplift of the TAM and
1461 potentially also downfaulting of the hinterland [Ferraccioli et al., 2009a], and we infer for the Devonian a
1462 single sedimentary basin system (the Beacon Basin) with low-elevation throughout. The system was divided
1463 along-strike into distinct depocenters with up to 9 major divisions along its length (Fig 13). The internal
1464 divisions are marked by changing thickness and morphology of the type 1 basins, while for type 2 basin in
1465 the TAM the variable extent of Beacon Supergroup exposures along strike may represent thickness
1466 variations coupled with differential uplift in later events [Brenn et al., 2017; Shen et al., 2017; Wannamaker
1467 et al., 2017]. Offsets to the basin margins and the uplifted parts are also seen (Fig 12). The end of this
1468 subsidence episode is not well constrained but must predate lower-Permian glaciogenic deposits that mark
1469 the onset of the second phase [Elliot et al., 2017].

1470 4.3 Phase 2 - Permian to Triassic

1471 Following the amalgamation of Pangea at ~320 Ma, the Permian marked a distinct change in the tectonic
1472 setting of Antarctica. Permian-Triassic Antarctica saw ongoing subduction at the West Antarctic-
1473 Panthalassan margin, while the Tethyan margin was subjected to rifting from ca 300 Ma to ca 200 Ma
1474 [Müller et al., 2019; Young et al., 2019]. During this period several microcontinents rifted at different times,
1475 but the main Cimmerian terranes separated from Pangea from 280 to 270 Ma (Fig 14a). The Antarctic
1476 Peninsula preserves arc-proximal sedimentary rocks from this period [Castillo et al., 2015], however the
1477 most extensive known sedimentary deposits are found along the Transantarctic Mountains, including
1478 exposures from Northern Victoria Land to the Shackleton Range [Elliot et al., 2017] all considered
1479 equivalents of the Victoria Group of the Beacon Supergroup. Similar rocks in the Ellsworth mountains may
1480 also be stratigraphic correlatives, since relocated due to motion of the Ellsworth-Whitmore block [Jordan et
1481 al., 2017a] (Fig 14a). A continuation of Victoria Group equivalent sequences into the Wilkes Subglacial basin,
1482 South Pole Basin and Pensacola-Pole Basin is likely [Ferraccioli et al., 2009a; Paxman et al., 2019a;
1483 Wannamaker et al., 2004].

1484 Exhumation of the East Antarctic coast at least from Prydz Bay to George IV Land occurred between ~350
1485 and ~200 Ma, likely in response to Tethyan rifting [Lisker et al., 2007; Maritati et al., 2020; Tochilin et al.,
1486 2012] although influenced by glacial erosion [Rolland et al., 2019]. This was accompanied by formation of
1487 several major basins including Lambert, Knox and Aurora basins [Maritati et al., 2020] and likely an extensive
1488 network of smaller basins within East Antarctica (Fig 14a). The Pangean landscape and basins persisted until
1489 the Early Jurassic Karoo-Ferrar LIP (183 Ma) when Gondwana breakup commenced.

1490 4.4 Phase 3 - Jurassic to Eocene

1491 The Jurassic to Eocene tectonic setting of Antarctica was dominated by the protracted and progressive
1492 fragmentation of Gondwana (Fig 14), which led to the formation of marginal basins and ultimately led to an
1493 isolated Antarctic continent. Rifting progressed in a 'clockwise' direction with first South America and Africa
1494 (from 177 Ma), India and Madagascar (from 135 Ma), Australia (from 100 Ma), and Zealandia (from 82 Ma).
1495 This process is relatively well recorded in the sedimentary basins of the Antarctic margin.

1496 Subsidence linked to Gondwana dispersal began in the Weddell Sea region ~180-177 Ma [Riley *et al.*, 2020].
1497 The pre-cursor to continental breakup is thought to have been extensive magmatism and emplacement of
1498 the Karoo-Ferrar Large Igneous Province at ~183 Ma [Burgess *et al.*, 2015]. For the main Weddell Sea basins,
1499 one suite of models suggest a two-stage development with Early Jurassic motion of the Haag Ellsworth–
1500 Whitmore microcontinent that led to the development of the Southern Weddell Sea Rift System [Jordan *et al.*,
1501 2017a], including rifting at the margins of the Weddell Sea (Evans-Rutford Basin and Filchner Trough).
1502 Subsequently, rifting occurred in the Northern Weddell Sea Rift Basin and the Riiser-Larsen Sea, beginning
1503 associated with breakup between Southern Africa and Antarctica before ~167 Ma [König and Jokat, 2006].
1504 The Weddell and Riiser-Larsen seas continued to open together, with associated basin formation offshore,
1505 until 126 Ma after which time Atlantic Ocean (Fig 14b) opening led to separate kinematics for these regions
1506 [König and Jokat, 2006]. In East Antarctica, the Jutul-Pencke-Graben system [Ferraccioli *et al.*, 2005b; Riedel
1507 *et al.*, 2012] and the Slessor Glacier Basin have experienced Jurassic to early Cretaceous extension in line
1508 with the departure of Africa and South America (Fig 14b). The thermal history of the Shackleton Range
1509 suggests a heating episode between 180 – 135 Ma indicating possible sedimentary burial during this time,
1510 before rapid cooling at ca 130 Ma [Krohne *et al.*, 2016].

1511 An alternative tectonic model for the Weddell Sea region suggests that the entire Weddell Sea Rift System is
1512 part of a single larger Skytrain tectonic plate, including much of the central and southern Antarctic Peninsula
1513 [Eagles and Eisermann, 2020]. In this model the Northern Weddell Sea Rift reflects separation of the Skytrain
1514 plate from Southern Africa and the Falkland Plateau between 180 and 156 Ma, followed by 90°
1515 counterclockwise rotation of the entire Skytrain plate into its current position by ~126 Ma [Eagles and
1516 Eisermann, 2020]. In contrast with the previous model this model does not include Jurassic opening of the
1517 southern Weddell Sea, and the plate-motion implies 200-400 km of shortening between the Skytrain plate
1518 and East Antarctica during the Cretaceous.

1519 Rifting of Madagascar and greater India from Antarctica had commenced by the early Cretaceous with
1520 oceanic crust forming in the Enderby Basin from 133 Ma [Jokat *et al.*, 2021]. This process may have involved
1521 an initial separation between East Antarctica and the Elan Bank and Southern Kerguelen Plateau, with by ~
1522 115 Ma a ridge-jump to north of the Elan Bank associated with the Kerguelen plume [Gaina *et al.*, 2007;

1523 *Gibbons et al.*, 2013], although an entirely pre-Kerguelen evolution is possible [*Jokat et al.*, 2021]. From 120
1524 Ma, igneous rocks from the Kerguelen plume formed much of the Southern Kerguelen Plateau and also are
1525 prominent in the basins of Enderby and Davis Seas [*Davis et al.*, 2018]. The potential effects of the rifting of
1526 greater India on East Antarctica's landscape and onshore basins remains ill-defined. Limited
1527 thermochronology detects early Cretaceous cooling in the Lambert region [*Lisker et al.*, 2007], linked to
1528 brittle deformation structures [*Phillips and Läufer*, 2009], although later studies propose an igneous origin
1529 for thermal resetting [*Tochilin et al.*, 2012], while the Shackleton range experienced rapid cooling at ca 130
1530 Ma [*Krohne et al.*, 2016].

1531 The geometry of the Lambert Rift is characteristic of two distinct structural orientations that dominate this
1532 sector of East Antarctica: one is aligned parallel to early spreading in the Cosmonauts Sea margin, and the
1533 other to early spreading direction of the Enderby Basin (Fig 14b). These structural orientations may be
1534 associated with much older events, and reactivation may have occurred in response to events associated
1535 with the opening of the Enderby Basin (130 – 115 Ma [*Gibbons et al.*, 2013]) and the Cosmonauts Sea (<120
1536 Ma [*Jokat et al.*, 2010]), either separately, or due to strain-partitioning associated with contemporaneous
1537 rifting.

1538 The impact of greater India rifting on the margin of Western Australia, at the time contiguous, is more well
1539 defined, and may form a key template to understand East Antarctica. After the end of Permian-Triassic
1540 rifting, renewed subsidence of the Perth and Mentelle basins occurred from the mid-Jurassic to early
1541 Cretaceous, with the breakup phase associated with oblique northwest-southeast extension aligned with
1542 spreading in the Perth Abyssal Plain [*Williams et al.*, 2013]. Onshore structures for this period include dextral
1543 strike-slip on north-south oriented structures, en-echelon folding and sinistral motion on northwest-
1544 southeast transfer faults [*Song and Cawood*, 2000]. The late Jurassic sedimentary fill of the Mentelle Basin
1545 suggests dominant detrital sources located in East Antarctica during this time, indicating active erosion of
1546 inland regions [*Maritati et al.*, 2021]. Following these a widespread Valanginian unconformity and eruption
1547 of the Bunbury Basalt at 137 - 130 Ma [*Olierook et al.*, 2016] mark breakup and widespread uplift. The Perth
1548 Basin is continuous with the Knox and Aurora Subglacial basins, which are structurally similar (Fig 14b).

1549 In the mid-Cretaceous the oblique motion of Australia from Antarctica (Fig 14c) commenced at ca. 100 Ma,
1550 however, did not proceed to separation until 83 Ma [*Williams et al.*, 2019]. In contrast to Africa and India,
1551 Australia did not rapidly move away, with slow spreading until ~45 Ma [*Williams et al.*, 2019], and the
1552 Tasman Gateway was not opened until 33 Ma [*Scher et al.*, 2015]. Spreading on this margin west of the
1553 George V fracture zone between 57-50 Ma may have been accommodated by sinistral transtension in East
1554 Antarctica and tectonic deepening of the Adventure and Astrolabe Subglacial Troughs [*Eagles*, 2019]. The
1555 adjacent margins preserve the evolution of this post-rift system including, since the early Paleogene, a major

1556 influence from evolving glacial and oceanographic systems [*De Santis et al., 2003; Escutia et al., 2005;*
1557 *Hochmuth et al., 2020; Sauermilch et al., 2019*].

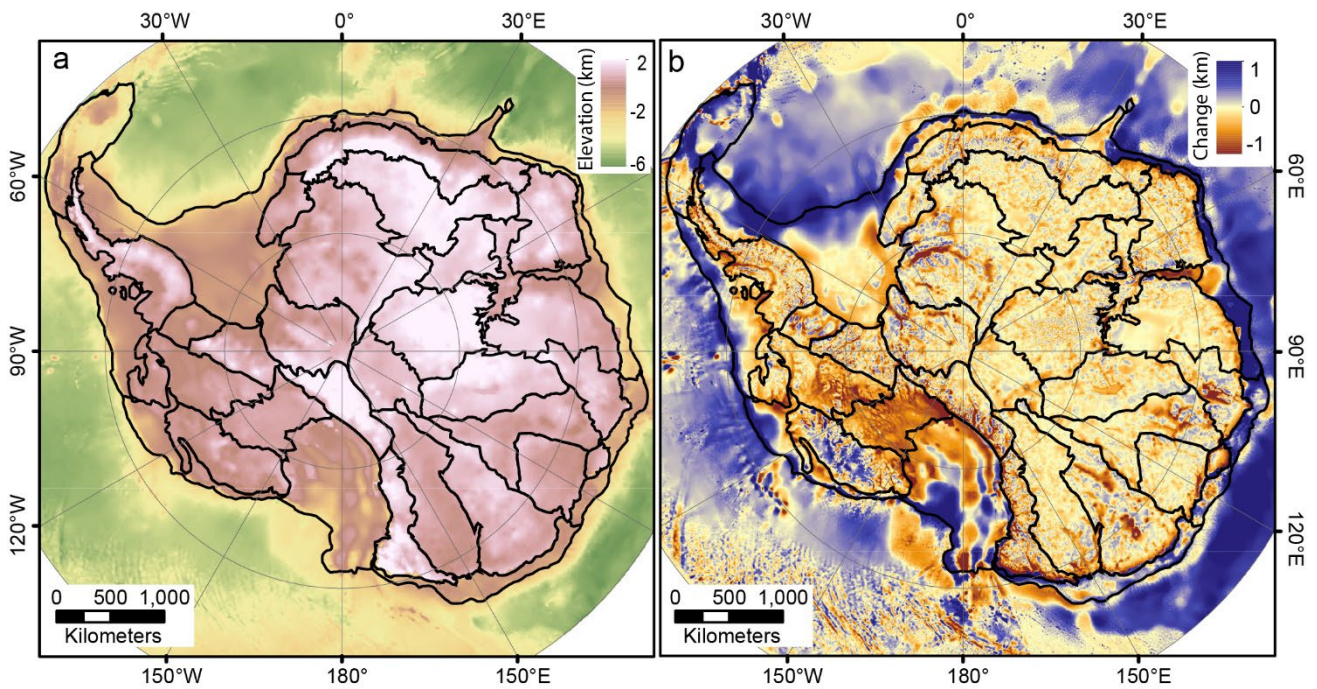
1558 Initial east-west extension in the Ross Sea is interpreted with a broad basin evolving between 105 to 83 Ma
1559 [*Jordan et al., 2020*]. This phase of rifting in the Ross Sea is characterized by lower-crustal exhumation along
1560 low-angle detachment faults [*Siddoway et al., 2004*]. Up to 100 km of diffuse extension may be
1561 accommodated on these shear zones [*Siddoway, 2008*], and this phase of extension is associated with
1562 crustal thinning and magmatism but not the development of major accommodation space [*Lindeque et al.,*
1563 *2016a*]. The predominance of crustal thinning over basin development may a consequence of weak lower
1564 crust [*Karner et al., 2005*]. This wide rift event has also been associated with a potential plateau collapse
1565 [*Bialas et al., 2007*]. With separation of Zealandia at 83 Ma the translation of Marie-Byrd Land trends
1566 towards the northwest and the rift system is interpreted to extend southward into the Siple Coast and
1567 Amundsen regions [*Jordan et al., 2020*], also evolving from a more diffuse wide-rift to a more focused
1568 narrow-rift mode, likely due to increasing rheological strength [*Harry et al., 2018; Huerta and Harry, 2007*].
1569 The opening of the Tasman Sea and Pacific-Antarctic Ridge from 83 Ma to 52 Ma accommodated the
1570 majority of the relative motion of Zealandia and the Pacific plate relative to Antarctica [*Gibbons et al., 2013*].
1571 In the northern Ross Sea, opening of the Central Basin is interpreted between 61- 53 Ma [*Davey et al., 2021*].
1572 From 52 Ma, the opening of the Macquarie Ridge and Adare basin is associated with translation and rotation
1573 of Marie-Byrd Land and the Eastern Basin, initially to the northeast, and then to the east (Fig 14).

1574 4.5 Phase 4 – Eocene to Present

1575 Post mid-Eocene, plate tectonic motions in Antarctica were restricted to a few key areas. The western Ross
1576 Sea was in extension with corresponding seafloor spreading in the Adare Basin from 43 to 26 Ma, and also
1577 extension in the Terror Rift [*Davey et al., 2016; Granot and Dyment, 2018*]. Although the amount of
1578 extension was limited, the effects on the bathymetry of the continental shelf, and the association with
1579 volcanism were important local drivers of basin evolution. Neogene rifting is interpreted to extend into the
1580 interior West Antarctica including the Bentley Subglacial Trough [*Lloyd et al., 2015*], Pine Island Rift [*Jordan*
1581 *et al., 2010b*], Byrd Subglacial Basin [*Shen et al., 2018*] and the Ferrigno Rift [*Bingham et al., 2012*]. Tectonic
1582 subsidence through this period has occurred in the Ross, Siple Coast and Central West Antarctica regions (Fig
1583 12) [*Paxman et al., 2019b*].

1584 Subduction of the Aluk plate (part of the Phoenix plate) progressively ceased from south to north over time,
1585 as the West Antarctic-Aluk ridge moved north and ultimately ceased subduction in the Neogene [*Burton-*
1586 *Johnson and Riley, 2015*]. The evolution of a more complex margin to the north occurred in line with
1587 complex tectonics of the Scotia Sea [*van de Lagemaat et al., 2021*]. This included the opening of the Powell
1588 (30-20 Ma) and Jane (18-14 Ma) basins in a back-arc setting, and the convergent South Shetland margin,

1589 comprising a fore-arc basin and accretionary prism [Maldonado et al., 1994], and, since 4 Ma rifting in the
1590 Bransfield Basin [Almendros et al., 2020]. In the Eocene tectonic processes occurring to the north of
1591 Antarctica remained important as the Drake Passage allowed throughflow by 42 Ma [Scher and Martin,
1592 2006] and the Tasman gateway by 33 Ma [Scher et al., 2015]. Through the Oligocene these gateways
1593 developed more fully [van de Lagemaat et al., 2021], allowing by the Miocene a fully developed Antarctic
1594 Circumpolar Current.



1595

1596 *Figure 15: a) paleotopography at the Eocene Oligocene boundary [Paxman et al., 2019b] and b) the*
1597 *difference with the present day. Negative values indicate surface lowering due to tectonic subsidence and or*
1598 *glacial erosion.*

1599 Despite these regional tectonic events, by far the major influence on Antarctica's basin forming processes in
1600 this period was the glacial influence as the ice sheet developed, with many cycles of advance and retreat
1601 causing major unconformities, substantial onshore erosion [Paxman et al., 2019b] and fluctuating sediment
1602 volumes deposited around the margins [Hochmuth and Gohl, 2019; Pérez et al., 2021]. The resulting
1603 landscape of eroded basement regions, post-glacial sedimentary basins and the geomorphological features
1604 from both tectonic and glacial processes are essential for understanding the past present and future
1605 behavior of the Antarctic Ice Sheet.

1606 5 Implications for Antarctic Ice Sheet dynamics

1607 5.1 Basin-associated processes and their potential impact on the cryosphere

1608 Ice sheets and glaciers flow by three main mechanisms: internal ice deformation, basal sliding and
1609 deformation of basal material. The first of these is ubiquitous among ice masses, but the second and third

1610 are conditional on the presence of basal water. Furthermore, the third is dependent on the availability of
1611 deformable sediments at the bed. For water to exist beneath an ice sheet basal heat is needed: This can
1612 come from geothermal sources and, especially if ice flow is rapid, from basal motion and internal ice-
1613 deformation. Thus, the dynamics of fast flowing ice is dominated by basal flow processes that allow speeds
1614 more than 50 m yr^{-1} , and often several 100 m yr^{-1} .

1615 The availability of subglacial water is essential to both basal sliding and sediment deformation. In addition to
1616 ice sheet melting, for a permeable bed, we must consider the potential for water to be exchanged between
1617 the ice sheet bed interface, the active deforming till layer, and the strata beneath which may tap deep
1618 groundwater reserves [Gustafson *et al.*, 2022]. The role of groundwater in subglacial hydrological systems is
1619 important to ice flow for two main reasons. The first reason is a source of water in addition to that melted
1620 from ice. For example, Christoffersen *et al.* [2014] suggest groundwater may contribute up to half of the
1621 water available beneath ice streams in the Siple Coast and Li *et al.* [2022] model groundwater discharge of
1622 similar scale to melt-derived water. The second reason is that groundwater flow allows heat to be
1623 transported vertically and laterally through the subglacial system [Gooch *et al.*, 2016; Kulesa *et al.*, 2019]
1624 thus representing a governing mechanism of advective heat transport to the ice sheet base.

1625 Hydraulic gradients in subglacial sedimentary basins vary over glacial cycles during the growth and decay of
1626 the ice sheet. This process has a positive feedback with ice sheet retreat and advance, as retreating ice
1627 sheets thin, unloading the basin causes groundwater to be discharged into the subglacial system [Gooch *et*
1628 *al.*, 2016; Li *et al.*, 2022; Person *et al.*, 2012,]. The opposite may occur when the ice sheet thickens, directing
1629 water away from the ice sheet base and storing it in subglacial sedimentary basins [Gooch *et al.*, 2016]. In
1630 this manner, the groundwater system modulates interactions between basal water systems and the
1631 underlying sedimentary basins to exert control on the lubrication of the ice sheet base and thus impact ice
1632 flow. Numerical modelling indicates that, even in situations of fast retreat, the groundwater discharge-rate
1633 can be of comparable magnitude to the expected basal melt rate, and this feedback is likely to contribute
1634 substantially to ice sheet dynamics [Li *et al.*, 2022]. Furthermore, past retreat and advance events can store
1635 'fossil' hydraulic head in aquifers for later release [Gooch *et al.*, 2016; Person *et al.*, 2012].

1636 From what we understand from formerly glaciated regions [Evans *et al.*, 2006] and from geophysical
1637 observations of subglacial Antarctica [Alley *et al.*, 2021; Anandakrishnan *et al.*, 1998; Christianson *et al.*,
1638 2016; Muto *et al.*, 2019a; Siegert *et al.*, 2016], the deformation of basal material is a dominant process
1639 within major ice streams and, consequently, exerts control on ice sheet flow. InSAR depiction of surface ice
1640 flow velocities [Mouginot *et al.*, 2019] and geophysical measurements of the subglacial system
1641 [Anandakrishnan *et al.*, 1998; Christianson *et al.*, 2016; Muto *et al.*, 2016; Muto *et al.*, 2019a; Peters *et al.*,
1642 2006] allow us to pinpoint the onset of enhanced ice flow and the basal boundary conditions that permit it:
1643 For example, the onset of Whillans Ice Stream coincides with the availability of sedimentary material

1644 identified through aerogeophysical [Bell et al., 1998] and seismic [Anandakrishnan et al., 1998] data. The
1645 mechanics of subglacial sediment is complex and time variable, with in general hydration and fluid
1646 overpressure leading to weaker rheology while compaction and de-watering lead to stiffer rheology. This
1647 sensitivity to water supply can lead to relatively abrupt changes in flow [Catania et al., 2012; Christoffersen
1648 et al., 2014; Smith et al., 2013]. Meanwhile, sediment deposition in a grounding zone wedge and subsequent
1649 compaction associated with tidal loading may stabilize the grounding zone [Christianson et al., 2016]. The
1650 deformation of the sediment commonly involves two layers: a relatively thin upper active zone, at most a
1651 few meters thick dilated by high-pressure water within pores that acts to reduce its material strength; and a
1652 thicker over-compacted basal unit that is stiffer and contributes little to flow [Evans et al., 2006].

1653 Basal sediments originate from two main sources: accumulations of marine sediments during previous times
1654 of deglaciation, and from the erosion of bedrock either locally or upstream. Recent marine deposits are likely
1655 to be present at lower-elevations and will often be widespread, prompting zones of more continuous bed
1656 deformation [Evans et al., 2006]. Without recent marine sediments, sediment supply must be sustained
1657 through glacial erosion, and this may be a limiting factor on till continuity. Glacial erosion is accomplished
1658 through a variety of processes, and these are fundamentally reliant on heterogeneities in the bedrock,
1659 including joints, especially their spacing and orientation [Hooyer et al., 2012], and lithological variations
1660 including competency contrasts, layer thicknesses, and structural orientation relative to flow [Krabbendam
1661 and Glasser, 2011; Lane et al., 2015]. In comparison to the competent and massive structure more typical of
1662 igneous and metamorphic basement, sedimentary rocks provide more opportunities for quarrying to occur,
1663 and also a higher likelihood of abrasion, where the rocks are less competent [Krabbendam and Glasser,
1664 2011]. Finally, to sustain a continuous till layer, sediments eroded upstream must be transported, which is
1665 predominantly achieved via the subglacial hydrology system, which depending on erosion rate and water
1666 flux may be supply-limited or transport capacity limited [Delaney et al., 2019].

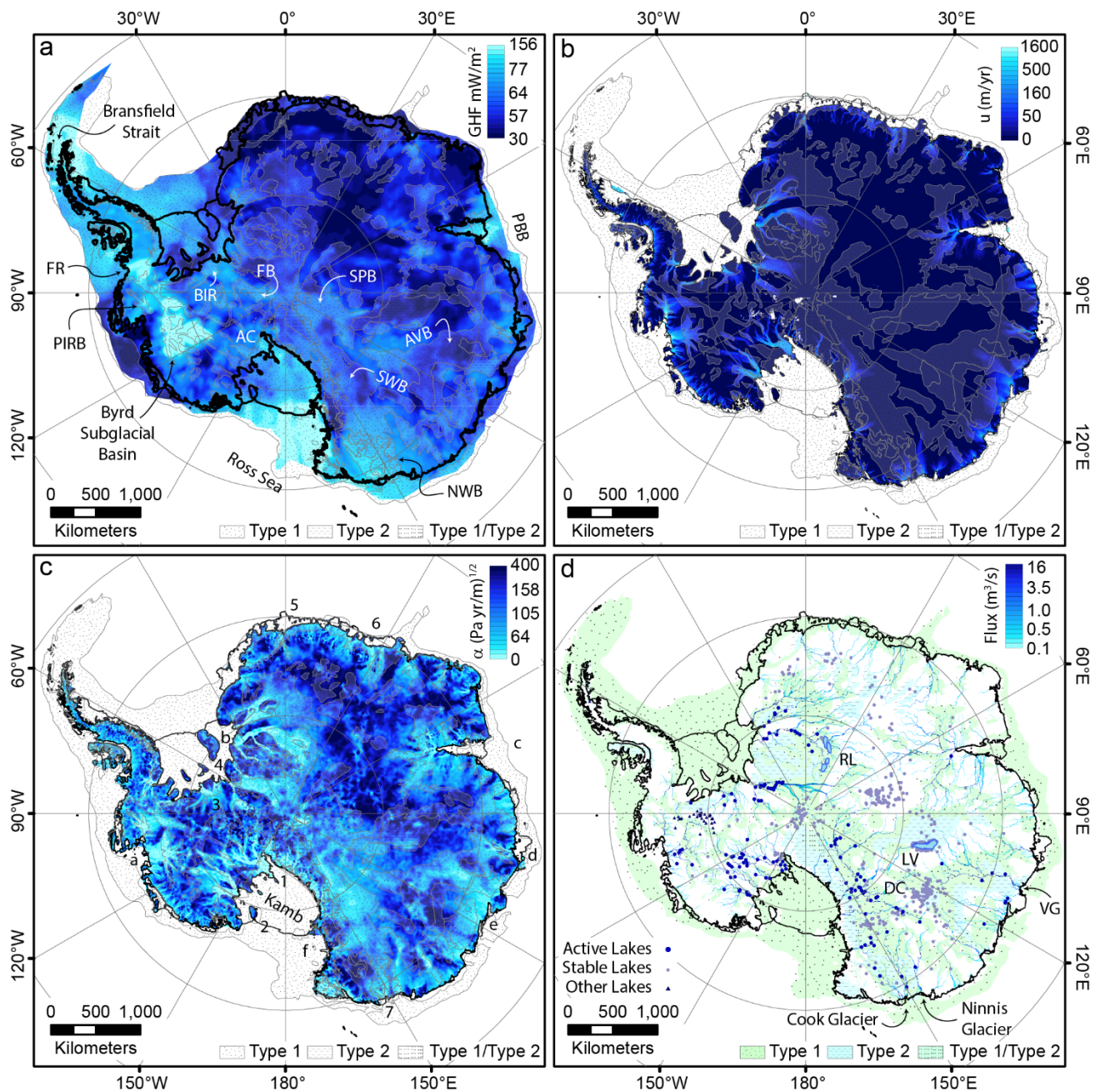
1667 Both subglacial water and thin horizons of weak basal sediments may be present in areas of crystalline
1668 basement as well as in sedimentary basin regions. Before considering basin settings, it is instructive to
1669 consider an ice stream catchment with a structurally massive and impermeable bed throughout, such as a
1670 granite or gneiss bedrock. For such a bed we may consider as a first priority the supply of basal water, which
1671 must be derived from basal melting and/or surface melting transported to the bed via fractures and moulins
1672 [Schoof, 2010]. The latter, while certainly an important processes, depends on surface melting conditions
1673 that in Antarctica are, for now, limited to certain coastal regions, although they may be more important in
1674 the future [Tuckett et al., 2019]. For the former, a sustained high flow-speed and/or geothermal heat flux is
1675 needed. With an impermeable bed, geothermal heat flux for a given location will be near constant, and so
1676 temporal variations in basal melt rate will depend solely on ice-stream flow processes. In addition to water,
1677 sediment must be supplied through erosion of the crystalline basement, which is likely to be highly resistant

1678 to erosion [Krabbendam and Glasser, 2011] potentially restricting supply. We may now consider how the
1679 presence of a sedimentary bed influences ice sheet dynamics.

1680 Several factors associated with sedimentary basin formation increase the likelihood that regions containing
1681 sedimentary basins will possess enhanced ice flow. These are 1) a favorable source for sustained supply of
1682 sediment from more erodible bedrock and/or recent marine sediments [Bell *et al.*, 1998]; 2) the supply of
1683 subglacial water through groundwater discharge, tied to glacial unloading [Christoffersen *et al.*, 2014; Siegert
1684 *et al.*, 2018]; 3) different organization of subglacial water systems including transitions between distributed
1685 and channelized flow, and routing between catchments [Christoffersen *et al.*, 2014; Schroeder *et al.*, 2013];
1686 4) the opportunity through groundwater circulation to advect heat from depth to the ice sheet bed [Gooch
1687 *et al.*, 2016]. In addition, the tendency for basin-dominated regions to possess relatively smooth topography
1688 at all scales promotes ice-stream boundaries defined by ice sheet dynamics, including basal processes
1689 [Catania *et al.*, 2012]. Finally, we may consider the effects of ongoing basin-forming processes on the
1690 morphology of ice shelf cavities that are critical for ice sheet stability [Smith *et al.*, 2019b].

1691 5.2 Antarctic sedimentary basins and ice sheet dynamics

1692 Although the specifics of when, where and how sedimentary basins have influenced ice sheet dynamics in
1693 Antarctica remain to be defined, the mechanisms listed above are more able to occur in catchments
1694 containing sedimentary basins. Consequently, we may consider if the presence of subglacial sedimentary
1695 basins within a glacial catchment is associated with more dynamic behaviour, and if this impact on ice sheet
1696 dynamics may be expressed for the modern-day ice sheet.



1697

1698 *Figure 16: a) deep-seated geothermal heat flux [Lösing and Ebbing, 2021] b) surface ice sheet velocity from*
 1699 *InSAR phase mapping [Mouginot et al., 2019] c) inferred basal friction coefficient derived by inverting for*
 1700 *basal conditions using the Ice sheet and Sea level System Model [Dawson et al., 2022]. Numbers indicate ice*
 1701 *stream systems with sedimentary basins beneath fast flowing ice including 1 – Mercer and Whillans, 2 –*
 1702 *Bindschadler and MacAyeal 3 – Insite , 4 - Academy and Support Force 5 – Jutulstraumen 6 – West and*
 1703 *Central Ragnhild, 7 – Cook. Letters indicate ice stream systems with basins upstream including a – Thwaites*
 1704 *and Pine Island, b – Recovery and Slessor d – Lambert, Mellor and Fisher, d – Denman and Scott e – Totten f –*
 1705 *David, Skelton and Byrd d) subglacial hydrology, including subglacial lakes [Livingstone et al., 2022], and a*
 1706 *modern-day drainage network [Le Brocq et al., 2013]. FR – Ferrigno Rift, PIRB – Pine Island Rift Basin, BIR –*
 1707 *Bungenstock Ice Rise, AC – Amundsen Coast Basin, FB – Foundation Basin, SPB – South Pole Basin, AVB –*

1708 *Aurora-Vincennes Basin, SWB – Southern Wilkes Basin, NWB – Northern Wilkes Basin, RL - Recovery Lakes, LV*
1709 *- Lake Vostok, DC – Dome C.*

1710 Basins are important modulating influence on geothermal heat flux (GHF) and can act either to inhibit or
1711 enhance surface GHF. In Antarctica, the overall statistical relationship with heat flux from deep-seated
1712 sources [Lösing and Ebbing, 2021] is almost null for type 1 basins relative to crystalline basement, although
1713 type 2 basins are systematically associated with lower GHF (small effect size). In West Antarctica where heat
1714 flux is generally high, higher heat flux is found within basin regions (Fig 15a). These regions include the Siple
1715 Coast with especially high heat flux in the Amundsen Coast Basin, but less to the north. From the Byrd
1716 Subglacial Basin to the Ferrigno Rift is an elevated high heat flux region, with concentrations beneath basins
1717 including the Byrd Subglacial basin and the Pine Island Rift Basin. The western Ross Sea, including the active
1718 Terror Rift and the similarly active Bransfield Strait region has high heat flux. Tectonically older regions such
1719 as the Weddell Sea possess more moderate heat flux, but higher towards the west and the south near
1720 Bungenstock Ice Rise (Fig 15a). Variations in heat flux in East Antarctica are not so clearly associated with
1721 basins except for the tendency for very low values to be restricted to areas without type 1 basins. Selected
1722 areas, including the Foundation Basin South Pole Basin, the Northern Wilkes Basin, and the Prydz Bay Basin
1723 show elevated heat flux relative to their surrounding area while the Aurora-Vincennes and southern Wilkes
1724 subglacial basins show reduced heat flux. With respect to ice sheet dynamics, the large-scale heat flux
1725 shown here represents the crustal structure beneath the basin, and excepting volcanism, is a stable
1726 boundary condition. The time-variable influence of basins on heat flux at the bed is likely to be substantial
1727 where fluid circulation is coupled with a high thermal gradient, with fluid conduits such as deformation
1728 zones also important [Tankersley et al., 2022].

1729 Fast flowing ice, as defined by surface ice velocity [Mouginot et al., 2019] has overall only a weak spatial
1730 association with the presence of basins (Fig 15b). Type 1 basins do have a higher average velocity (24 m yr^{-1})
1731 than either crystalline bed (19 m yr^{-1}) or type 2 basins (11 m yr^{-1}), but with very small effect size given the
1732 large spatial variability ($\sigma \approx 70 \text{ m yr}^{-1}$). However, although many of Antarctica's fastest flowing glaciers flow
1733 over crystalline bedrock or a mixed bed, many of these possess sedimentary basins preserved in the upper
1734 catchment (Fig 15b).

1735 The slipperiness at the ice-bed interface is expressed by the basal friction coefficient, which relates basal
1736 sliding velocity to basal shear stress. It is a direct measure of the subglacial environment and encapsulates
1737 the effect of both subglacial water and deformable sediment. Model inferred basal friction coefficient is
1738 generally lower where there is fast flowing ice and higher near topographic divides, but also may associate
1739 with the presence of basins (Fig 15c). In comparison with velocity, model-inferred basal friction coefficient is
1740 closely correlated with the basin distribution, with a mean for type 1 basins of $93 \text{ (Pa yr/m)}^{1/2}$ contrasting

1741 with a mean of 127 and 134 (Pa yr/m)^{1/2} in crystalline basement and type 2 basins respectively. Overall, this
1742 relationship has a medium effect size given regional variability ($\sigma \approx 70$ (Pa yr/m)^{1/2}).

1743 Basal friction coefficient is related to basin coverage in several ways. In several ice stream systems, basin
1744 coverage occurs in the fast-flowing lower catchment and low basal friction coefficient is seen. Examples
1745 include Mercer and Whillans; MacAyeal and Bindschadler; and Institute ice streams draining the West
1746 Antarctic Ice sheet and Academy and Support Force; Jutulstraumen; West and Central Ragnhild; and Cook ice
1747 streams draining the East Antarctic Ice Sheet. Often however for major catchments the fast-flowing lower
1748 catchments flows over a crystalline or mixed bed, with the basin confined to the upper catchment, the
1749 downstream part having been eroded [Aitken *et al.*, 2016b; Paxman *et al.*, 2017]. Examples include Thwaites
1750 and Pine Island; Recovery and Slessor; Lambert, Mellor and Fisher; Denman and Scott; Totten and the ice
1751 streams draining from the southern Wilkes Subglacial Basin through the TAM including Byrd, Skelton and
1752 David glaciers. For these ice streams low basal friction coefficient extends far into the sedimentary basin
1753 region despite the surface velocity being relatively slow, suggesting that basal sliding can propagate into the
1754 upstream basin. A final relationship is that for slow-moving ice such as at Kamb Ice Stream, and at drainage
1755 divides (e.g. for South Pole) where we see basin regions associated with moderate to high basal friction
1756 coefficient, indicating that basal sliding is limited in these areas.

1757 We may also review the association of basins with the subglacial hydrology system (Fig 13d). Subglacial
1758 lakes are found throughout Antarctica [Livingstone *et al.*, 2022] and occur across all bed classes. Of 675
1759 lakes, 260 (39%) occur over crystalline bedrock, while 239 (35%) occur over type 1 basins, and 114 (17%)
1760 over type 2 basins. In comparison, the areas taken up by these bed classes is 40%, 47% and 8% respectively.
1761 Furthermore, of 140 hydraulically active lakes we find 96 (69%) occur over type 1 basins, while of 502 stable
1762 lakes only 137 occur over this class (27%). This represents a tendency for stable lakes to occur close to ice
1763 divides, while active lakes occur more frequently towards the ice sheet margins [Livingstone *et al.*, 2022].
1764 Besides subglacial lakes, basal fluid flux is driven by hydraulic potential gradients from the high-potential
1765 divides towards the ice sheet margins. These networks do not necessarily follow the same flow-routing as
1766 the ice and can cross boundaries to ice flow (Fig 15d). Unless the ice sheet surface slope is steep and
1767 oriented transverse to the bed slope, the subglacial water flux will be preferentially concentrated into
1768 topographic basins and form highly dynamic flow networks [Dow *et al.*, 2022; Le Brocq *et al.*, 2013], and so
1769 there is a natural association of high-volume subglacial water flux and sedimentary basins (Fig 13d). Several
1770 notable examples include the Recovery Lakes that overly the Recovery Basin with flow directed towards
1771 Recovery glaciers, the Pensacola-Pole Basin with flow directed to Academy and Support Force glaciers, the
1772 Byrd Subglacial Basin with flow directed towards Thwaites Glacier. Lake Vostok draining into the Wilkes
1773 Subglacial Basin, and from there flow directed towards Cook Glacier, and also through the TAM, and Finally
1774 Dome C with flow directed into the Aurora Subglacial Basin and towards Vanderford Glacier.

1775 At Thwaites, the transition from distributed to channelized flow may be correlated to the change from
1776 sedimentary basin to crystalline bed [Schroeder *et al.*, 2013] and bed-type transitions in other catchments
1777 (Fig 15d) may also be critical thresholds for the hydrology system. The interaction of high-flux hydrology
1778 networks including active lakes with higher-permeability sedimentary beds is fundamental to the subglacial
1779 hydrology of Antarctica and may exert a critical influence on ice sheet dynamics. An important consideration
1780 is where subglacial hydrology follows different routing to the ice flow: Ice retreat and unloading in one
1781 catchment, along with increased basal melting, may enhance water flux that is potentially routed into
1782 another catchment, and so may help propagate dynamic behavior from one catchment to another [Wright
1783 *et al.*, 2008].

1784 The preceding indicates associations between the presence of sedimentary basins and enhanced ice sheet
1785 flow. In a sedimentary basin setting, this sliding may occur in deformable till layers facilitated by more
1786 extensive basal till and from hydrogeological processes that may provide substantial amounts of subglacial
1787 water. Enhanced groundwater discharge to the bed is associated with additional feedbacks, including heat
1788 advection within the basin and temporally variable water discharge and recharge coupled with ice unloading
1789 and loading histories. The expected groundwater response includes an ongoing long-term response from
1790 deep aquifers activated by unloading since Last Glacial Maximum, and shorter-term responses from
1791 shallower aquifers activated by more recent mass loss [Christoffersen *et al.*, 2014; Gustafson *et al.*, 2022; Li
1792 *et al.*, 2022]. In some regions, high sensitivity to variable subglacial hydrology network structure may lead to
1793 cross-catchment vulnerabilities and the propagation of dynamic behavior between ice streams [Alley *et al.*,
1794 1994; Vaughan *et al.*, 2008; Wright *et al.*, 2008].

1795 A substantial role for subglacial sedimentary basins in governing the basal conditions of the ice sheet is well
1796 supported by both models and data, but a well-defined relationship between subglacial sedimentary basins
1797 and ice sheet flow remains elusive, with many cross-associations with other boundary conditions and
1798 complex time and space variable interactions. In particular, the potential effects of these basin processes on
1799 large scale glacial flow are yet to be systematically assessed.

1800 6 Future directions in Antarctic Subglacial Sedimentary Basins research

1801 Knowledge of sedimentary basins beneath the Antarctic ice sheet has expanded greatly in recent decades,
1802 and key concepts relating to their influence on ice sheet dynamics are identified. Despite this, for a full
1803 realization of their value for understanding global tectonics, paleolandscape evolution and the dynamic
1804 behavior of ice sheets with changing climate, there is a pressing need to continue to progress several key
1805 themes.

1806 6.1 Sedimentary basin definition and characterization

1807 Despite substantial recent advances, mapping the presence of sedimentary rocks beneath thick ice remains a
1808 significant challenge. The more widely available datasets from airborne geophysics can provide a strong
1809 indication of the presence of a sedimentary basin, subject to certain ambiguities.

1810 Small-scale variations in the solid earth, for example heat flux [McCormack *et al.*, 2022] and topography
1811 [Mackie *et al.*, 2020] may have large impacts on ice sheet dynamics. For consistent mapping at a continent
1812 scale, improved coverage is needed both to fill remaining data gaps, and in areas with typically older, low
1813 resolution, less accurate or poorly geolocated data. The newest compilation Bedmap3 [Frémand *et al.*,
1814 2022b] is based on a 500m along-line resolution. Taking this as a benchmark, we summarize the
1815 requirements for airborne data to reach this resolution: To maximize non-aliased signal, magnetic intensity
1816 data should be collected with a line-separation comparable to the source-sensor separation [Reid, 1980].
1817 Gravity data may be more widely separated without loss of non-aliased signal. In much of Antarctica, due to
1818 thick ice, the source-sensor separation is several kilometers, and there is little gain from closely spaced
1819 magnetic and gravity surveys. Regions with thinner ice however may benefit in principle but are limited by
1820 several additional factors. Airborne gravity systems require along-line data filtering that, for fixed-wing
1821 platforms, limit viable resolution to 5 -10 kilometers wavelength.

1822 Radar has no similar physical limitation on resolution and the bed can be sampled at fine scales along lines.
1823 The fine scale along line sampling allows for sub-survey resolution data products to be generated in 2D using
1824 physical and/or statistical techniques [Frémand *et al.*, 2022b; Mackie *et al.*, 2020; Morlighem *et al.*, 2020].
1825 The need for closely spaced data, depends on the characteristics of the ice sheet bed and the ice sheet flow,
1826 and a variable radar line-spacing of 500 to 2.5 km across the continent is likely to improve the fidelity of bed
1827 topography data products across all scales. To enable finer resolution it is necessary to reduce aircraft
1828 velocity, and helicopter surveys are one practical solution [Wei *et al.*, 2020], or alternatively, slow-flying
1829 UAVs may be an emerging technology for practical deployment in the future [Teisberg *et al.*, 2022]. Ship-
1830 based operation may also allow to reach key coastal data gaps.

1831 Ground-based geophysical data collection, including by active and passive seismic and magnetotelluric
1832 methods, remains limited in Antarctica and it is a significant challenge to achieve a systematic continent-
1833 wide coverage. Large-scale passive seismic deployments, with stations spaced tens of kilometers apart or
1834 more, have been used with success to image the nature of the crust and the mantle including basins [Shen *et al.*,
1835 2018; Zhou *et al.*, 2022]. The current network of passive seismic stations ($n \sim 1600$), mostly in West
1836 Antarctica could feasibly be expanded to a continent-scale network with accompanying magnetotelluric data
1837 within a manageable logistical footprint. Smaller-scale deployments with station spacings of kilometers are
1838 capable of imaging the geology conditions at the bed of individual ice streams and are fundamental to

1839 understanding the impact of sedimentary basins on ice sheet dynamics [*Anandkrishnan and Winberry,*
1840 *2004; Gustafson et al., 2022; Peters et al., 2006*]. Active seismic experiments remain resource-intensive and
1841 logistically challenging although the implementation of vibrator sources and snow-streamer technologies is a
1842 substantial step forward to increase the efficiency, resolution and accuracy of data collection [*Eisen et al.,*
1843 *2015*]. These more intensive approaches initially may be targeted towards key catchments, however
1844 expanded deployment of these technologies would be of immense benefit to understanding geologic bed
1845 conditions for ice dynamics.

1846 Finally, it is necessary to enhance capability for field-verification of bed characteristics to inform and
1847 constrain geophysical observations. Several initiatives are under way to develop further drilling technologies
1848 to access the subglacial geology, including systems designed with differing logistical footprints and with
1849 different capacity to reach the bed through thick ice [*Gong et al., 2019; Goodge et al., 2021; Hodgson et al.,*
1850 *2016; Kuhl et al., 2021; Talalay et al., 2021*]. Maintaining strong engagement with ice-coring and hot-water
1851 drilling communities is desirable to synergize efforts where feasible. For the context of basins research, and
1852 the study of their interactions with glacial systems, a critical problem remains that representative samples
1853 are likely to be found under thick and especially wet-based ice, for which drilling technologies are not yet
1854 optimized. The capacity to recover long stratigraphic cores is of particular value to basins research.

1855 As well as the detection of basins, we may seek to better define the geometry of basins, including their
1856 thickness and overall morphology but also their internal structure. Defining the thickness of Antarctica's
1857 sedimentary basins is a clear next step that demands a new approach able to combine multiple diverse
1858 datasets so that all are accommodated in the problem formulation, and the solution. Also important are
1859 faults and stratigraphy, which provide critical controls on fluid flow within the basins. Consequently, these
1860 dictate the hydrogeological response to changing glacial load and so advective heat transport to the ice
1861 sheet bed [*Tankersley et al., 2022*]. The sensitivity of gravity and magnetic data to internal basin structure
1862 may be limited by density and magnetization contrasts between sedimentary rocks which are relatively low
1863 in comparison to the contrast with the basement and other features such as intrusions and volcanic rocks.
1864 While passive seismic and magnetotelluric data provide some additional constraints, active seismic data are
1865 most effective for developing a good appreciation of intra-basin structure.

1866 Finally, while the physical properties of the basins, including density, seismic velocity and its anisotropy,
1867 electrical conductivity and other characteristics may be defined from geophysical data, to define their
1868 relationship with ice sheet dynamics it is necessary to translate these into mechanical and hydrogeological
1869 properties. A particular challenge are 'topological' properties defined largely by orientations and
1870 connections (e.g. permeability, stratigraphic layering and its orientation, fracture density and orientation)
1871 that have most bearing on both the hydrogeological system [*Person et al., 2012*] and also the erodibility of
1872 sedimentary bedrock [*Krabbendam and Glasser, 2011; Lane et al., 2015*].

1873 6.2 Sedimentary basins as a record of glacial change

1874 A profound quality of sedimentary basins is their capacity to record sensitively the conditions of their
1875 formation, which amongst other things provides knowledge of tectonic and surface processes, and past ice,
1876 ocean, and climate conditions. Sampling of sedimentary records from basins provides key benchmarks and
1877 constraints on the behavior of the ice sheet in the past, which supports the capacity to define ice sheet
1878 processes in models of potential future ice sheet change. While many studies have investigated the Antarctic
1879 margin, these studies remain limited in extent and are clustered in a few areas (Fig 1). With dynamic
1880 instabilities dominating catchment scale ice stream behavior, more comprehensive coverage is required to
1881 understand the dynamic response of the Antarctic ice sheet to changing climate. Innovative approaches to
1882 marine drilling [e.g. *Gohl et al., 2017*] may allow more agile, safer and less logistically demanding
1883 investigations.

1884 In addition to obtaining records of changing conditions from drill cores, spatial patterns of erosion and
1885 sedimentation are closely linked to past glacial cycles [*Anderson et al., 2019; Hochmuth et al., 2020; Pérez et*
1886 *al., 2021*] and can be used to understand systematic instabilities within catchments [*Aitken et al., 2016b*].
1887 The structure of sedimentary basins can be used for the reconstruction of paleo-landscapes, offshore and
1888 onshore, which is important for understanding the long-term stability of the ice sheet structure [*Hochmuth*
1889 *et al., 2020; Jamieson et al., 2010; Paxman et al., 2019b*]. Paleotopographic reconstruction is also critical in
1890 the effort to model past ice sheet behavior with realistic topographic and basal boundary conditions, rather
1891 than relying on modern-day formulations [*Hochmuth and Gohl, 2019; Paxman et al., 2020*]. An important
1892 factor here is not just the reconstruction of topographic elevation, but also the changing nature of the ice
1893 sheet bed through time.

1894 6.3 Understanding cryosphere interactions

1895 While the fundamental principles of the interactions between sedimentary basins, sediments and water at
1896 the ice sheet bed and ice sheet flow have been known for some time [*Alley et al., 1987; Bell et al., 1998;*
1897 *Blankenship et al., 1986; Christoffersen et al., 2014*] their overall role in controlling Antarctic ice sheet
1898 dynamics is ill-defined. Knowledge of these interactions in Antarctica is growing, but it is evident that much
1899 further work needs be done to provide a systematic understanding of how these complex boundary
1900 conditions interact with the ice sheet to focus, enhance, constrain or otherwise influence glacial change
1901 processes associated with a warming climate [*Kennicutt et al., 2019*].

1902 Hydrogeologic interactions of sedimentary basins with subglacial hydrology and cryosphere are understood
1903 largely through model studies [*Christoffersen et al., 2014; Gooch et al., 2016; Li et al., 2022*] and through
1904 studies of the former northern hemisphere ice sheets [*Person et al., 2007*]. It is not clear yet how these
1905 model concepts may affect Antarctic conditions, and a robust and Antarctic-specific understanding of their

1906 role in the dynamics of the Antarctic ice sheet is a core challenge requiring both targeted model studies and
1907 expanded observations of the bed. Critical concepts to be defined further include the role of sedimentary
1908 basins for sustaining subglacial water supply, and the interactions of aquifer systems with subglacial lakes
1909 and hydrological flow organization on different timescales. Understanding how Antarctica's aquifers respond
1910 to a changing ice sheet may be an essential factor in understanding their vulnerability in retreat, as the
1911 release of water during glacial unloading, if substantial, could be a critical positive feedback promoting
1912 accelerated ice sheet flow [Schoof, 2010] and also ice-shelf destabilization [Le Brocq et al., 2013].

1913 Sedimentary basins are an important factor in controlling heat flux, firstly through the tendency to insulate
1914 the crust beneath, leading to warmer conditions beneath and secondly, the capacity for fluid circulation
1915 within the basin to efficiently transport heat from depth to the surface, also potentially accessing saline
1916 waters [Gustafson et al., 2022]. Heat advection is especially important as a positive feedback associated
1917 with ice sheet unloading [Gooch et al., 2016]. Essential concepts to be defined further include mapping
1918 temperature gradients, water contents and salinity within basins, as well as the association of these with
1919 high ambient temperatures associated with rifting, magmatism, or high crustal heat production. Perhaps the
1920 most limiting factor is the identification of the internal basin structure, and so the necessary conduits for
1921 fluid circulation, their orientation and connectivity.

1922 A sustained supply of flow-capable sediment is an important factor enabling sustained fast ice sheet flow.
1923 This requires either a base of marine sediments, deposited during a past retreat, or a reliably erodible
1924 bedrock. In the latter case, while the presence of the sedimentary bed is known to be an important
1925 condition, studies of formerly glaciated regions show there is a high degree of sensitivity to the nature of the
1926 sedimentary rocks, including the dip and strike of the strata, bedding-layer thicknesses, the competency of
1927 the different lithologies, and the intensity and spacing of joints and other fractures [Hooyer et al., 2012;
1928 Krabbendam and Glasser, 2011; Lane et al., 2015]. Characterization of these fine-scale details in a subglacial
1929 setting is problematic in the absence of high-resolution seismic reflection data, however, an understanding
1930 of the depositional setting, large-scale structure and broad lithology variations within basins may allow these
1931 factors to be assessed in a probabilistic sense bearing in mind analogues from formerly glaciated regions.

1932 6.4 Coupling mapping with ice sheet models for predictive capacity

1933 A major frontier for basins research in Antarctica is the coupling of the knowledge of subglacial geology with
1934 ice sheet models to understand the influence of the main processes and to enable better predictions of sea
1935 level change and other impacts on ocean and climate. The first challenge in doing so is the identification of
1936 the basin characteristics and processes that are most relevant to dynamic ice sheet behavior, in particular
1937 we may wish to understand more precisely the influence of basin location within the catchment relative to
1938 the grounding zone, the effects of variable basin thickness, and variations at different scales of properties

1939 such as porosity, lithology, permeability, structural orientation and mechanical erodibility. The incorporation
1940 of these in ice sheet models may in the future be enabled through inclusion of adaptive sliding laws and
1941 better coupled hydrology and hydrogeology modelling.

1942 Other challenges include the successful representation in ice sheet models of evolving sedimentary systems
1943 under ice, including spatially variable and anisotropic bedrock erosion, the re-distribution of subglacial
1944 sediments through subglacial sediment transport and time-variable subglacial hydrology on ice sheet flow,
1945 water outflux and sediment deposition on ice shelves and their cavities. Many ice sheet models are now able
1946 to accommodate at least some of these processes in parameterized forms, allowing their influence to be
1947 assessed alongside other processes [e.g. *Delaney et al.*, 2019; *Lowry et al.*, 2020; *Pollard and DeConto*, 2020].

1948 7 Conclusion

1949 The presence of sedimentary basins in Antarctica, their potential impact on ice sheet dynamics, and their
1950 ability to record change has long been known. Except in some regions with access to outcrops and/or ship-
1951 based science, a comprehensive understanding has been lacking due to ice cover and remoteness restricting
1952 access. The geophysical community has in recent years developed improved approaches to characterize
1953 subglacial geology, through improved equipment and data collection, and advances in data processing and
1954 analysis targeted to the unique environment of Antarctica. The community also has collected large amounts
1955 of data, and crucially these are available to the community in compilations at continent-scale. Numerical
1956 data analysis techniques including machine learning are providing advanced capability to map the
1957 distribution of sedimentary basins.

1958 Key outcomes from the growing understanding of Antarctica's basins are the definition of feedbacks with ice
1959 sheet processes that have the capacity to influence the future Antarctic Ice Sheet, in particular through the
1960 potential supply of increased water and heat to the ice sheet bed as a consequence of retreat. Around the
1961 continent, a system-level understanding is emerging that ties subglacial processes at the ice sheet bed and
1962 marine depositional systems [*Hochmuth et al.*, 2020; *Paxman et al.*, 2019b; *Pollard and DeConto*, 2020]. A
1963 persistent finding beneath the ice sheet, on the continental shelf and beyond is that glacial processes are the
1964 dominant factor in the development of Antarctica's basins since at least the Eocene, signifying the dynamic
1965 nature of the Antarctic Ice Sheet [*Noble et al.*, 2020].

1966 Despite the progress made it is notable that the records we have are, relative to many other parts of the
1967 world, very limited in their distribution, resolution and scope. Across all data, critical gaps remain in our
1968 coverage of Antarctica's basins, and, due to high logistical thresholds, data redundancy and repeatability is
1969 often low. There is a critical need to define in expanded form the importance of subglacial sedimentary
1970 basins for controlling dynamic ice sheet flow, especially to characterize the feedbacks and instabilities that
1971 may dictate the response of Antarctica's ice sheet to changing climate. Finally, it is essential that these

1972 findings are incorporated in future numerical ice sheet models to underpin a better predictive capacity for
1973 future ice sheet change.

1974 8 Acknowledgements

1975 This work rests upon an enormous body of knowledge, and we thank all who have contributed to the
1976 acquisition, processing, analysis and modelling of data and to providing a rich base of interpretations to draw
1977 on. We thank a broad range of collaborators for conversations that helped to develop the manuscript,
1978 including Pippa Whitehouse, Jamin Greenbaum and Katharina Hochmuth. We thank the Editorial Board for
1979 the invitation for this review article. The authors acknowledge funding support from the following bodies
1980 Australian Research Council Special Research Initiative, Australian Centre for Excellence in Antarctic Science
1981 (Project Number SR200100008). China Scholarship Council–The University of Western Australia joint Ph.D.
1982 scholarship (201806170054). Natural Environment Research Council grants NE/S006621/1, NE/R010838/1
1983 NE/G013071/2, NE/F016646/2. British Antarctic Survey Palaeo Environments, Ice Sheets and Climate Change
1984 team. National Science Foundation Graduate Research Fellowship under Grant No. DGE-1656518.

1985 9 Open Research

1986 The map of Antarctica’s sedimentary basins presented here is available from the Pangaea repository (Details
1987 TBC) via [DOI, persistent identifier link] with [license, access conditions]. A version for ongoing development
1988 is available form GitHub []. Data used in mapping are available from sources as cited in text.

1989 10 References

- 1990 Aitken, A. R. A., et al. (2014), The subglacial geology of Wilkes Land, East Antarctica, *Geophysical Research*
1991 *Letters*, 41(7), 2390-2400.
- 1992 Aitken, A. R. A., et al. (2016a), The Australo-Antarctic Columbia to Gondwana transition, *Gondwana*
1993 *Research*, 29(0), 136-152.
- 1994 Aitken, A. R. A., et al. (2016b), Repeated large-scale retreat and advance of Totten Glacier indicated by inland
1995 bed erosion., *Nature*, 533, 385-389.
- 1996 Aitken, A. R. A., et al. (2018), A role for data richness mapping in exploration decision making, *Ore Geology*
1997 *Reviews*, 99, 398-410.
- 1998 Aitken, A. R. A., et al. (2020), A Magnetic Data Correction Workflow for Sparse, Four-Dimensional Data,
1999 *Journal of Geophysical Research: Solid Earth*, 125(10).
- 2000 Allen, P. A., et al. (2015), Chapter 2 Classification of basins, with special reference to Proterozoic examples,
2001 *Geological Society, London, Memoirs*, 43(1), 5-28.
- 2002 Alley, R. B., et al. (1987), Till beneath ice stream B: 3. Till deformation: Evidence and implications, *Journal of*
2003 *Geophysical Research: Solid Earth*, 92(B9), 8921-8929.
- 2004 Alley, R. B., et al. (1994), A water-piracy hypothesis for the stagnation of Ice Stream C, Antarctica, *Annals of*
2005 *Glaciology*, 20, 187-194.

- 2006 Alley, R. B., et al. (2021), Bedforms of Thwaites Glacier, West Antarctica: Character and Origin, *Journal of*
2007 *Geophysical Research: Earth Surface*, 126(12).
- 2008 Almendros, J., et al. (2020), BRAVOSEIS: Geophysical investigation of rifting and volcanism in the Bransfield
2009 Strait, Antarctica, *Journal of South American Earth Sciences*, 104, 102834.
- 2010 Ammon, C. J. (1991), The isolation of receiver effects from teleseismic P waveforms, *Bulletin - Seismological*
2011 *Society of America*, 81(6), 2504-2510.
- 2012 An, M., et al. (2015), S-velocity model and inferred Moho topography beneath the Antarctic Plate from
2013 Rayleigh waves, *Journal of Geophysical Research: Solid Earth*, 120(1), 2014JB011332.
- 2014 Anandakrishnan, S., et al. (1998), Influence of subglacial geology on the position of a West Antarctic ice
2015 stream from seismic observations, *Nature*, 394(6688), 62-65.
- 2016 Anandakrishnan, S., et al. (2000), Deployment of a broadband seismic network in West Antarctica,
2017 *Geophysical Research Letters*, 27(14), 2053-2056.
- 2018 Anandakrishnan, S., and J. P. Winberry (2004), Antarctic subglacial sedimentary layer thickness from receiver
2019 function analysis, *Global and Planetary Change*, 42(1-4), 167-176.
- 2020 Anderson, J. B., et al. (2019), Seismic and geomorphic records of Antarctic Ice Sheet evolution in the Ross Sea
2021 and controlling factors in its behaviour, *Geological Society, London, Special Publications*, 475(1), 223-240.
- 2022 Anderson, J. J. (1965), Bedrock Geology of Antarctica: A Summary of Exploration, 1831–1962, in *Geology and*
2023 *Paleontology of the Antarctic*, edited by J. B. Hadley, pp. 1-70, AGU, Washington, DC, USA.
- 2024 Arndt, J. E., et al. (2017), Evidence for a dynamic grounding line in outer Filchner Trough, Antarctica, until the
2025 early Holocene, *Geology*, 45(11), 1035-1038.
- 2026 Arnold, E., et al. (2020), CReSIS airborne radars and platforms for ice and snow sounding, *Annals of*
2027 *Glaciology*, 61(81), 58-67.
- 2028 Bailey, J. T., et al. (1964), Radio echo sounding of polar ice sheets, *Nature*, 204(4957), 420-421.
- 2029 Bamber, J. L., et al. (2006), East Antarctic ice stream tributary underlain by major sedimentary basin, *Geology*,
2030 34(1), 33-36.
- 2031 Baranov, A., et al. (2021), ANTASed – An Updated Sediment Model for Antarctica, *Frontiers in Earth Science*,
2032 9.
- 2033 Bart, P. J., et al. (2000), Seismic data from the Northern basin, Ross Sea, record extreme expansions of the
2034 East Antarctic Ice Sheet during the late Neogene, *Marine Geology*, 166(1-4), 31-50.
- 2035 Bart, P. J. (2003), Were West Antarctic ice sheet grounding events in the Ross Sea a consequence of East
2036 Antarctic ice sheet expansion during the middle Miocene?, *Earth and Planetary Science Letters*, 216(1-2), 93-
2037 107.
- 2038 Batchelor, C. L., et al. (2020), New insights into the formation of submarine glacial landforms from high-
2039 resolution Autonomous Underwater Vehicle data, *Geomorphology*, 370.
- 2040 Beaman, R. J., et al. (2011), A new high-resolution bathymetry model for the Terre Adélie and George V
2041 continental margin, East Antarctica, *Antarctic Science*, 23(1), 95-103.
- 2042 Behrendt, J. C., et al. (1966), Airborne geophysical study in the Pensacola Mountains of Antarctica, *Science*,
2043 153(3742), 1373-1376.
- 2044 Bell, R., et al. (1999a), Development of a new generation gravity map of Antarctica: ADGRAV Antarctic Digital
2045 Gravity Synthesis, *Annali di Geofisica*, 42.
- 2046 Bell, R. E., et al. (1998), Influence of subglacial geology on the onset of a West antarctic ice stream from
2047 aerogeophysical observations, *Nature*, 394(6688), 58-62.

- 2048 Bell, R. E., et al. (1999b), Airborne gravity and precise positioning for geologic applications, *Journal of*
2049 *Geophysical Research: Solid Earth*, 104(B7), 15281-15292.
- 2050 Bentley, C. R., et al. (1960), Structure of West Antarctica, *Science*, 131(3394), 131-136.
- 2051 Bialas, R., et al. (2007), Plateau collapse model for the Transantarctic Mountains--West Antarctic Rift System:
2052 Insights from numerical experiments, *Geology*, 35, 687-690.
- 2053 Bienert, N. L., et al. (2022), Post-Processing Synchronized Bistatic Radar for Long Offset Glacier Sounding,
2054 *IEEE Transactions on Geoscience and Remote Sensing*, 1-1.
- 2055 Bingham, R. G., and M. J. Siegert (2007a), Radio-echo sounding over polar ice masses, *Journal of*
2056 *Environmental and Engineering Geophysics*, 12(1), 47-62.
- 2057 Bingham, R. G., and M. J. Siegert (2007b), Radar-derived bed roughness characterization of Institute and
2058 Möller ice streams, West Antarctica, and comparison with Siple Coast ice streams, *Geophysical Research*
2059 *Letters*, 34(21).
- 2060 Bingham, R. G., and M. J. Siegert (2009), Quantifying subglacial bed roughness in Antarctica: implications for
2061 ice-sheet dynamics and history, *Quaternary Science Reviews*, 28(3), 223-236.
- 2062 Bingham, R. G., et al. (2012), Inland thinning of West Antarctic Ice Sheet steered along subglacial rifts,
2063 *Nature*, 487(7408), 468-471.
- 2064 Blankenship, D. D., et al. (1986), Seismic measurements reveal a saturated porous layer beneath an active
2065 Antarctic ice stream, *Nature*, 322(6074), 54-57.
- 2066 Boger, S. D. (2011), Antarctica — Before and after Gondwana, *Gondwana Research*, 19(2), 335-371.
- 2067 Bohoyo, F., et al. (2002), Basin development subsequent to ridge-trench collision: The Jane Basin, Antarctica,
2068 *Marine Geophysical Research*, 23(5-6), 413-421.
- 2069 Bowman, V., et al. (2016), The Paleocene of Antarctica: Dinoflagellate cyst biostratigraphy,
2070 chronostratigraphy and implications for the palaeo-Pacific margin of Gondwana, *Gondwana Research*, 38,
2071 132-148.
- 2072 Bradshaw, M. A. (2013), The Taylor Group (Beacon Supergroup): the Devonian sediments of Antarctica,
2073 *Geological Society, London, Special Publications*, 381(1), 67-97.
- 2074 Brenn, G. R., et al. (2017), Variable thermal loading and flexural uplift along the Transantarctic Mountains,
2075 Antarctica, *Geology*, 45(5), 463-466.
- 2076 Brisbane, A. M., et al. (2017), Bed conditions of Pine Island Glacier, West Antarctica, *Journal of Geophysical*
2077 *Research: Earth Surface*, 122(1), 419-433.
- 2078 Broome, A. L., and D. M. Schroeder (2022), A Radiometrically Precise Multi-Frequency Ice-Penetrating Radar
2079 Architecture, *IEEE Transactions on Geoscience and Remote Sensing*, 60, 1-15.
- 2080 Burgess, S. D., et al. (2015), High-precision geochronology links the Ferrar large igneous province with early-
2081 Jurassic ocean anoxia and biotic crisis, *Earth and Planetary Science Letters*, 415, 90-99.
- 2082 Burton-Johnson, A., and T. R. Riley (2015), Autochthonous v. accreted terrane development of continental
2083 margins: a revised in situ tectonic history of the Antarctic Peninsula, *Journal of the Geological Society*, 172(6),
2084 822-835.
- 2085 Cande, S. C., and J. M. Stock (2004), Cenozoic reconstructions of the Australia-New Zealand-South Pacific
2086 sector of Antarctica, in *Geophysical Monograph Series*, edited, pp. 5-17.
- 2087 Capponi, M., et al. (2022), Antarctica 3-D crustal structure investigation by means of the Bayesian gravity
2088 inversion: the Wilkes Land case study, *Geophysical Journal International*, 229(3), 2147-2161.

2089 Castillo, P., et al. (2015), Petrography and geochemistry of the Carboniferous-Triassic Trinity Peninsula
2090 Group, West Antarctica: Implications for provenance and tectonic setting, *Geological Magazine*, 152(4), 575-
2091 588.

2092 Castillo, P., et al. (2017), Provenance and age constraints of Paleozoic siliciclastic rocks from the Ellsworth
2093 Mountains in West Antarctica, as determined by detrital zircon geochronology, *GSA Bulletin*, 129(11-12),
2094 1568-1584.

2095 Catania, G., et al. (2012), Variability in the mass flux of the Ross ice streams, West Antarctica, over the last
2096 millennium, *Journal of Glaciology*, 58(210), 741-752.

2097 Chaput, J., et al. (2014), The crustal thickness of West Antarctica, *Journal of Geophysical Research: Solid
2098 Earth*, 119(1), 378-395.

2099 Christianson, K., et al. (2016), Basal conditions at the grounding zone of Whillans Ice Stream, West
2100 Antarctica, from ice-penetrating radar, *Journal of Geophysical Research: Earth Surface*, 121(11), 1954-1983.

2101 Christoffersen, P., et al. (2014), Significant groundwater contribution to Antarctic ice streams hydrologic
2102 budget, *Geophysical Research Letters*, 41(6), 2003-2010.

2103 Chu, W., et al. (2018), Complex Basal Thermal Transition Near the Onset of Petermann Glacier, Greenland,
2104 *Journal of Geophysical Research: Earth Surface*, 123(5), 985-995.

2105 Cianfarra, P., and F. Salvini (2016), Origin of the Adventure Subglacial Trench linked to Cenozoic extension in
2106 the East Antarctic Craton, *Tectonophysics*, 670, 30-37.

2107 Cooper, M. A., et al. (2019), Subglacial roughness of the Greenland Ice Sheet: relationship with
2108 contemporary ice velocity and geology, *The Cryosphere*, 13(11), 3093-3115.

2109 Corr, H., et al. (2007), Airborne radio-echo sounding of the Wilkes Subglacial Basin, the Transantarctic
2110 Mountains, and the Dome C region, 55-63.

2111 Cox, S. C., et al. (2019), ATA SCAR GeoMAP geology, edited by G. Science¹.

2112 Craddock, J. P., et al. (2017), Detrital zircon provenance of upper Cambrian-Permian strata and tectonic
2113 evolution of the Ellsworth Mountains, West Antarctica, *Gondwana Research*, 45, 191-207.

2114 Cui, X., et al. (2020), Bed topography of Princess Elizabeth Land in East Antarctica, *Earth Syst. Sci. Data*, 12(4),
2115 2765-2774.

2116 Curtis, M. L., and S. A. Lomas (1999), Late Cambrian stratigraphy of the Heritage Range, Ellsworth Mountains:
2117 Implications for basin evolution, *Antarctic Science*, 11(1), 63-77.

2118 Curtis, M. L. (2002), Palaeozoic to Mesozoic polyphase deformation of the Patuxent Range, Pensacola
2119 Mountains, Antarctica, *Antarctic Science*, 14(2), 175-183.

2120 Curtis, M. L., et al. (2004), Structural and geochronological constraints of early Ross orogenic deformation in
2121 the Pensacola Mountains, Antarctica, *Bulletin of the Geological Society of America*, 116(5-6), 619-636.

2122 Dall, J., et al. (2010), ESA'S POLarimetric Airborne Radar Ice Sounder (POLARIS): design and first
2123 results, *IET Radar, Sonar & Navigation*, 4(3), 488-496.

2124 Damaske, D., et al. (2003), Aeromagnetic anomaly investigations along the antarctic coast between Yule Bay
2125 and Mertz Glacier, *Terra Antarctica*, 10, 85-96.

2126 Davey, F. J., and G. Brancolini (1995), The Late Mesozoic and Cenozoic structural setting of the Ross Sea
2127 region, *Geology and Seismic Stratigraphy of the Antarctic Margin*, 68, 167-182.

2128 Davey, F. J., et al. (2000), A revised correlation of the seismic stratigraphy at the Cape Roberts drill sites with
2129 the seismic stratigraphy of the Victoria Land Basin, Antarctica, *Terra Antarctica*, 7(3), 215-220.

2130 Davey, F. J., et al. (2016), Synchronous oceanic spreading and continental rifting in West Antarctica,
2131 *Geophysical Research Letters*, 43(12), 6162-6169.

- 2132 Davey, F. J., et al. (2021), Cenozoic continental rifting in the north-western Ross Sea, *New Zealand Journal of*
2133 *Geology and Geophysics*, 1-8.
- 2134 Davies, D., et al. (2017), High-resolution sub-ice-shelf seafloor records of twentieth century ungrounding and
2135 retreat of Pine Island Glacier, West Antarctica, *Journal of Geophysical Research: Earth Surface*, 122(9), 1698-
2136 1714.
- 2137 Davis, J. K., et al. (2018), The crustal structure of the Enderby Basin, East Antarctica, *Marine Geophysical*
2138 *Research*, 40, 1-16.
- 2139 Dawson, E. J., et al. (2022), Ice mass loss sensitivity to the Antarctic ice sheet basal thermal state, *Nature*
2140 *Communications*, 13(1), 4957.
- 2141 De Santis, L., et al. (1999), The Eastern Ross Sea continental shelf during the Cenozoic: Implications for the
2142 West Antarctic ice sheet development, *Global and Planetary Change*, 23(1-4), 173-196.
- 2143 De Santis, L., et al. (2003), Seismo-stratigraphic analysis of the Wilkes Land continental margin (East
2144 Antarctica): Influence of glacially driven processes on the Cenozoic deposition, *Deep-Sea Research Part II:*
2145 *Topical Studies in Oceanography*, 50(8-9), 1563-1594.
- 2146 Delaney, I., et al. (2019), A Numerical Model for Fluvial Transport of Subglacial Sediment, *Journal of*
2147 *Geophysical Research: Earth Surface*, 124(8), 2197-2223.
- 2148 Dow, C. F., et al. (2022), Antarctic basal environment shaped by high-pressure flow through a subglacial river
2149 system, *Nature Geoscience*, 15(11), 892-898.
- 2150 Dowdeswell, J. A., et al. (2008), Autonomous underwater vehicles (AUVs) and investigations of the ice-ocean
2151 interface in Antarctic and Arctic waters, *Journal of Glaciology*, 54(187), 661-672.
- 2152 Dunham, C. K., et al. (2020), A joint inversion of receiver function and Rayleigh wave phase velocity
2153 dispersion data to estimate crustal structure in West Antarctica, *Geophysical Journal International*, 223(3),
2154 1644-1657.
- 2155 Eagles, G., and R. A. Livermore (2002), Opening history of Powell Basin, Antarctic Peninsula, *Marine Geology*,
2156 185(3-4), 195-205.
- 2157 Eagles, G., et al. (2018), Erosion at extended continental margins: Insights from new aerogeophysical data in
2158 eastern Dronning Maud Land, *Gondwana Research*, 63, 105-116.
- 2159 Eagles, G. (2019), A little spin in the Indian Ocean plate circuit, *Tectonophysics*, 754, 80-100.
- 2160 Eagles, G., and H. Eisermann (2020), The Skytrain plate and tectonic evolution of southwest Gondwana since
2161 Jurassic times, *Scientific Reports*, 10(1), 19994.
- 2162 Ebbing, J., et al. (2018), Earth tectonics as seen by GOCE - Enhanced satellite gravity gradient imaging,
2163 *Scientific Reports*, 8(1).
- 2164 Ebbing, J., et al. (2021), East Antarctica magnetically linked to its ancient neighbours in Gondwana, *Scientific*
2165 *Reports*, 11(1).
- 2166 Eisen, O., et al. (2015), On-ice vibroseis and snowstreamer systems for geoscientific research, *Polar Science*,
2167 9(1), 51-65.
- 2168 Eisen, O., et al. (2020), Basal roughness of the East Antarctic Ice Sheet in relation to flow speed and basal
2169 thermal state, *Annals of Glaciology*, 61(81), 162-175.
- 2170 Eisermann, H., et al. (2020), Bathymetry Beneath Ice Shelves of Western Dronning Maud Land, East
2171 Antarctica, and Implications on Ice Shelf Stability, *Geophysical Research Letters*, 47(12), e2019GL086724.
- 2172 Elliot, D. H., et al. (2017), The Permo-Triassic Gondwana sequence, central Transantarctic Mountains,
2173 Antarctica: Zircon geochronology, provenance, and basin evolution, *Geosphere*, 13(1), 155-178.

- 2174 Enkin, R. J., et al. (2020), The Henkel Petrophysical Plot: Mineralogy and Lithology From Physical Properties, *Geochemistry, Geophysics, Geosystems*, 21(1), e2019GC008818.
2175
- 2176 Escutia, C., et al. (2005), Cenozoic ice sheet history from East Antarctic Wilkes Land continental margin
2177 sediments, *Global and Planetary Change*, 45(1), 51-81.
- 2178 Evans, D. J. A., et al. (2006), Subglacial till: Formation, sedimentary characteristics and classification, *Earth-
2179 Science Reviews*, 78(1), 115-176.
- 2180 Evans, K. R., et al. (2018), Geology of the Nelson Limestone, Postel Nunatak, Patuxent Range, Antarctica,
2181 *Antarctic Science*, 30(1), 29-43.
- 2182 Evans, S., and G. D. Q. Robin (1966), Glacier depth-sounding from the air, *Nature*, 210(5039), 883-885.
- 2183 Evenick, J. C. (2021), Glimpses into Earth's history using a revised global sedimentary basin map, *Earth-
2184 Science Reviews*, 215.
- 2185 Ferraccioli, F., and E. Bozzo (2003), Cenozoic strike-slip faulting from the eastern margin of the Wilkes
2186 Subglacial Basin to the western margin of the Ross Sea Rift: an aeromagnetic connection, *Geological Society,
2187 London, Special Publications*, 210(1), 109-133.
- 2188 Ferraccioli, F., et al. (2005a), Subglacial imprints of early Gondwana break-up as identified from high
2189 resolution aerogeophysical data over western Dronning Maud Land, East Antarctica, *Terra Nova*, 17(6), 573-
2190 579.
- 2191 Ferraccioli, F., et al. (2005b), Tectonic and magmatic patterns in the Jutulstraumen rift (?) region, East
2192 Antarctica, as imaged by high-resolution aeromagnetic data, *Earth, Planets and Space*, 57(8), 767-780.
- 2193 Ferraccioli, F., et al. (2009a), Aeromagnetic exploration over the East Antarctic Ice Sheet: A new view of the
2194 Wilkes Subglacial Basin, *Tectonophysics*, 478(1), 62-77.
- 2195 Ferraccioli, F., et al. (2009b), Magmatic and tectonic patterns over the Northern Victoria Land sector of the
2196 Transantarctic Mountains from new aeromagnetic imaging, *Tectonophysics*, 478(1-2), 43-61.
- 2197 Ferraccioli, F., et al. (2011), East Antarctic rifting triggers uplift of the Gamburtsev Mountains, *Nature*,
2198 479(7373), 388-392.
- 2199 Ferraccioli, F., et al. (2020), Processed line aeromagnetic data over the Recovery Lakes region and interior
2200 Dronning Maud Land, East Antarctica (2013) [Data set]. UK Polar Data Centre, Natural Environment Research
2201 Council, UK Research & Innovation. , edited.
- 2202 Ferrar, H. (1907), Report on the field-geology of the region explored during the "Discovery" Antarctic
2203 Expedition, 1901-1904, Natl. Antarctic Expedition 1901-1904, Nat. Hist., Geol.
- 2204 Fielding, C. R., et al. (2008), Seismic facies and stratigraphy of the Cenozoic succession in McMurdo Sound,
2205 Antarctica: Implications for tectonic, climatic and glacial history, *Palaeogeography, Palaeoclimatology,
2206 Palaeoecology*, 260(1-2), 8-29.
- 2207 Fitzgerald, P. G., and J. W. Goodge (2022), Exhumation and tectonic history of inaccessible subglacial interior
2208 East Antarctica from thermochronology on glacial erratics, *Nature Communications*, 13(1), 6217.
- 2209 Foley, N., et al. (2015), Helicopter-borne transient electromagnetics in high-latitude environments: An
2210 application in the McMurdo Dry Valleys, Antarctica, *GEOPHYSICS*, 81, WA87-WA99.
- 2211 Forsberg, R., et al. (2018), Exploring the Recovery Lakes region and interior Dronning Maud Land, East
2212 Antarctica, with airborne gravity, magnetic and radar measurements, *Geological Society, London, Special
2213 Publications*, 461(1), 23-34.
- 2214 Francis, J. E., et al. (2006), *Cretaceous–Tertiary High-Latitude Palaeoenvironments: James Ross Basin*,
2215 *Antarctica*, Geological Society of London.

- 2216 Frederick, B. C., et al. (2016), Distribution of subglacial sediments across the Wilkes Subglacial Basin, East
2217 Antarctica, *Journal of Geophysical Research F: Earth Surface*, 121(4), 790-813.
- 2218 Frémand, A. C., et al. (2022a), British Antarctic Survey's aerogeophysical data: releasing 25 years of airborne
2219 gravity, magnetic, and radar datasets over Antarctica, *Earth Syst. Sci. Data*, 14(7), 3379-3410.
- 2220 Frémand, A. C., et al. (2022b), Antarctic Bedmap data: FAIR sharing of 60 years of ice bed, surface and
2221 thickness data, *Earth Syst. Sci. Data Discuss.*, 2022, 1-25.
- 2222 Fretwell, P., et al. (2013), Bedmap2: Improved ice bed, surface and thickness datasets for Antarctica,
2223 *Cryosphere*, 7(1), 375-393.
- 2224 Gaina, C., et al. (2007), Breakup and early seafloor spreading between India and Antarctica, *Geophysical
2225 Journal International*, 170(1), 151-169.
- 2226 Gibbons, A. D., et al. (2013), The breakup of East Gondwana: Assimilating constraints from Cretaceous ocean
2227 basins around India into a best-fit tectonic model, *Journal of Geophysical Research: Solid Earth*, 118(3), 808-
2228 822.
- 2229 Gibson, C., et al. (2020), RAM-2 Drill system development: an upgrade of the Rapid Air Movement Drill,
2230 *Annals of Glaciology*, 62, 1-10.
- 2231 Glover, P. (2016), Archie's law – a reappraisal, *Solid Earth*, 7, 1157-1169.
- 2232 Gogineni, S., et al. (1998), An improved coherent radar depth sounder, *Journal of Glaciology*, 44(148), 659-
2233 669.
- 2234 Gohl, K., et al. (2013a), Deciphering tectonic phases of the Amundsen Sea Embayment shelf, West
2235 Antarctica, From a magnetic anomaly grid, *Tectonophysics*, 585, 113-123.
- 2236 Gohl, K., et al. (2013b), Seismic stratigraphic record of the Amundsen Sea Embayment shelf from pre-glacial
2237 to recent times: Evidence for a dynamic West Antarctic ice sheet, *Marine Geology*, 344, 115-131.
- 2238 Gohl, K., et al. (2017), MeBo70 Seabed Drilling on a Polar Continental Shelf: Operational Report and Lessons
2239 From Drilling in the Amundsen Sea Embayment of West Antarctica, *Geochemistry, Geophysics, Geosystems*,
2240 18(11), 4235-4250.
- 2241 Gohl, K., et al. (2021), Evidence for a Highly Dynamic West Antarctic Ice Sheet During the Pliocene,
2242 *Geophysical Research Letters*, 48(14), e2021GL093103.
- 2243 Golynsky, A., et al. (2001), ADMAP – Magnetic anomaly map of the Antarctic, 1: 10 000 000 scale map,
2244 British Antarctic Survey, Cambridge, UK.
- 2245 Golynsky, A., et al. (2006), ADMAP — A Digital Magnetic Anomaly Map of the Antarctic, in *Antarctica:
2246 Contributions to Global Earth Sciences*, edited by D. K. Fütterer, et al., pp. 109-116, Springer Berlin
2247 Heidelberg, Berlin, Heidelberg.
- 2248 Golynsky, A. V., et al. (2018), New Magnetic Anomaly Map of the Antarctic, *Geophysical Research Letters*,
2249 45(13), 6437-6449.
- 2250 Golynsky, D. A., and A. V. Golynsky (2007), Gaussberg rift - illusion or reality?, in *Antarctica: A Keystone in a
2251 Changing World--Online Proceedings of the 10th ISAES*, edited by A. K. Cooper and C. R. Raymond, USGS
2252 Open-File Report 2007-1047, Extended Abstract 168, 5 p.
- 2253 Gong, D., et al. (2019), Coring of antarctic subglacial sediments, *Journal of Marine Science and Engineering*,
2254 7(6).
- 2255 Gooch, B. T., et al. (2016), Potential groundwater and heterogeneous heat source contributions to ice sheet
2256 dynamics in critical submarine basins of East Antarctica, *Geochemistry, Geophysics, Geosystems*, 17(2), 395-
2257 409.

- 2258 Goodge, J. W. (2020), Geological and tectonic evolution of the Transantarctic Mountains, from ancient
2259 craton to recent enigma, *Gondwana Research*, 80, 50-122.
- 2260 Goodge, J. W., et al. (2021), Deep ice drilling, bedrock coring and dust logging with the Rapid Access Ice Drill
2261 (RAID) at Minna Bluff, Antarctica, *Annals of Glaciology*.
- 2262 Granot, R., and J. Dymant (2018), Late Cenozoic unification of East and West Antarctica, *Nature*
2263 *Communications*, 9(1), 3189.
- 2264 Grikurov, G., et al. (2003), Antarctic tectonic and minerogenic provinces, *Arctic and Antarctic, Russian*
2265 *Academy of Sciences*, 2, 26-47.
- 2266 Grima, C., et al. (2019), Surface and basal boundary conditions at the Southern McMurdo and Ross Ice
2267 Shelves, Antarctica, *Journal of Glaciology*, 65(252), 675-688.
- 2268 Gulick, S. P. S., et al. (2017), Initiation and long-term instability of the East Antarctic Ice Sheet, *Nature*,
2269 552(7684), 225-229.
- 2270 Gustafson, C. D., et al. (2022), A dynamic saline groundwater system mapped beneath an Antarctic ice
2271 stream, *Science*, 376(6593), 640-644.
- 2272 Haeger, C., and M. K. Kaban (2019), Decompensative Gravity Anomalies Reveal the Structure of the Upper
2273 Crust of Antarctica, *Pure and Applied Geophysics*, 176(10), 4401-4414.
- 2274 Halberstadt, A. R. W., et al. (2018), Characteristics of the deforming bed: Till properties on the deglaciated
2275 Antarctic continental shelf, *Journal of Glaciology*, 64(248), 1014-1027.
- 2276 Hale, R., et al. (2016), Multi-channel ultra-wideband radar sounder and imager, paper presented at 2016
2277 IEEE International Geoscience and Remote Sensing Symposium (IGARSS), 10-15 July 2016.
- 2278 Hambrey, M. J., and B. McKelvey (2000), Major Neogene fluctuations of the East Antarctic ice sheet:
2279 Stratigraphic evidence from the Lambert Glacier region, *Geology*, 28(10), 887-890.
- 2280 Harry, D. L., et al. (2018), Geodynamic models of the West Antarctic Rift System: Implications for the mantle
2281 thermal state, *Geosphere*, 14(6), 2407-2429.
- 2282 Hathway, B. (2000), Continental rift to back-arc basin: Jurassic-Cretaceous stratigraphical and structural
2283 evolution of the Larsen Basin, Antarctic Peninsula, *Journal of the Geological Society*, 157(2), 417-432.
- 2284 Haynes, M. S., et al. (2018), Geometric Power Fall-Off in Radar Sounding, *IEEE Transactions on Geoscience*
2285 *and Remote Sensing*, 56(11), 6571-6585.
- 2286 Hazzard, J., et al. (2022), Probabilistic Assessment of Antarctic Thermomechanical Structure: Impacts on Ice
2287 Sheet Stability, *EarthArXiv*.
- 2288 Heliere, F., et al. (2007), Radio Echo Sounding of Pine Island Glacier, West Antarctica: Aperture Synthesis
2289 Processing and Analysis of Feasibility From Space, *IEEE Transactions on Geoscience and Remote Sensing*,
2290 45(8), 2573-2582.
- 2291 Hill, G. J. (2020), On the Use of Electromagnetics for Earth Imaging of the Polar Regions, *Surveys in*
2292 *Geophysics*, 41(1), 5-45.
- 2293 Hillenbrand, C. D., et al. (2014), Reconstruction of changes in the Weddell Sea sector of the Antarctic Ice
2294 Sheet since the Last Glacial Maximum, *Quaternary Science Reviews*, 100, 111-136.
- 2295 Hirt, C., et al. (2016), A new degree-2190 (10 km resolution) gravity field model for Antarctica developed
2296 from GRACE, GOCE and Bedmap2 data, *Journal of Geodesy*, 90(2), 105-127.
- 2297 Hochmuth, K., and K. Gohl (2019), Seaward growth of Antarctic continental shelves since establishment of a
2298 continent-wide ice sheet: Patterns and mechanisms, *Palaeogeography, Palaeoclimatology, Palaeoecology*,
2299 520, 44-54.

- 2300 Hochmuth, K., et al. (2020), The Evolving Paleobathymetry of the Circum-Antarctic Southern Ocean Since 34
2301 Ma: A Key to Understanding Past Cryosphere-Ocean Developments, *Geochemistry, Geophysics, Geosystems*,
2302 21(8), e2020GC009122.
- 2303 Hochmuth, K., et al. (2022), Southern Ocean biogenic blooms freezing-in Oligocene colder climates, *Nature*
2304 *Communications*, 13(1), 6785.
- 2305 Hodgson, D. A., et al. (2016), Technologies for retrieving sediment cores in Antarctic subglacial settings,
2306 *Philosophical Transactions of the Royal Society A: Mathematical, Physical and Engineering Sciences*,
2307 374(2059).
- 2308 Holschuh, N., et al. (2020), Linking postglacial landscapes to glacier dynamics using swath radar at Thwaites
2309 Glacier, Antarctica, *Geology*, 48(3), 268-272.
- 2310 Hooyer, T. S., et al. (2012), Control of glacial quarrying by bedrock joints, *Geomorphology*, 153-154, 91-101.
- 2311 Horgan, H., et al. (2005), Seismic stratigraphy of the Plio-Pleistocene Ross Island flexural moat-fill: A
2312 prognosis for ANDRILL Program drilling beneath McMurdo-Ross Ice Shelf, *Global and Planetary Change*,
2313 45(1-3 SPEC. ISS.), 83-97.
- 2314 Horgan, H. J., et al. (2021), Grounding zone subglacial properties from calibrated active-source seismic
2315 methods, *Cryosphere*, 15(4), 1863-1880.
- 2316 Huang, X., and W. Jokat (2016), Sedimentation and potential venting on the rifted continental margin of
2317 Dronning Maud Land, *Marine Geophysical Research*, 37.
- 2318 Huerta, A. D., and D. L. Harry (2007), The transition from diffuse to focused extension: Modeled evolution of
2319 the West Antarctic Rift system, *Earth and Planetary Science Letters*, 255(1), 133-147.
- 2320 Hunter, M. A., and D. J. Cantrill (2006), A new stratigraphy for the Latady Basin, Antarctic Peninsula: Part 2,
2321 Latady Group and basin evolution, *Geological Magazine*, 143(6), 797-819.
- 2322 Hunter, R. J., et al. (1996), Aeromagnetic data from the southern Weddell Sea embayment and adjacent
2323 areas: Synthesis and interpretation, in *Geological Society Special Publication*, edited, pp. 143-154.
- 2324 Isanina, E., et al. (2009), Deep structure of the Vostok Basin, East Antarctica as deduced from seismological
2325 observations, *Geotectonics*, 43, 221-225.
- 2326 Isbell, J. L., et al. (2008), Permian glacial deposits in the Transantarctic Mountains, Antarctica, in *Special*
2327 *Paper of the Geological Society of America*, edited, pp. 59-70.
- 2328 Jamieson, S. S., et al. (2010), The evolution of the subglacial landscape of Antarctica, *Earth and Planetary*
2329 *Science Letters*, 293(1-2), 1-27.
- 2330 Jamieson, S. S. R., et al. (2014), The glacial geomorphology of the Antarctic ice sheet bed, *Antarctic Science*,
2331 26(6), 724-741.
- 2332 Jamieson, S. S. R., et al. (2016), An extensive subglacial lake and canyon system in Princess Elizabeth Land,
2333 East Antarctica, *Geology*, 44(2), 87-90.
- 2334 Jensen, T. E., and R. Forsberg (2018), Helicopter Test of a Strapdown Airborne Gravimetry System, *Sensors*
2335 (*Basel, Switzerland*), 18(9), 3121.
- 2336 Johnston, L., et al. (2008), Cenozoic basin evolution beneath the southern McMurdo Ice Shelf, Antarctica,
2337 *Global and Planetary Change*, 62, 61-76.
- 2338 Jokat, W., et al. (2010), New aeromagnetic data from the western Enderby Basin and consequences for
2339 Antarctic-India break-up, *Geophysical Research Letters*, 37(21).
- 2340 Jokat, W., and U. Herter (2016), Jurassic failed rift system below the Filchner-Ronne-Shelf, Antarctica: New
2341 evidence from geophysical data, *Tectonophysics*, 688, 65-83.
- 2342 Jokat, W., et al. (2021), The early drift of the Indian plate, *Sci Rep*, 11(1), 10796.

- 2343 Jones, P., et al. (2002), Detecting rift basins in the Evans Ice Stream region of West Antarctica using airborne
2344 gravity data, *Tectonophysics*, 347, 25-41.
- 2345 Jordan, T. A., et al. (2010a), Hypothesis for mega-outburst flooding from a palaeo-subglacial lake beneath
2346 the East Antarctic Ice Sheet, *Terra Nova*, 22(4), 283-289.
- 2347 Jordan, T. A., et al. (2010b), Aerogravity evidence for major crustal thinning under the Pine Island Glacier
2348 region (West Antarctica), *Bulletin of the Geological Society of America*, 122(5-6), 714-726.
- 2349 Jordan, T. A., et al. (2013a), Crustal architecture of the Wilkes Subglacial Basin in East Antarctica, as revealed
2350 from airborne gravity data, *Tectonophysics*, 585, 196-206.
- 2351 Jordan, T. A., et al. (2013b), Inland extent of the Weddell Sea Rift imaged by new aerogeophysical data,
2352 *Tectonophysics*, 585, 137-160.
- 2353 Jordan, T. A., et al. (2017a), New geophysical compilations link crustal block motion to Jurassic extension and
2354 strike-slip faulting in the Weddell Sea Rift System of West Antarctica, *Gondwana Research*, 42, 29-48.
- 2355 Jordan, T. A., and D. Becker (2018), Investigating the distribution of magmatism at the onset of Gondwana
2356 breakup with novel strapdown gravity and aeromagnetic data, *Physics of the Earth and Planetary Interiors*,
2357 282, 77-88.
- 2358 Jordan, T. A., et al. (2020), The geological history and evolution of West Antarctica, *Nature Reviews Earth &*
2359 *Environment*, 1(2), 117-133.
- 2360 Jordan, T. A., et al. (2022), An embayment in the East Antarctic basement constrains the shape of the
2361 Rodinian continental margin, *Communications Earth & Environment*, 3(1), 52.
- 2362 Jordan, T. M., et al. (2017b), Self-affine subglacial roughness: consequences for radar scattering and basal
2363 water discrimination in northern Greenland, *The Cryosphere*, 11(3), 1247-1264.
- 2364 Karner, G. D., et al. (2005), Gravity anomalies of sedimentary basins and their mechanical implications:
2365 Application to the Ross Sea basins, West Antarctica, *Earth and Planetary Science Letters*, 235(3-4), 577-596.
- 2366 Kennicutt, M. C., et al. (2019), Sustained Antarctic Research: A 21st Century Imperative, *One Earth*, 1(1), 95-
2367 113.
- 2368 Key, K., and M. R. Siegfried (2017), The feasibility of imaging subglacial hydrology beneath ice streams with
2369 ground-based electromagnetics, *Journal of Glaciology*, 63(241), 755-771.
- 2370 Kim, S., et al. (2018), Seismic stratigraphy of the Central Basin in northwestern Ross Sea slope and rise,
2371 Antarctica: Clues to the late Cenozoic ice-sheet dynamics and bottom-current activity, *Marine Geology*, 395,
2372 363-379.
- 2373 Kjær, K. H., et al. (2018), A large impact crater beneath Hiawatha Glacier in northwest Greenland, *Sci Adv*,
2374 4(11), eaar8173.
- 2375 König, M., and W. Jokat (2006), The Mesozoic breakup of the Weddell Sea, *Journal of Geophysical Research:*
2376 *Solid Earth*, 111(12).
- 2377 Kovesi, P. (1999), Image Features from Phase Congruency, *VIDERE*, 1(3), 2-26.
- 2378 Krabbendam, M., and N. F. Glasser (2011), Glacial erosion and bedrock properties in NW Scotland: Abrasion
2379 and plucking, hardness and joint spacing, *Geomorphology*, 130(3), 374-383.
- 2380 Kristoffersen, Y., et al. (2014), Reassembling Gondwana: A new high quality constraint from vibroseis
2381 exploration of the sub-ice shelf geology of the East Antarctic continental margin, *Journal of Geophysical*
2382 *Research: Solid Earth*, 119(12), 9171-9182.
- 2383 Krohne, N., et al. (2016), The Shackleton Range (East Antarctica): an alien block at the rim of Gondwana?,
2384 *Geological Magazine*, 155(4), 841-864.

- 2385 Kuhl, T., et al. (2021), Agile Sub-Ice Geological (ASIG) Drill development and Pirrit Hills field project, *Annals of*
2386 *Glaciology*, 62(84), 53-66.
- 2387 Kulesa, B., et al. (2006), Time-lapse imaging of subglacial drainage conditions using three-dimensional
2388 inversion of borehole electrical resistivity data, *Journal of Glaciology*, 52(176), 49-57.
- 2389 Kulesa, B. (2007), A Critical Review of the Low-Frequency Electrical Properties of Ice Sheets and Glaciers,
2390 *Journal of Environmental Engineering Geophysics*, 12, 23-36.
- 2391 Kulesa, B., et al. (2019), Heat and groundwater transport between the Antarctic Ice Sheet and subglacial
2392 sedimentary basins from electromagnetic geophysical measurements, in *SEG Technical Program Expanded*
2393 *Abstracts* edited by D. Bevc and O. Nedorub, pp. 4819-4823.
- 2394 Kulhanek, D. K., et al. (2019), Revised chronostratigraphy of DSDP Site 270 and late Oligocene to early
2395 Miocene paleoecology of the Ross Sea sector of Antarctica, *Global and Planetary Change*, 178, 46-64.
- 2396 Kvas, A., et al. (2021), GOCO06s – a satellite-only global gravity field model, *Earth Syst. Sci. Data*, 13(1), 99-
2397 118.
- 2398 Lane, T. P., et al. (2015), Controls on bedrock bedform development beneath the Uummannaq Ice Stream
2399 onset zone, West Greenland, *Geomorphology*, 231, 301-313.
- 2400 Lawrence, J. F., et al. (2006), Rayleigh wave phase velocity analysis of the Ross Sea, Transantarctic
2401 Mountains, and East Antarctica from a temporary seismograph array, *Journal of Geophysical Research: Solid*
2402 *Earth*, 111(B6).
- 2403 Le Brocq, A. M., et al. (2013), Evidence from ice shelves for channelized meltwater flow beneath the
2404 Antarctic Ice Sheet, *Nature Geosci*, 6(11), 945-948.
- 2405 Leitchenkov, G. L., and G. A. Kudryavtzev (1997), Structure and Origin of the Earth's Crust in the Weddell Sea
2406 Embayment (beneath the Front of the Filchner and Ronne Ice Shelves) from Deep Seismic Sounding data,
2407 *Polarforschung*, 67(3), 143-154.
- 2408 Leitchenkov, G. L., et al. (2016), Geology and environments of subglacial Lake Vostok, *Philosophical*
2409 *Transactions of the Royal Society A: Mathematical, Physical and Engineering Sciences*, 374(2059).
- 2410 Levy, R., et al. (2016), Antarctic ice sheet sensitivity to atmospheric CO₂ variations in the early to mid-
2411 Miocene, *Proceedings of the National Academy of Sciences*, 113(13), 3453-3458.
- 2412 Li, L., et al. (2022), Sedimentary basins reduce stability of Antarctic ice streams through groundwater
2413 feedbacks, *Nature Geoscience*, 15(8), 645-650.
- 2414 Lin, F.-C., et al. (2012), Joint inversion of Rayleigh wave phase velocity and ellipticity using USArray:
2415 Constraining velocity and density structure in the upper crust, *Geophysical Research Letters*, 39(12).
- 2416 Lindeque, A., et al. (2013), Deep-sea pre-glacial to glacial sedimentation in the Weddell Sea and southern
2417 Scotia Sea from a cross-basin seismic transect, *Marine Geology*, 336, 61-83.
- 2418 Lindeque, A., et al. (2016a), Seismic stratigraphy along the Amundsen Sea to Ross Sea continental rise: A
2419 cross-regional record of pre-glacial to glacial processes of the West Antarctic margin, *Palaeogeography,*
2420 *Palaeoclimatology, Palaeoecology*, 443, 183-202.
- 2421 Lindeque, A., et al. (2016b), Preglacial to glacial sediment thickness grids for the Southern Pacific Margin of
2422 West Antarctica, *Geochemistry, Geophysics, Geosystems*, 17(10), 4276-4285.
- 2423 Lisker, F., et al. (2007), Thermal history of the Vestfold Hills (East Antarctica) between Lambert rifting and
2424 Gondwana break-up, evidence from apatite fission track data, *Antarctic Science*, 19(1), 97-106.
- 2425 Livingstone, S. J., et al. (2022), Subglacial lakes and their changing role in a warming climate, *Nature Reviews*
2426 *Earth & Environment*, 3(2), 106-124.

2427 Lloyd, A. J., et al. (2015), A seismic transect across West Antarctica: Evidence for mantle thermal anomalies
2428 beneath the Bentley Subglacial Trench and the Marie Byrd Land Dome, *Journal of Geophysical Research:*
2429 *Solid Earth*, 120(12), 8439-8460.

2430 Lloyd, A. J., et al. (2020), Seismic Structure of the Antarctic Upper Mantle Imaged with Adjoint Tomography,
2431 *Journal of Geophysical Research: Solid Earth*, 125(3).

2432 Lösing, M., and J. Ebbing (2021), Predicting Geothermal Heat Flow in Antarctica With a Machine Learning
2433 Approach, *Journal of Geophysical Research: Solid Earth*, 126(6), e2020JB021499.

2434 Lowry, D. P., et al. (2020), Geologic controls on ice sheet sensitivity to deglacial climate forcing in the Ross
2435 Embayment, Antarctica, *Quaternary Science Advances*, 1, 100002.

2436 Luyendyk, B. P., et al. (2001), Structural and tectonic evolution of the Ross Sea rift in the Cape Colbeck
2437 region, Eastern Ross Sea, Antarctica, *Tectonics*, 20(6), 933-958.

2438 Lythe, M. B., and D. G. Vaughan (2001), BEDMAP: A new ice thickness and subglacial topographic model of
2439 Antarctica, *Journal of Geophysical Research: Solid Earth*, 106(B6), 11335-11351.

2440 MacGregor, J. A., et al. (2021), The Scientific Legacy of NASA's Operation IceBridge, *Reviews of Geophysics*,
2441 59(2).

2442 MacKie, E. J., et al. (2020), Antarctic Topographic Realizations and Geostatistical Modeling Used to Map
2443 Subglacial Lakes, *Journal of Geophysical Research: Earth Surface*, 125(3), e2019JF005420.

2444 MacKie, E. J., et al. (2021), Stochastic modeling of subglacial topography exposes uncertainty in water
2445 routing at Jakobshavn Glacier, *Journal of Glaciology*, 67(261), 75-83.

2446 Maggi, M., et al. (2016), Erosion by tectonic carving in the Concordia Subglacial Fault Zone, East Antarctica,
2447 *Earth and Planetary Science Letters*, 433, 99-108.

2448 Maldonado, A., et al. (1994), Forearc tectonic evolution of the South Shetland margin, Antarctic Peninsula,
2449 *Tectonics*, 13(6), 1345-1370.

2450 Maldonado, A., et al. (2006), Ocean basins near the Scotia-Antarctic plate boundary; influence of tectonics
2451 and paleoceanography on the Cenozoic deposits, *Marine Geophysical Researches*, 27(2), 83-107.

2452 Maritati, A., et al. (2016), The tectonic development and erosion of the Knox Subglacial Sedimentary Basin,
2453 East Antarctica, *Geophysical Research Letters*, 43(20), 10,728-710,737.

2454 Maritati, A., et al. (2019), Fingerprinting Proterozoic Bedrock in Interior Wilkes Land, East Antarctica,
2455 *Scientific Reports*, 9(1).

2456 Maritati, A., et al. (2020), Pangea Rifting Shaped the East Antarctic Landscape, *Tectonics*, 39(8),
2457 e2020TC006180.

2458 Maritati, A., et al. (2021), Provenance of Upper Jurassic–Lower Cretaceous strata in the Mentelle Basin,
2459 southwestern Australia, reveals a trans-Gondwanan fluvial pathway, *Gondwana Research*, 93, 128-141.

2460 Marschalek, J. W., et al. (2021), A large West Antarctic Ice Sheet explains early Neogene sea-level amplitude,
2461 *Nature*, 600(7889), 450-455.

2462 Marschall, H. R., et al. (2013), Mesoproterozoic subduction under the eastern edge of the Kalahari-
2463 Grunehogna Craton preceding Rodinia assembly: The Ritscherflya detrital zircon record, Ahlmannryggen
2464 (Dronning Maud Land, Antarctica), *Precambrian Research*, 236, 31-45.

2465 Matsuoka, K. (2011), Pitfalls in radar diagnosis of ice-sheet bed conditions: Lessons from englacial
2466 attenuation models, *Geophysical Research Letters*, 38(5).

2467 Mawson, D. (1928), Unsolved Problems of Antarctic Exploration and Research, *American Geographical*
2468 *Society Special Publication*, 7, 253-266.

- 2469 Mawson, D. (1940), Sedimentary Rocks, Australasian Antarctic Expedition, 1911-1914, Sci. Rept., Ser. A,
2470 Geol., vol. 4, pt.
2471 11, pp. 347-367.
- 2472 McCormack, F. S., et al. (2022), Fine-Scale Geothermal Heat Flow in Antarctica Can Increase Simulated
2473 Subglacial Melt Estimates, *Geophysical Research Letters*, 49(15), e2022GL098539.
- 2474 McKay, R., et al. (2012a), Antarctic and Southern Ocean influences on Late Pliocene global cooling,
2475 *Proceedings of the National Academy of Sciences of the United States of America*, 109(17), 6423-6428.
- 2476 McKay, R., et al. (2012b), Pleistocene variability of Antarctic Ice Sheet extent in the Ross Embayment,
2477 *Quaternary Science Reviews*, 34, 93-112.
- 2478 McKay, R. M., et al. (2016), Antarctic Cenozoic climate history from sedimentary records: ANDRILL and
2479 beyond, *Philosophical Transactions of the Royal Society A: Mathematical, Physical and Engineering Sciences*,
2480 374(2059).
- 2481 McLean, M. A., et al. (2008), Three-dimensional inversion modelling of a Neoproterozoic basin in the
2482 southern Prince Charles Mountains, East Antarctica, *Tectonophysics*, 456(3-4), 180-193.
- 2483 McLean, M. A., et al. (2009), Basement interpretations from airborne magnetic and gravity data over the
2484 Lambert rift region of east Antarctica, *Journal of Geophysical Research B: Solid Earth*, 114(6).
- 2485 McLoughlin, S., and A. N. Drinnan (1997), Revised stratigraphy of the Permian Bainmedart Coal Measures,
2486 northern Prince Charles Mountains, East Antarctica, *Geological Magazine*, 134(3), 335-353.
- 2487 McMahan, K. L., and M. A. Lackie (2006), Seismic reflection studies of the Amery Ice Shelf, East Antarctica:
2488 delineating meteoric and marine ice, *Geophysical Journal International*, 166(2), 757-766.
- 2489 Mieth, M., and W. Jokat (2014), New aeromagnetic view of the geological fabric of southern Dronning Maud
2490 Land and Coats Land, East Antarctica, *Gondwana Research*, 25(1), 358-367.
- 2491 Mikhalsky, E. V., et al. (2020), Low-grade Sandow Group metasediments of the Denman Glacier area (East
2492 Antarctica): Chemical composition, age and provenance from U–Pb detrital zircon data, with some
2493 palaeotectonic implications, *Polar Science*, 26, 100587.
- 2494 Mishra, D. C., et al. (1999), Crustal structure based on gravity-magnetic modelling constrained from seismic
2495 studies under Lambert Rift, Antarctica and Godavari and Mahanadi rifts, India and their interrelationship,
2496 *Earth and Planetary Science Letters*, 172(3-4), 287-300.
- 2497 Montelli, A., et al. (2019), Seismic stratigraphy of the Sabrina Coast shelf, East Antarctica: Early history of
2498 dynamic meltwater-rich glaciations, *GSA Bulletin*, 132(3-4), 545-561.
- 2499 Morlighem, M. (2020), MEaSURES BedMachine Antarctica, Version 2, edited, NASA National Snow and Ice
2500 Data Center Distributed Active Archive Center, Boulder, Colorado USA.
- 2501 Morlighem, M., et al. (2020), Deep glacial troughs and stabilizing ridges unveiled beneath the margins of the
2502 Antarctic ice sheet, *Nature Geoscience*, 13(2), 132-137.
- 2503 Mougnot, J., et al. (2019), Continent-Wide, Interferometric SAR Phase, Mapping of Antarctic Ice Velocity,
2504 *Geophysical Research Letters*, 46(16), 9710-9718.
- 2505 Mulder, J. A., et al. (2019), A Multiproxy provenance approach to uncovering the assembly of East Gondwana
2506 in Antarctica, *Geology*, 47(7), 645-649.
- 2507 Müller, R. D., et al. (2019), A Global Plate Model Including Lithospheric Deformation Along Major Rifts and
2508 Orogens Since the Triassic, *Tectonics*, 38(6), 1884-1907.
- 2509 Muto, A., et al. (2016), Subglacial bathymetry and sediment distribution beneath Pine Island Glacier ice shelf
2510 modeled using aerogravity and in situ geophysical data: New results, *Earth and Planetary Science Letters*,
2511 433, 63-75.

- 2512 Muto, A., et al. (2019a), Bed-type variability and till (dis)continuity beneath Thwaites Glacier, West
2513 Antarctica, *Annals of Glaciology*, 60(80), 82-90.
- 2514 Muto, A., et al. (2019b), Relating bed character and subglacial morphology using seismic data from Thwaites
2515 Glacier, West Antarctica, *Earth and Planetary Science Letters*, 507, 199-206.
- 2516 Naish, T., et al. (2009), Obliquity-paced Pliocene West Antarctic ice sheet oscillations, *Nature*, 458(7236),
2517 322-328.
- 2518 Naylor, S., et al. (2008), The IGY and the ice sheet: surveying Antarctica, *Journal of Historical Geography*,
2519 34(4), 574-595.
- 2520 Noble, T. L., et al. (2020), The Sensitivity of the Antarctic Ice Sheet to a Changing Climate: Past, Present, and
2521 Future, *Reviews of Geophysics*, 58(4), e2019RG000663.
- 2522 Olesen, A., et al. (2020), Processed line aerogravity data over the Recovery Lakes region and interior
2523 Dronning Maud Land, East Antarctica (2013) [Data set]. UK Polar Data Centre, Natural Environment Research
2524 Council, UK Research & Innovation., edited.
- 2525 Olierook, H. K. H., et al. (2016), Bunbury Basalt: Gondwana breakup products or earliest vestiges of the
2526 Kerguelen mantle plume?, *Earth and Planetary Science Letters*, 440, 20-32.
- 2527 Paden, J., et al. (2010), Ice-sheet bed 3-D tomography, *Journal of Glaciology*, 56(195), 3-11.
- 2528 Pappa, F., et al. (2019a), Moho Depths of Antarctica: Comparison of Seismic, Gravity, and Isostatic Results,
2529 *Geochemistry, Geophysics, Geosystems*, 20(3), 1629-1645.
- 2530 Pappa, F., et al. (2019b), Modeling Satellite Gravity Gradient Data to Derive Density, Temperature, and
2531 Viscosity Structure of the Antarctic Lithosphere, *Journal of Geophysical Research: Solid Earth*, 124(11),
2532 12053-12076.
- 2533 Paxman, G. J. G., et al. (2017), Uplift and tilting of the Shackleton Range in East Antarctica driven by glacial
2534 erosion and normal faulting, *Journal of Geophysical Research: Solid Earth*, 122(3), 2390-2408.
- 2535 Paxman, G. J. G., et al. (2019a), Subglacial Geology and Geomorphology of the Pensacola-Pole Basin, East
2536 Antarctica, *Geochemistry, Geophysics, Geosystems*, 20(6), 2786-2807.
- 2537 Paxman, G. J. G., et al. (2019b), Reconstructions of Antarctic topography since the Eocene–Oligocene
2538 boundary, *Palaeogeography, Palaeoclimatology, Palaeoecology*, 535, 109346.
- 2539 Paxman, G. J. G., et al. (2020), Long-Term Increase in Antarctic Ice Sheet Vulnerability Driven by Bed
2540 Topography Evolution, *Geophysical Research Letters*, 47(20), e2020GL090003.
- 2541 Pérez, L. F., et al. (2021), Early and middle Miocene ice sheet dynamics in the Ross Sea: Results from
2542 integrated core-log-seismic interpretation, *GSA Bulletin*, 134(1-2), 348-370.
- 2543 Person, M., et al. (2007), Pleistocene hydrology of North America: The role of ice sheets in reorganizing
2544 groundwater flow systems, *Reviews of Geophysics*, 45(3).
- 2545 Person, M., et al. (2012), Models of ice-sheet hydrogeologic interactions: A review, *Geofluids*, 12(1), 58-78.
- 2546 Peters, L. E., et al. (2006), Subglacial sediments as a control on the onset and location of two Siple Coast ice
2547 streams, West Antarctica, *Journal of Geophysical Research: Solid Earth*, 111(1).
- 2548 Peters, M. E., et al. (2007), Along-Track Focusing of Airborne Radar Sounding Data From West Antarctica for
2549 Improving Basal Reflection Analysis and Layer Detection, *IEEE Transactions on Geoscience and Remote
2550 Sensing*, 45(9), 2725-2736.
- 2551 Phillips, G., and A. L. Läufer (2009), Brittle deformation relating to the Carboniferous–Cretaceous evolution
2552 of the Lambert Graben, East Antarctica: A precursor for Cenozoic relief development in an intraplate and
2553 glaciated region, *Tectonophysics*, 471(3–4), 216-224.

- 2554 Pollard, D., and R. M. DeConto (2020), Continuous simulations over the last 40 million years with a coupled
2555 Antarctic ice sheet-sediment model, *Palaeogeography, Palaeoclimatology, Palaeoecology*, 537, 109374.
- 2556 Pourpoint, M., et al. (2019), Constraints on shallow subglacial structure beneath Thwaites Glacier from joint
2557 inversion of receiver function and surface wave data. abstract #NS11B-0632, in *AGU Fall Meeting 2019*
2558 *Abstracts* edited by AGU.
- 2559 Pyle, M. L., et al. (2010), Crustal structure of the Transantarctic Mountains near the Ross Sea from ambient
2560 seismic noise tomography, *Journal of Geophysical Research: Solid Earth*, 115(11).
- 2561 Reid, A. B. (1980), Aeromagnetic survey design, *Geophysics*, 45(5), 973-976.
- 2562 Reid, A. B., et al. (1990), Magnetic interpretation in three dimensions using Euler deconvolution, *Geophysics*,
2563 55(1), 80-91.
- 2564 Riedel, S., et al. (2012), Mapping tectonic provinces with airborne gravity and radar data in Dronning Maud
2565 Land, East Antarctica, *Geophysical Journal International*, 189(1), 414-427.
- 2566 Riedel, S., et al. (2013), Interpretation of new regional aeromagnetic data over Dronning Maud Land (East
2567 Antarctica), *Tectonophysics*, 585, 161-171.
- 2568 Riley, T. R., et al. (2012), Chrono- and lithostratigraphy of a Mesozoic-Tertiary fore- to intra-arc basin:
2569 Adelaide Island, Antarctic Peninsula, *Geological Magazine*, 149(5), 768-782.
- 2570 Riley, T. R., et al. (2020), Magmatism of the Weddell Sea rift system in Antarctica: Implications for the age
2571 and mechanism of rifting and early stage Gondwana breakup, *Gondwana Research*, 79, 185-196.
- 2572 Rippin, D. M., et al. (2014), Basal roughness of the Institute and Möller Ice Streams, West Antarctica: Process
2573 determination and landscape interpretation, *Geomorphology*, 214, 139-147.
- 2574 Robin, G. d. Q. (1958), Glaciology III: Seismic Shooting and Related Investigations, *Norwegian-British-
2575 Swedish Antarctic Expedition, 1949-52, Scientific Results*, 5.
- 2576 Rogenhagen, J., et al. (2004), Improved seismic stratigraphy of the Mesozoic Weddell Sea, *Marine
2577 Geophysical Research*, 25(3-4), 265-282.
- 2578 Rolland, Y., et al. (2019), Late Paleozoic Ice Age glaciers shaped East Antarctica landscape, *Earth and
2579 Planetary Science Letters*, 506, 123-133.
- 2580 Rosier, S. H. R., et al. (2018), A New Bathymetry for the Southeastern Filchner-Ronne Ice Shelf: Implications
2581 for Modern Oceanographic Processes and Glacial History, *Journal of Geophysical Research: Oceans*, 123(7),
2582 4610-4623.
- 2583 Ruppel, A., et al. (2018), New geophysical data from a key region in East Antarctica: Estimates for the spatial
2584 extent of the Tonian Oceanic Arc Super Terrane (TOAST), *Gondwana Research*, 59, 97-107.
- 2585 Salvini, F., et al. (1997), Cenozoic geodynamics of the Ross Sea region, Antarctica: Crustal extension,
2586 intraplate strike-slip faulting, and tectonic inheritance, *Journal of Geophysical Research B: Solid Earth*,
2587 102(11), 24669-24696.
- 2588 Sanchez, G., et al. (2021), PetroChron Antarctica: A Geological Database for Interdisciplinary Use,
2589 *Geochemistry, Geophysics, Geosystems*, 22(12).
- 2590 Sandwell, D. T., et al. (2014), New global marine gravity model from CryoSat-2 and Jason-1 reveals buried
2591 tectonic structure, *Science*, 346(6205), 65-67.
- 2592 Sauermilch, I., et al. (2019), Tectonic, Oceanographic, and Climatic Controls on the Cretaceous-Cenozoic
2593 Sedimentary Record of the Australian-Antarctic Basin, *Journal of Geophysical Research: Solid Earth*, 124(8),
2594 7699-7724.
- 2595 Sauli, C., et al. (2021), Neogene Development of the Terror Rift, Western Ross Sea, Antarctica, *Geochemistry,
2596 Geophysics, Geosystems*, 22(3).

- 2597 Scambos, T. A., et al. (2017), How much, how fast?: A science review and outlook for research on the
2598 instability of Antarctica's Thwaites Glacier in the 21st century, *Global and Planetary Change*, 153, 16-34.
- 2599 Scanlan, K. M., et al. (2022), Polarimetric Airborne Radar Sounding as an Approach to Characterizing
2600 Subglacial R othlisberger Channels, *IEEE Journal of Selected Topics in Applied Earth Observations and Remote*
2601 *Sensing*, 15, 4455-4467.
- 2602 Scheinert, M., et al. (2016), New Antarctic gravity anomaly grid for enhanced geodetic and geophysical
2603 studies in Antarctica, *Geophysical Research Letters*, 43(2), 600-610.
- 2604 Scher, H. D., and E. E. Martin (2006), Timing and climatic consequences of the opening of Drake Passage,
2605 *Science*, 312(5772), 428-430.
- 2606 Scher, H. D., et al. (2015), Onset of Antarctic Circumpolar Current 30 million years ago as Tasmanian
2607 Gateway aligned with westerlies, *Nature*, 523(7562), 580-583.
- 2608 Schoof, C. (2010), Ice-sheet acceleration driven by melt supply variability, *Nature*, 468(7325), 803-806.
- 2609 Schroeder, D. M., et al. (2013), Evidence for a water system transition beneath Thwaites Glacier, West
2610 Antarctica, *Proceedings of the National Academy of Sciences*, 110(30), 12225-12228.
- 2611 Schroeder, D. M., et al. (2015), Estimating Subglacial Water Geometry Using Radar Bed Echo Specularity:
2612 Application to Thwaites Glacier, West Antarctica, *IEEE Geoscience and Remote Sensing Letters*, 12(3), 443-
2613 447.
- 2614 Schroeder, D. M., et al. (2019), Multidecadal observations of the Antarctic ice sheet from restored analog
2615 radar records, *Proceedings of the National Academy of Sciences*, 116(38), 18867-18873.
- 2616 Schroeder, D. M., et al. (2020), Five decades of radioglaciology, *Annals of Glaciology*, 61(81), 1-13.
- 2617 Shen, W., et al. (2017), Seismic evidence for lithospheric foundering beneath the southern Transantarctic
2618 Mountains, Antarctica, *Geology*, 46.
- 2619 Shen, W., et al. (2018), The Crust and Upper Mantle Structure of Central and West Antarctica From Bayesian
2620 Inversion of Rayleigh Wave and Receiver Functions, *Journal of Geophysical Research: Solid Earth*, 123(9),
2621 7824-7849.
- 2622 Siddoway, C. S., et al. (2004), Ross Sea mylonites and the timing of intracontinental extension within the
2623 West Antarctic rift system, *Geology*, 32(1), 57-60.
- 2624 Siddoway, C. S. (2008), Tectonics of the West Antarctic Rift System: new light on the history and dynamics of
2625 distributed intracontinental extension, *Antarctica: A keystone in a changing world*, 91-114.
- 2626 Siegert, M., et al. (2011), Vostok Subglacial Lake: A Review of Geophysical Data Regarding Its Discovery and
2627 Topographic Setting, *Washington DC American Geophysical Union Geophysical Monograph Series*, 192, 45-
2628 60.
- 2629 Siegert, M. J., et al. (2005), Spectral roughness of subglacial topography and implications for former ice-sheet
2630 dynamics in East Antarctica, *Global and Planetary Change*, 45(1), 249-263.
- 2631 Siegert, M. J., et al. (2016), Subglacial controls on the flow of Institute Ice Stream, West Antarctica, *Annals of*
2632 *Glaciology*, 57(73), 19-24.
- 2633 Siegert, M. J., et al. (2018), Antarctic subglacial groundwater: A concept paper on its measurement and
2634 potential influence on ice flow, in *Geological Society Special Publication*, edited, pp. 197-213.
- 2635 Smellie, J. L., and K. D. Collerson (2021), Chapter 5.5 Gaussberg: volcanology and petrology, in *Volcanism in*
2636 *Antarctica: 200 Million Years of Subduction, Rifting and Continental Break-up*, edited by J. L. Smellie, et al., p.
2637 0, Geological Society of London.

2638 Smith, A. M., et al. (2013), Influence of subglacial conditions on ice stream dynamics: Seismic and potential
2639 field data from Pine Island Glacier, West Antarctica, *Journal of Geophysical Research: Solid Earth*, *118*(4),
2640 1471-1482.

2641 Smith, C., et al. (2019a), New species from the Sabrina Flora: an early Paleogene pollen and spore
2642 assemblage from the Sabrina Coast, East Antarctica, *Palynology*, *43*(4), 650-659.

2643 Smith, E. C., et al. (2020), Detailed Seismic Bathymetry Beneath Ekström Ice Shelf, Antarctica: Implications
2644 for Glacial History and Ice-Ocean Interaction, *Geophysical Research Letters*, *47*(10), e2019GL086187.

2645 Smith, J. A., et al. (2019b), The marine geological imprint of Antarctic ice shelves, *Nature Communications*,
2646 *10*(1), 5635.

2647 Song, T., and P. A. Cawood (2000), Structural styles in the Perth Basin associated with the Mesozoic break-up
2648 of Greater India and Australia, *Tectonophysics*, *317*(1-2), 55-72.

2649 Stagg, H., et al. (2004), Geology of the Continental Margin of Enderby and Mac. Robertson Lands, East
2650 Antarctica: Insights from a Regional Data Set, *Marine Geophysical Researches*, *25*, 183-219.

2651 Stål, T., et al. (2019), A Multivariate Approach for Mapping Lithospheric Domain Boundaries in East
2652 Antarctica, *Geophysical Research Letters*, *46*(17-18), 10404-10416.

2653 Straume, E. O., et al. (2019), GlobSed: Updated Total Sediment Thickness in the World's Oceans,
2654 *Geochemistry, Geophysics, Geosystems*, *20*(4), 1756-1772.

2655 Studinger, M., et al. (2001), Subglacial sediments: A regional geological template for iceflow in West
2656 Antarctica, *Geophysical Research Letters*, *28*(18), 3493-3496.

2657 Studinger, M., et al. (2003), Geophysical models for the tectonic framework of the Lake Vostok region, East
2658 Antarctica, *Earth and Planetary Science Letters*, *216*(4), 663-677.

2659 Studinger, M., et al. (2004), Sub-ice geology inland of the Transantarctic Mountains in light of new
2660 aerogeophysical data, *Earth and Planetary Science Letters*, *220*(3-4), 391-408.

2661 Studinger, M., et al. (2008), Comparison of AIRGrav and GT-1A airborne gravimeters for research
2662 applications, *GEOPHYSICS*, *73*(6), I51-I61.

2663 Swink, M., and C. Speier (1999), Presenting geographic information: effects of data aggregation, dispersion,
2664 and users' spatial orientation, *Decision sciences*, *30*(1), 169-195.

2665 Tabacco, I. E., et al. (2006), Physiography and tectonic setting of the subglacial lake district between Vostok
2666 and Belgica subglacial highlands (Antarctica), *Geophysical Journal International*, *165*(3), 1029-1040.

2667 Talalay, P., et al. (2021), Antarctic subglacial drilling rig: Part II. Ice and Bedrock Electromechanical Drill
2668 (IBED), *Annals of Glaciology*, *62*(84), 12-22.

2669 Tankersley, M. D., et al. (2022), Basement topography and sediment thickness beneath Antarctica's Ross Ice
2670 Shelf imaged with airborne magnetic data, *Earth and Space Science Open Archive*, *17*.

2671 Teisberg, T. O., et al. (2022), Development of a Uav-Borne Pulsed ICE-Penetrating Radar System, paper
2672 presented at IGARSS 2022 - 2022 IEEE International Geoscience and Remote Sensing Symposium, 17-22 July
2673 2022.

2674 Thomson, S. N., et al. (2013), The contribution of glacial erosion to shaping the hidden landscape of East
2675 Antarctica, *Nature Geoscience*, *6*(3), 203-207.

2676 Tinto, K. J., et al. (2019), Ross Ice Shelf response to climate driven by the tectonic imprint on seafloor
2677 bathymetry, *Nature Geoscience*, *12*(6), 441-449.

2678 Tochilin, C. J., et al. (2012), Erosional history of the Prydz Bay sector of East Antarctica from detrital apatite
2679 and zircon geo-and thermochronology multidating, *Geochemistry, Geophysics, Geosystems*, *13*(11).

- 2680 Trey, H., et al. (1999), Transect across the West Antarctic rift system in the Ross Sea, Antarctica,
2681 *Tectonophysics*, 301(1-2), 61-74.
- 2682 Tuckett, P. A., et al. (2019), Rapid accelerations of Antarctic Peninsula outlet glaciers driven by surface melt,
2683 *Nature Communications*, 10(1).
- 2684 Tulaczyk, S. M., and N. T. Foley (2020), The role of electrical conductivity in radar wave reflection from
2685 glacier beds, *The Cryosphere*, 14(12), 4495-4506.
- 2686 Turchetti, S., et al. (2008), Accidents and Opportunities: A History of the Radio Echo-Sounding of Antarctica,
2687 1958-79, *The British Journal for the History of Science*, 41(3), 417-444.
- 2688 van de Lagemaat, S. H. A., et al. (2021), Subduction initiation in the Scotia Sea region and opening of the
2689 Drake Passage: When and why?, *Earth-Science Reviews*, 215, 103551.
- 2690 Vaughan, D. G., et al. (2008), Flow-switching and water piracy between Rutford ice stream and Carlson inlet,
2691 West Antarctica, *Journal of Glaciology*, 54(184), 41-48.
- 2692 Voigt, D. E., et al. (2013), 'Georods': the development of a four-element geophone for improved seismic
2693 imaging of glaciers and ice sheets, *Annals of Glaciology*, 54(64), 142-148.
- 2694 Wannamaker, P., et al. (2017), Uplift of the central Transantarctic Mountains, *Nature Communications*, 8(1),
2695 1588.
- 2696 Wannamaker, P. E., et al. (2004), Structure and thermal regime beneath the South Pole region, East
2697 Antarctica, from magnetotelluric measurements, *Geophysical Journal International*, 157(1), 36-54.
- 2698 Wei, W., et al. (2020), Getz Ice Shelf melt enhanced by freshwater discharge from beneath the West
2699 Antarctic Ice Sheet, *The Cryosphere*, 14(4), 1399-1408.
- 2700 Wenman, C. P., et al. (2020), Post Middle Miocene Tectonomagmatic and Stratigraphic Evolution of the
2701 Victoria Land Basin, West Antarctica, *Geochemistry, Geophysics, Geosystems*, 21(3).
- 2702 Whitehead, J., et al. (2006), A review of the Cenozoic stratigraphy and glacial history of the Lambert
2703 Graben—Prydz Bay region, East Antarctica, *Antarctic Science*, 18(1), 83-99.
- 2704 Willan, R. C. R. (2003), Provenance of Triassic-Cretaceous sandstones in the Antarctic Peninsula: Implications
2705 for terrane models during Gondwana breakup, *Journal of Sedimentary Research*, 73(6), 1062-1077.
- 2706 Williams, S. E., et al. (2013), Early India-Australia spreading history revealed by newly detected Mesozoic
2707 magnetic anomalies in the Perth Abyssal Plain, *Journal of Geophysical Research: Solid Earth*, 118(7), 3275-
2708 3284.
- 2709 Williams, S. E., et al. (2019), Australian-Antarctic breakup and seafloor spreading: Balancing geological and
2710 geophysical constraints, *Earth-Science Reviews*, 188, 41-58.
- 2711 Wilson, C. G., et al. (2019), How can geologic decision-making under uncertainty be improved?, *Solid Earth*,
2712 10(5), 1469-1488.
- 2713 Wilson, D. S., and B. P. Luyendyk (2006), Bedrock platforms within the Ross Embayment, West Antarctica:
2714 Hypotheses for ice sheet history, wave erosion, Cenozoic extension, and thermal subsidence, *Geochemistry,*
2715 *Geophysics, Geosystems*, 7(12).
- 2716 Wilson, D. S., et al. (2012), Antarctic topography at the Eocene-Oligocene boundary, *Palaeogeography,*
2717 *Palaeoclimatology, Palaeoecology*, 335-336, 24-34.
- 2718 Wilson, G., et al. (2007), The geological evolution of southern McMurdo Sound - New evidence from a high-
2719 resolution aeromagnetic survey, *Geophysical Journal International*, 170(1), 93-100.
- 2720 Wilson, T. J. (1999), Cenozoic structural segmentation of the Transantarctic Mountains rift flank in southern
2721 Victoria Land, *Global and Planetary Change*, 23(1-4), 105-127.

2722 Wright, A. P., et al. (2008), High sensitivity of subglacial hydrological pathways in Antarctica to small ice-
2723 sheet changes, *Geophysical Research Letters*, 35(17).

2724 Yakymchuk, C., et al. (2015), Paleozoic evolution of western Marie Byrd Land, Antarctica, *Bulletin of the*
2725 *Geological Society of America*, 127(9-10), 1464-1484.

2726 Young, A., et al. (2019), Global kinematics of tectonic plates and subduction zones since the late Paleozoic
2727 Era, *Geoscience Frontiers*, 10(3), 989-1013.

2728 Young, D. A., et al. (2016), The distribution of basal water between Antarctic subglacial lakes from radar
2729 sounding, *Philosophical Transactions of the Royal Society A: Mathematical, Physical and Engineering*
2730 *Sciences*, 374(2059).

2731 Young, D. A., et al. (2017a), Gravity disturbance data over central Marie Byrd Land, West Antarctica
2732 (GIMBLE.GGCMG2) U.S. Antarctic Program (USAP) Data Center <https://doi.org/10.15784/601003>., edited.

2733 Young, D. A., et al. (2017b), Magnetic anomaly data over central Marie Byrd Land, West Antarctica
2734 (GIMBLE.GMGEO2) U.S. Antarctic Program (USAP) Data Center. doi: <https://doi.org/10.15784/601002>.,
2735 edited.

2736 Young, T. J., et al. (2018), Resolving the internal and basal geometry of ice masses using imaging phase-
2737 sensitive radar, *Journal of Glaciology*, 64(246), 649-660.

2738 Zhang, Y., et al. (2018), Hydromechanical Impacts of Pleistocene Glaciations on Pore Fluid Pressure
2739 Evolution, Rock Failure, and Brine Migration Within Sedimentary Basins and the Crystalline Basement, *Water*
2740 *Resources Research*, 54(10), 7577-7602.

2741 Zhou, Z., et al. (2022), Radial Anisotropy and Sediment Thickness of West and Central Antarctica Estimated
2742 From Rayleigh and Love Wave Velocities, *Journal of Geophysical Research: Solid Earth*, 127(3),
2743 e2021JB022857.

2744